

# Carnegie Mellon University

CARNEGIE INSTITUTE OF TECHNOLOGY

## THESIS

SUBMITTED IN PARTIAL FULFILLMENT OF THE REQUIREMENTS

FOR THE DEGREE OF Doctor of Philosophy

**TITLE** Mixing and Phase Behavior of Organic Particles

**PRESENTED BY** Ellis Robinson

**ACCEPTED BY THE DEPARTMENT OF**

Chemical Engineering

NEIL DONAHUE

9/30/14

NEIL DONAHUE, ADVISOR

DATE

LORENZ BIEGLER

9/30/14

LORENZ BIEGLER, DEPARTMENT HEAD

DATE

**APPROVED BY THE COLLEGE COUNCIL**

VIJAYAKUMAR BHAGAVATULA

9/30/14

DEAN

DATE

## **Mixing and Phase Behavior of Organic Particles**

Submitted in partial fulfillment of the requirements for  
the degree of  
Doctor of Philosophy  
in  
Chemical Engineering

Ellis Shipley Robinson  
B.S., Chemical & Biomolecular Engineering, The Ohio State University

Carnegie Mellon University  
Pittsburgh, PA  
August, 2014

The views and conclusions contained in this document are those of the author, and should not be interpreted as representing the official policies, either expressed or implied, of any sponsoring institution, the U.S. government, or any other entity.

**Keywords:** organic aerosol, atmospheric chemistry, air pollution, mass spectrometry, phase thermodynamics.

## Abstract

We have developed novel experiments aimed at understanding whether and how quickly organic aerosols (OA) mix using single-particle mass spectrometry, as different treatments of mixing in regional models significantly affect predicted mass and composition. First, we designed experiments that separate OA formation chemistry from thermodynamics to test whether two populations of particles equilibrate with each other through the gas phase on experimental timescales. Single-particle mass spectrometry measurements from the aerosol mass spectrometer (AMS) allowed us to quantify the extent of mixing that had occurred. We calibrated this technique using pure-component aerosols with known vapor pressure and phase state, the results of which agreed with a condensation-evaporation model. We then applied these techniques to three atmospherically-relevant situations to determine that: 1) anthropogenic secondary OA (aSOA) does not mix with a surrogate for hydrophobic primary OA (POA), 2) biogenic SOA (bSOA) does not mix with hydrophobic POA, and 3) bSOA shows significant mixing with aSOA. The sum of these experiments show that these complex interactions can be measured for atmospherically important systems, a first step towards quantifying activity coefficients for complex OA mixtures.

We also investigated mixing within individual particles, using mixed-particles of squalane (a surrogate for hydrophobic POA) and SOA from  $\alpha$ -pinene +  $O_3$  that we determined to contain two separate phases. In these experiments, after formation of the mixed-particles, we perturbed smog chamber with a heat ramp. These data revealed that squalane is able to quickly evaporate from the mixed-particles, and that almost all of the SOA is comprised of material lower in volatility than squalane (a low-volatility constituent of pump oil). For this latter “comparative volatility analysis,” we had to correct for the highly variable collection efficiency (CE) of the mixed particles to correctly calculate the mass fraction of SOA remaining. One of the larger implications of this work is highly dependent on the particle morphology, which we were not able to determine definitively: if indeed the particles are core-shell with squalane inside a thick layer of SOA, our results show that diffusivity within SOA is not ultra-low.

Lastly, we present work that furthers our understanding of single-particle CE in the AMS, a quantity especially important for experiments where particle phase is dynamic or there are two separate populations of particles. We report the particle CE of SOA, ammonium sulfate, ammonium nitrate, and squalane. We also determine that half of SOA particles that give meaningful signal, do so at a time later than would be predicted based on their optically-measured flight time through the

instrument. We present convincing evidence that the nature of this delay is due to particles ricocheting around the ionization region of the instrument before vaporizing on an auxiliary surface near the vaporizer. This process affects how much mass signal comes from a particle, the particle mass spectrum, and the bulk mass distribution derived from particle time-of-flight mode. Our results also show that while there is no size dependence to CE for SOA, particles that have passed through a thermodenuder have lower CE, implicating oxidation state and/or volatility as a controller of particle bounce.

## **Acknowledgments**

Being at Carnegie Mellon has been a great experience for me. I learned how to be a scientist, and I fell in love with the city of Pittsburgh. More than anything, those are the two things that I will remember the most about my time here.

I have been incredibly lucky to have Neil Donahue as my advisor. I have had this thought more and more the longer I have been his student, and I think I will continue to have it as I progress to the next steps in my path through science. Neil always spoke to me as a peer, even when I very much wasn't (at times, this was confusing). But his respect of others' intelligence and faith in their abilities to work hard and be excited about science, even in their own way/style, gave me the agency to succeed with my project. And nearing the end of my Ph.D., his trust in me to explore my own questions has very much influenced my decision to continue in atmospheric research. I truly respect the way Neil treats people and how committed he is to science. Thanks, Neil!

The Division of Chemistry at the National Science Foundation largely provided the funds that supported my research (grant number: CHE1012293). This grant was awarded to Neil and another committee member of mine, Allen Robinson, and allowed me freedom to pursue this research without having to worry about limited resources. For this I am very thankful. I would also like to acknowledge the Wallace Research Foundation, who partially funded the purchase of the Aerosol Mass Spectrometers used in this research.

Thanks must also go out to the rest of my Ph.D. committee—Spyros Pandis, Allen Robinson, and Bob Tilton. All of you were helpful in your feedback on my proposed research and the results I presented in my defense. Other professors of mine who deserve considerable thanks are Albert Presto for his help early on in B201, Peter Adams for his truly excellent courses that set the stage for me being an aerosol scientist, and Eric Lipsky for his commitment to the holistic betterment of the CAPS lab.

One of the most influential people I have had the opportunity to do research beside is Rawad Saleh. Rawad, you are an awesome scientist and I know I am not the only person who looks up to you for wisdom "on and off the field" (that's a sports metaphor). In all seriousness, I would not be as engaged in work or have near as much confidence in my ability to be a Real Scientist without your help over the years. The same goes for Adam Ahern, who I admire very much as a scientist (despite him being two years "my junior"). You have been a great collaborator, and I hope we will get the chance to do science again.

I would also like to mention Neil (again) for allowing me to pursue my interests

in science media, which are nearly as important to me as the practice of science itself. What good is our work here if we can't tell people about it? And indeed, as beneficiaries of tax-dollars, I feel that a responsibility rests on our shoulders to do so. During the summer of 2013, I had the wonderful opportunity to work as a science reporter as a mass media fellow of the American Association for the Advancement of Science, something that many advisors would not so easily let their students do. On that note, the Aspen Public Radio crew—most notably Roger Adams, Marci Krivonen, and Elise Thatcher—also deserve thanks for letting me run wild with my science stories. Daniel Tkacik, more than anyone else, has been a big part of the science communication side of my life, and also deserves a huge thanks for being a partner in crime as well as a great friend.

There are so many other people to thank on a personal level that have made my time in Pittsburgh rich and meaningful. Friends from CAPS and CMU (you know who you are—especially you, Andrea. You too, German.), from the city, and from the crag have all been a big part of the last 5 years. As has my girlfriend Margaret, whose support was unconditional and full of energy at all times :). And lastly, to the Peanut Gallery, who has been a part of my life for as long as I can remember, and somehow, awesomely, continues to be just as ever.

Finally, I'd like to thank my family for their support and visits to Pittsburgh: my brother Ethan, my mom Karen, and my dad. Especially I want to thank my scientist-father, John, who I would like to dedicate this thesis too. I know nobody could be more proud.

## Contents

<b>Abstract</b>	<b>iii</b>
<b>Acknowledgments</b>	<b>v</b>
<b>1 Introduction</b>	<b>1</b>
1.1 Motivation . . . . .	1
1.2 Atmospheric particles . . . . .	3
1.3 Organic aerosols . . . . .	5
1.4 Partitioning theory . . . . .	7
1.5 Research questions . . . . .	10
1.6 Thesis overview . . . . .	11
<b>2 Background and Related work</b>	<b>19</b>
2.1 Representations of phase-separation in organic aerosol models . . .	19
2.2 Experimental studies of organic aerosol phase-separation . . . . .	20
2.3 Experimental & modeling studies of diffusivity in organic aerosol . .	22
<b>3 Organic aerosol mixing</b>	<b>26</b>
3.1 Introduction . . . . .	27
3.2 Background . . . . .	29
3.3 Methods . . . . .	32
3.3.1 Experimental design of mixing experiments . . . . .	32
3.3.2 Aerosol preparation . . . . .	33
3.3.3 Measurement suite . . . . .	34
3.3.4 Single-particle mass spectrometer measurements . . . . .	35
3.4 Results and Discussion . . . . .	37
3.4.1 External mixtures . . . . .	37
3.4.2 Vapor pressure-driven mixing . . . . .	45
3.4.3 Mixing between $\alpha$ -pinene-derived SOA and toluene-derived SOA . . . . .	49
3.5 Conclusions . . . . .	53
<b>4 Dynamics of mixed SOA/Squalane particles</b>	<b>61</b>
4.1 Introduction . . . . .	61
4.2 Methods . . . . .	64
4.2.1 Two-population experiments . . . . .	65
4.2.2 Mixed-particle experiments . . . . .	66
4.2.3 Instrument suite . . . . .	67
4.3 Results . . . . .	68
4.3.1 Two-population SOA/Squalane mixing . . . . .	68
4.3.2 Evaporation dynamics of mixed SOA/Squalane particles . . .	70
4.3.3 Collection efficiency of mixed SOA/Squalane particles . . . .	75
4.3.4 Comparative volatility analysis of mixed-particles . . . . .	77
4.4 Discussion . . . . .	79

4.5	Conclusions and future work . . . . .	84
<b>5</b>	<b>Collection efficiency of <math>\alpha</math>-pinene SOA</b>	<b>88</b>
5.1	Introduction . . . . .	89
5.2	Methods . . . . .	93
5.2.1	Aerosol generation . . . . .	93
5.2.2	Operation of light-scattering module . . . . .	95
5.2.3	Calculation of collection efficiency . . . . .	96
5.3	Results and Discussion . . . . .	97
5.3.1	Delayed vaporization PToF artifact . . . . .	97
5.3.2	Delayed particle signal strengths . . . . .	100
5.3.3	Nature of particle-vaporizer interactions . . . . .	103
5.3.4	Collection efficiency as a function of size . . . . .	108
5.3.5	Collection efficiency as a function of volatility . . . . .	109
5.4	Conclusions . . . . .	110
<b>6</b>	<b>Conclusions</b>	<b>114</b>

## List of Figures

2.1	Ideal-mixing versus phase-separation simulation in PM-CAMx . . . . .	20
3.1	Mixing experiment schematic. . . . .	32
3.2	Experimental setup for mixing experiments. . . . .	35
3.3	Docosane/D <sub>46</sub> -docosane mixing experiment time-series and condensation-evaporation model. . . . .	38
3.4	Average mass spectra for two populations in docosane/D <sub>46</sub> -docosane mixing experiment. . . . .	39
3.5	Coagulation simulation for squalane/D <sub>62</sub> -squalane mixing experiment. . . . .	41
3.6	Docosane/D <sub>46</sub> -docosane mixing experiment time-series with heat ramp. . . . .	42
3.7	Squalane/D <sub>46</sub> -docosane mixing experiment time-series and model. . . . .	43
3.8	Squalane/D <sub>8</sub> -toluene SOA mixing experiment time-series. . . . .	44
3.9	Squalane/D <sub>62</sub> -squalane mixing experiment time-series. . . . .	46
3.10	Average mass spectra two populations in squalane/D <sub>62</sub> -squalane mixing experiment at $t = 0$ and $t = 4$ hours . . . . .	47
3.11	Correlation plots for unique MS fragments in squalane/D <sub>62</sub> -squalane and docosane/D <sub>46</sub> -docosane experiments. . . . .	49
3.12	Time-series for $\alpha$ -pinene SOA mixing experiments. . . . .	50
3.13	Histograms of single-particle MS fragments in $\alpha$ -pinene SOA mixing experiments. . . . .	51
3.14	Time-resolved mass distributions of $\alpha$ -pinene SOA/D <sub>8</sub> -toluene SOA mixing experiment. . . . .	52
4.1	Squalane/ $\alpha$ -pinene SOA two-population mixing experiment time-series and single-particle histogram . . . . .	69
4.2	Mixed-particles: SOA condensing on squalane seeds. Time series and single-particle data. . . . .	71
4.3	Size-resolved composition in each stage of mixed-particle experiment where squalane particles serve as seeds for SOM condensation. . . . .	74
4.4	Mixed-particles: squalane condensing on SOA seeds. Time series and PToF data. . . . .	76
4.5	AMS collection efficiency of mixed SOA/squalane particles. . . . .	77
4.6	Time series for comparative volatility analysis. . . . .	79
4.7	Schematic of hypothetical morphologies for mixed-particles prepared from SOM condensation on squalane seeds. . . . .	81
5.1	Experimental setup for size-selected CE study. . . . .	94
5.2	Comparison of size-distributions between SMPS, PToF, and LSSP. . . . .	98
5.3	Illustration of LS and MS signals for a typical, delayed single-particle in AMS. . . . .	99
5.4	Size-distribution comparison between bulk PToF and prompt and delayed single-particles. . . . .	100

5.5	Histogram of ions per particle for null, delayed, and prompt SOA particles . . . . .	101
5.6	Average ions per particle as a function of delay time for SOA. . . . .	102
5.7	Cumulative particle counts as a function of delay time for SOA, $\text{NH}_4\text{NO}_3$ , $(\text{NH}_4)_2\text{SO}_4$ , D <sub>6</sub> 2-squalane, and SOA. . . . .	104
5.8	Mass spectral signal profiles for two (prompt and delayed) ToF arrival times for SOA. . . . .	105
5.9	Test test . . . . .	107
5.10	Difference plot for average prompt and delayed mass spectra for SOA and ammonium sulfate. . . . .	108
5.11	Collection efficiency of SOA as a function of $D_{va}$ and thermodeuder temperature . . . . .	109

# Chapter 1

## Introduction

### 1.1 Motivation

We care about fine particles (aerosol) in the atmosphere for three main reasons: **1.)** they kill people, **2.)** they have strong but uncertain climate effects, and **3.)** they can make it very hard to see.

Fine particles are implicated in three of the top 10 leading causes of mortality, according to the Global Burden of disease: ischaemic heart disease, lower respiratory infections, and chronic obstructive pulmonary disease (Lozano et al., 2012). Roughly 50,000 people per year die in the US from inhalation of excessive levels of fine particles in ambient air (Pope, Ezzati, and Dockery, 2009). According to Pope et al in a population-based study of large metropolitan areas in the U.S, a decrease of 10  $\mu\text{g}$  per cubic meter in concentration of fine particulate matter during the 1980s and 1990s accounted for an increase in average life expectancy of almost a year. Despite the tightening of air quality standards in the U.S.—there have been five reductions in the annual average federal standard for PM mass from 1971 to 2012—the majority of evidence suggests that there exists no threshold between the association of particles with mortality (Schwartz et al., 2007). Aside from mortality, fine particulate pollution is associated with respiratory hospitalizations and illness, exacerbated asthma, premature birth, birth defects, and school absences, among others. These health consequences are disproportionately felt by at-risk populations such as those with pre-existing respiratory and cardiovascular disease, diabetes, asthma, and low socioeconomic status (Pope and Dockery, 2006). Despite the vast variety in the physical and chemical characteristics of fine particles (which will be detailed further in section 1.2 below), exactly how aerosol

health effects are influenced by chemical composition remains poorly understood (Kelly and Fussell, 2012).

The largest uncertainty in estimating earth's energy budget is the radiative forcing associated with both aerosols and clouds (clouds themselves are highly influenced by the nature of collocated aerosols). According to the IPCC's 5th Assessment report, the radiative forcing associated with aerosols is  $-0.9 \pm 1 \text{ W/m}^2$  ( $-0.27$  [ $-0.77$  to  $0.23$ ]  $\text{W/m}^2$  and  $-0.55$  [ $-1.33$  to  $-0.06$ ]  $\text{W/m}^2$  for the direct and indirect effects, respectively) (Solomon et al., 2007). For comparison, the single largest positive radiative forcing term—absorption of out-going infrared radiation by carbon dioxide—is  $1.68 \text{ W/m}^2$ . Fine particles contribute directly to radiative forcing by scattering or absorbing incoming radiation, which is determined by aerosol composition and size. For example, while sulfate particles purely scatter light and black carbon particles purely absorb light, organic aerosol particles can do one or the other depending on their chemical makeup (Lack et al., 2012). Aerosol particles can also have “indirect” effects on the radiative budget through their influence on cloud properties. If cloud droplet-forming aerosol (cloud condensation nuclei or CCN) are high in number, cloud droplets themselves will be smaller in size than for a lower number concentration of CCN. Known as the Twomey Effect or “first aerosol indirect effect,” smaller droplets due to high CCN concentrations increases scattering and thus brighten clouds, a cooling effect on climate (Twomey, 1977). The Albrecht Effect or “second indirect effect,” also contributes negatively to radiative forcing. High CCN concentrations, leading to a large number of relatively smaller cloud droplets, increases the time that cloud droplets take to coalesce into raindrops, increasing the lifetime (and thus scattering ability) of the cloud (Albrecht, 1989). The associated changes to cloud droplet number, and thus cloud albedo, from preindustrial times are one of the largest uncertainties in understanding climate forcing (Solomon et al., 2007). In all of these effects, aerosol composition is

a critical variable influencing not only the magnitude but also the sign of climate forcing.

Finally, haze—a term used to describe the visibility effects from direct light scattering by aerosols—is simply difficult to see through. In some cases, haze is not unwelcome: for instance, the Great Smoky Mountain and Blue Ridge Mountain Ranges derive their namesakes from the presence of secondary organic aerosol particles that form above the canopy of the surrounding forests. Haze is also welcomed when it provides a stunning multi-hued sunset (as documented by many of paintings great masters, whose work has since been used to estimate aerosol optical depths during pre-industrial times, Zerefos et al., 2014). On the other hand, the visibility consequences of haze can be seen as a threat to cultural heritage (Nava et al., 2010): For example, the EPA has intervened in the emissions of power-generating stations on behalf of the scenic vistas in the Grand Canyon National Park (Randazzo, 2014). Aside from when the horizon is obscured, it poses a threat to pilots; this may have been the cause of the small plane crash that claimed the lives of John F. Kennedy Jr. and his companions in 1999 (Showstack, 2000). Aerosols clearly have substantial environmental, social, and economic importance.

## **1.2 Atmospheric particles**

Aerosol refers to a suspension of condensed phase particles (solid or liquid) in a gaseous medium (Hinds, 1999). The most ubiquitous aerosol is our earth's atmosphere, a gaseous medium containing an immense variety of different particles. Colloquially, "aerosols" or "aerosol particles" can refer to the particles themselves.

The diversity of aerosol composition in the atmosphere reflects the large number of sources of particles and processes that act on them during their atmospheric lifetime. There are many kinds: crustal particles of dusts lofted by wind, smoke from incomplete combustion of fossil fuels, suspended bacterial cells, salt particles from

ocean spray, and photochemically-generated aerosols from atmospheric oxidation reactions; these are a select few from a vast array. Photochemically-generated particles (a type of organic aerosol) that form without the presence of a surface to condense on can be on the order of nanometers in width, while fungal spores (a bioaerosol) can span hundreds of microns (Després et al., 2012).

Submicron particles are the size fraction most important for climate, due a the confluence of factors: their size is on the same order of the wavelength of light, meaning that they can efficiently absorb or scatter light; and they have long lifetimes relative to larger particles more influenced by gravitational settling, meaning they can be transported over long distances (and that there simply are more of them); and they are the most common CCN (Seinfeld and Pandis, 2012). Similarly, this submicron size range is interesting for health effects, as small particles have the deepest penetration efficiency in the lungs, making it possible for them to cross into the bloodstream (Kelly and Fussell, 2012). Evidence suggests that smaller particles are more toxic than larger ones (Natusch and Wallace, 1974).

Within the submicron size fraction of atmospheric particles, mass is largely described by two main classes: inorganic and organic, either of which can dominate submicron particle mass depending on location. Comprised of a small number of major ions ( $\text{NH}_4^+$ ,  $\text{Na}^+$ ,  $\text{K}^+$ ,  $\text{Mg}^{2+}$ ,  $\text{Ca}^{2+}$ ,  $\text{NO}_3^-$ ,  $\text{Cl}^-$ ,  $\text{SO}_4^{2-}$ ), the sources, mechanisms of formation, and molecular interactions (e.g. water uptake, aqueous thermodynamics) for inorganic particles are relatively well-understood (e.g. Wexler, 2002). Inorganic particles can be emitted directly into the atmosphere from their source (primary particles), or can be generated through atmospheric chemical reactions to form condensible products (secondary particles).

### 1.3 Organic aerosols

Less understood is the organic fraction of atmospheric aerosols. Organic compounds can comprise up to 90% of submicron aerosol mass, and are globally ubiquitous in particles, from urban areas to remote environments (Jimenez et al., 2009). They play an important role in climate, as condensation of secondary organic matter is a dominant mechanism of growth of particles to CCN sizes (Pierce et al., 2012), and nucleation of organics is a significant source of new particle formation in the atmosphere (Kulmala et al., 2004). Aside from contributing significantly to fine particulate mass less than 2.5 microns ( $PM_{2.5}$ ), one of the most robust indicators for health effects from air pollution, there is growing evidence that organics within  $PM_{2.5}$  contribute specifically to toxicity (Cassee et al., 2012; Sioutas, 2011).

The entire range of organic functional groups are present in OA. From the oxidation of  $\alpha$ -pinene with  $O_3$ , much of which condenses to form secondary OA (SOA), there are an estimated  $\sim 1,000$  molecular products, including alcohol, dicarboxylic, ketone, and aldehyde functional groups (Tolocka et al., 2004). There are an estimated 20,000 different organic compounds in diesel exhaust alone, only a very small fraction of which have been positively identified ( $< 5\%$ ) (Sehlstedt et al., 2007). And for a C10 alkane, over 100 possible isomers exist, the number of which increases exponentially with each additional carbon atom (Goldstein and Galbally, 2007). While many techniques do exist for molecular identification of OA components—such as two-dimensional gas chromatography, high-resolution mass spectrometry, and various spectroscopic techniques—the majority of molecules ( $> 70\%$  as a lower estimate) are as yet unspciated (Williams et al., 2006).

The molecular complexity of OA gives rise to equally vast ranges of important physical properties, such as vapor pressure, polarity and oxidation state, density, and molecular weight. Condensable vapors from first-generation reactions in the  $\alpha$ -

pinene + O<sub>3</sub> system can have saturation mass concentrations as low 10<sup>-5</sup> μg/m<sup>-3</sup> (equivalent to ~10<sup>-12</sup> torr, which is essentially non-volatile), while other products from the same reaction can have vapor pressures as high as 10<sup>4</sup> μg/m<sup>-3</sup> (Ehn et al., 2015; Pathak et al., 2007). Within atmospheric OA exist both highly-oxidized (oxygen-to-carbon (O:C) ratios of >1), extremely-low volatility particles and completely hydrophobic semi-volatile particles (e.g. fresh diesel exhaust) with O:C ~0.

Despite the significance and abundance of organic aerosols (OA), their chemical and physical properties are poorly understood, owing largely to this complexity. There persists a strong gap between ambient OA mass measurements, across a variety of environments, and what regional and global model predict in those same places (Volkamer et al., 2006; Heald et al., 2011)). In the vast majority of cases, the air quality model under-predicts the ambient concentration, sometimes by up to a factor of ten. Missing sources (e.g. Robinson et al., 2010; Heald et al., 2005; Liggio and Li, 2013) and poorly understood atmospheric processes (e.g. new particle formation) have both been invoked as contributing to the discrepancy between models and measurements.

Traditionally, OA has been split into two broad classes based on formation: primary organic aerosol (POA), and SOA. POA refers to particles emitted directly as particles into the atmosphere (e.g. from combustion sources like diesel or biomass-burning). POA was once considered nonvolatile, indicating that emissions testing at the tailpipe was indicative of primary exhaust emissions under all atmospheric conditions (Code of Federal Regulations, 2008). We now know that primary exhaust consists largely of volatile and semi-volatile compounds, and that POA is highly dynamic: the emissions factor for primary PM mass is highly dependent on the dilution factor at which it is measured (Lipsky and Robinson, 2006). The evaporated emissions from POA, like any other reduced organics in the troposphere, are very subject to chemical reactions with atmospheric oxidants (e.g. OH radical).

Through this mechanism, “POA” becomes SOA, blurring the traditional distinction between the two broad classes of organic particles. Accounting for the SOA potential of these semi-volatiles, is one source of organic PM mass that may help close the model-measurement gap (Presto et al., 2009).

## 1.4 Partitioning theory

Chemical lifetimes of organics in the gas-phase are short ( $\sim$ hours), due to rapid reaction with OH radicals, relative to particle lifetimes that can be up to a week (Donahue et al., 2013). These reactions generally result in substitution of a hydrogen with a oxygen-containing functional group, thus lowering the vapor pressure, which is then followed by condensation. This repeated evaporation, reaction, and condensation cycle generally leads to highly-oxidized, low-volatility organic particles. These organics spend most of their time in the condensed phase. The interplay between gas-to-particle partitioning and chemistry is dubbed the “evolution of volatility.”

The ability of a molecule at the end of the evaporation-reaction-condensation cycle to partition into the condensed-phase is a crucial factor determining OA properties (e.g. oxidation state, volatility), as chemical reactions in the condensed phase are much slower than in the gas-phase. General partitioning theory describes the fraction ( $\xi_i$ ) of a given molecule  $i$  that will be found in the condensed-phase (the remainder residing in the gas-phase):

$$\xi_i = \frac{1}{1 + \frac{C_i^*}{C_{OA}}} \quad (1.1)$$

where  $C_{OA}$  is the total mass concentration of the absorbing organic phase.  $C_i^*$  is the effective mass saturation concentration of compound  $i$  in  $\mu\text{g m}^{-3}$ , but can simply be related to sub-cooled liquid saturation vapor pressure through the ideal gas

law (Pankow, 1994; Donahue et al., 2006). In general partitioning theory, organics in the condensed phase are assumed to form a solution and to be in equilibrium with the gas-phase (or relaxing towards it).

Highly pertinent to this thesis, from equation 1.1, is the  $C_{OA}$  term. Finding a compound in the condensed-phase depends strongly on the concentration of OA into which  $i$  can be absorbed into. This is nicely illustrated by the dependence of SOA yields on  $C_{OA}$  from single-precursors in smog chamber experiments: with a higher absorbing mass, compounds with larger saturation concentrations can partition into the aerosol, thus increasing the observed yield. But in the atmosphere, if there are different organic phases present, how does one define  $C_{OA}$  with respect to compound  $i$  and equation 1.1?

Embedded in  $C_i^*$  is the activity coefficient for compound  $i$  in the absorbing phase. In SOA yield experiments, activity coefficients are assumed to be constant for a given compound “over the range of the conditions of interest” (e.g. a given experiment) (Donahue, Robinson, and Pandis, 2009). This is likely a good assumption for a smog chamber yield experiment, where all SOA is uniform in composition, but possibly not in, for instance, urban areas with a diverse set of sources producing chemically-dissimilar OA (e.g. Moffet et al., 2008). The oxidation products from a semi-volatile biogenic precursor (e.g.  $\alpha$ -pinene) likely does not have the same activity coefficient in SOA as it does in highly-reduced, hydrophobic diesel exhaust. This drives one of the main foci of this thesis: do different OA types (e.g. SOA and POA) form mixtures, or remain phase-separated (Asa-Awuku et al., 2009)? If the answer is that different organic phases are present, then a given compound  $i$  would (likely) have different  $\xi_i$  values respective to each phase. Activity coefficients of organics in the condensed organic phase(s) thus control how much a given compound will be found in the gas-phase, which governs the chemical lifetime and the chemical composition of a given particle.

Traditionally—and almost always, still—OA models assume a single, well-mixed organic phase (Strader, Lurmann, and Pandis, 1999). In practical terms, this means that, as an example, SOA is able to partition into POA. First, this assumes that all classes of OA are miscible in one-another. Further, it implies that the organic phase(s) is(are) in equilibrium, or quickly relaxing towards equilibrium, with the gas-phase. Despite our knowledge that externally-mixed particles do exist in source-rich environments (e.g. Moffet et al., 2008), meaning that there are indeed separate organic phases, if the equilibration with the gas-phase to form a uniform organic phase occurs on short timescales relative to the time steps in regional or global aerosol models, then this is likely a good assumption.

It has been hypothesized that, because many of the atmospherically-identified OA constituents have sufficient volatilities to diffuse through the gas-phase and establish equilibrium with neighboring particles on fast timescales, organics tend to form an internally-mixed aerosol (Marcolli et al., 2004). However, this process has not been observed experimentally to date. Experimental investigations of phase behavior between different types of OA are limited to a small number of studies, most of which rely on indirect evidence to diagnose mixing (or lack there-of), (e.g. Song et al., 2007; Hildebrandt et al., 2011). However, the implications for mixing have the potential to be profound, as the more absorbing organic mass there is, the greater the partial pressure reduction for all components in the mixture by Raoult's Law. This has the potential to influence the total OA mass from models, which is further discussed in Chapter 2. Chapter 3 of this thesis describes experiments aimed at observing mixing in between different types of OA, a first step towards quantifying activity coefficients in OA systems.

While improving our understanding of the thermodynamics of organic aerosols has the potential to bring models closer to measurements, there is the issue of kinetics as well: for models to assume a single, well-mixed organic phase, not only

do OA from different sources have to be miscible with one another, the process of gas-phase exchange leading to equilibration between OA types must occur on timescales shorter than the time steps of regional or global models (e.g.  $\sim 1$  hour, Lee, Pierce, and Adams, 2013). Recent research, however, has called into question this assumption about the equilibration timescales of SOA for several reasons. First, a large fraction of biogenic SOA has been found to have vapor-pressures much lower than previously thought, limiting the timescale for gas-phase exchange between dissimilar particles. Secondly, it has been reported that SOA exists in a highly-viscous semi-solid phase, leading to extremely low internal diffusivity ( $D_{org} = 10^{-20} \text{ cm}^2 \text{ s}^{-1}$ ) and long mixing timescales *within* particles ( $\tau_{eq} > \text{days}$ ). Further, it has been argued that slow diffusion could explain some of the model-measurement gap for OA (e.g. Shrivastava et al., 2011). Chapter 4 of this thesis aims to probe the volatility of SOA and the possibility of long diffusion timescales within SOA.

## 1.5 Research questions

*In this thesis, I make the following contributions: I present novel mixing experiments that determine the ability of two organic aerosol populations to mix (or not). I present data on mixed-particles that suggests that SOA does not present significant diffusive limitations to evaporation though is comprised largely of material less volatile than squalane (a low-volatility constituent of pump oil). Lastly, I demonstrate the capacity of single-particle measurements from the AMS to shed new light on mixing processes, phase state of organic aerosols, and collection efficiency in the AMS.*

The following list contains the simplest phrasings of the single research question driving each of the chapters in this thesis. These are followed by sub-questions also posed in each chapter. The questions themselves do not necessarily reveal

the implications that the answers to the questions might have, but rather describe the most fundamental problem each that chapter attempts to solve.

1. Does vapor-pressure driven mixing happen, and can it be observed in smog chamber experiments? (Chapter 3)
  - (a) Can externally-mixed aerosol populations of different organics be differentiated in smog chamber experiments, allowing us to see when two populations do not mix?
  - (b) Is the degree of mixing between two populations quantifiable?
2. Is squalane able to evaporate from mixed SOA/squalane particles when subjected to a perturbation of elevated heat? (Chapter 4)
  - (a) Do squalane and SOA (from  $\alpha$ -pinene +  $O_3$ ) mix or phase-separate?
  - (b) Can we diagnose the morphology of these mixed-particles using the AMS?
  - (c) What are the implications of this work?
3. What is the nature of the disagreement for mass measurements of SOA between the AMS and other co-located instruments (e.g. Scanning Mobility Particle Sizer)? (Chapter 5)
  - (a) What is the mechanism of delay for a “delayed” single-particle signal in the AMS?
  - (b) How do size and composition affect collection efficiency?

## 1.6 Thesis overview

**Chapter 2** details the broad literature review that has informed the writing of this thesis and the research questions it poses. Summarized in **Chapter 2** are some different approaches to dealing with phase-separation in OA modeling, which serve as motivation for the relatively short list of pre-existing experimental studies of OA mixing. Additionally, this chapter contains a review of recent work relating to organic diffusivity in SOA, which has important implications for almost all aspects of OA modeling, including mixing, evaporation, and heterogeneous chemistry. Lastly, as it relates to the science questions of chapters 3 and 4, a description of single-

particle mass spectrometry is presented, focusing on techniques specific to the light-scattering single-particle capability of the aerosol mass spectrometer (AMS).

**Chapter 3** describes smog chamber experiments that investigated how different populations of organic particles mixed (or didn't) with each other. There have been (very few) attempts at determining mixing behavior between different aerosol populations, but a.) most of these used indirect measurements to infer mixing, and b.) many of these studies do not fully separate formation chemistry from phase thermodynamics. Here, we present experiments that reveal whether or not two populations mix or don't, and we attempt to quantify the extent of mixing in some systems. The experimental design of these mixing experiments is first described, followed by data from calibration experiments between populations of pure-compound particles that followed expected behavior. These experiments served as important benchmarks for the efficacy of the mixing technique. Next, experiments between laboratory-surrogates for atmospherically-relevant organic aerosols are presented where mixing behavior was determined. This chapter presents an experimental method from which further studies of organic aerosol mixing can be conducted, and also directly answers questions of atmospheric importance regarding how the interactions between different organic aerosols sources should be considered in models.

**Chapter 4** details experiments aimed at assessing the diffusivity and morphology of mixed-particles made of squalane and SOA derived from  $\alpha$ -pinene ozonolysis. Recent work has thrown into question the validity of treating secondary organic aerosols as being capable of equilibrating on atmospheric timescales. Equilibration timescales are highly important to determining phase-partitioning in OA systems, and in this chapter we attempted to assess the ability of squalane to equilibrate with the gas-phase in heat ramp perturbation experiments. First, the mixing behavior between SOA and squalane was assessed according to the procedure outlined in

Chapter 3. These experiments informed the assessment that squalane and SOA form separate phases within particles. Subsequent experiments were performed on “mixed-particles,” where one material (squalane or SOA) served as the seed for the condensation of the other material. The particles were then heated from 23 to 40 °C, and the evaporation of squalane from the mixed particles was quantified to assess any diffusive limitations presented by the presence of SOA. We also use this method to perform a comparative volatility analysis between squalane and SOA, and demonstrate how collection efficiency in mixed-organic systems can vary with time, and needs to be accounted for for full mass quantification.

**Chapter 5** presents novel data analysis of single-particle data from the AMS aimed at better understanding the nature of collection efficiency (CE), the major limitation to full quantification in the instrument. Collection efficiency is especially important in both mixing experiments (Chapter 3), where different particle types may be counted with different sensitivities, and in mixed-particle experiments (Chapter 4), where the presence of one material affects the mass measurement of the other. Using data from both mixing experiments and careful, size-selected experiments of “pure” aerosol, we present an analysis of single-particle data that adds to our understanding of how the AMS works. First, the nature of a well-known AMS artifact—the “delayed tail” of the mass distribution, which misrepresents the mass distribution at large particle diameters—is discussed in the context of single-particle measurements. The data strongly suggest that the tail arises from delayed particle signals, due to non-ideal interactions with the AMS vaporizer, which is dictated by the particle phase state. In addition to results presented for SOA derived from  $\alpha$ -pinene ozonolysis, we compare the SOA data with ammonium nitrate, ammonium sulfate, and squalane particles. This chapter represents a step forward in better understanding the nature of CE through the collection of single-particle data.

Finally, in **Chapter 6**, the key findings of this thesis are summarized. The atmo-

spheric implications of this work are discussed, and future work is suggested.

## Bibliography

- [1] Bruce A Albrecht. "Aerosols, cloud microphysics, and fractional cloudiness". *Science* 245.4923 (1989), pp. 1227–1230.
- [2] A Asa-Awuku et al. "Mixing and phase partitioning of primary and secondary organic aerosols". *Geophysical Research Letters* 36.15 (Aug. 2009).
- [3] Flemming R Cassee et al. "Environmental Research". *Environmental Research* 115.C (May 2012), pp. 1–10.
- [4] Code of Federal Regulations. *Engine Testing Procedures*. Tech. rep. Title 40. Jan. 2008.
- [5] Viviane R Després et al. "Primary biological aerosol particles in the atmosphere: a review". *Tellus B* 64.0 (Feb. 2012), p. 296.
- [6] N M Donahue et al. "Coupled Partitioning, Dilution, and Chemical Aging of Semivolatile Organics". *Environmental Science & Technology* 40.8 (Apr. 2006), pp. 2635–2643.
- [7] N M Donahue et al. "Why do organic aerosols exist? Understanding aerosol lifetimes using the two-dimensional volatility basis set". *Environmental Chemistry* 10.3 (2013), p. 151.
- [8] Neil M Donahue, Allen L Robinson, and Spyros N Pandis. "Atmospheric Environment". *Atmospheric Environment* 43.1 (Jan. 2009), pp. 94–106.
- [9] Mikael Ehn et al. "A large source of low-volatility secondary organic aerosol". *Nature* 506.7489 (Apr. 2015), pp. 476–479.
- [10] Allen H Goldstein and Ian E Galbally. "Known and unexplored organic constituents in the earth's atmosphere". *Environmental Science & Technology* 41.5 (2007), pp. 1514–1521.
- [11] C L Heald et al. "Exploring the vertical profile of atmospheric organic aerosol: comparing 17 aircraft field campaigns with a global model". *Atmospheric Chemistry and Physics* 11.24 (2011), pp. 12673–12696.
- [12] Colette L Heald et al. "A large organic aerosol source in the free troposphere missing from current models". *Geophysical Research Letters* 32.18 (Sept. 2005), n/a–n/a.
- [13] Lea Hildebrandt et al. "Evaluating the Mixing of Organic Aerosol Components Using High-Resolution Aerosol Mass Spectrometry". *Environmental Science & Technology* 45.15 (Aug. 2011), pp. 6329–6335.
- [14] William C Hinds. *Aerosol technology : properties, behavior, and measurement of airborne particles*. New York: Wiley, 1999.
- [15] J L Jimenez et al. "Evolution of Organic Aerosols in the Atmosphere". *Science* 326.5959 (Dec. 2009), pp. 1525–1529.

- [16] Frank J Kelly and Julia C Fussell. "Size, source and chemical composition as determinants of toxicity attributable to ambient particulate matter". *Atmospheric Environment* 60.C (Dec. 2012), pp. 504–526.
- [17] M Kulmala et al. "Formation and growth rates of ultrafine atmospheric particles: a review of observations". *Journal of Aerosol Science* 35.2 (Mar. 2004), pp. 143–176.
- [18] Daniel A Lack et al. "Brown carbon and internal mixing in biomass burning particles". *Proceedings of the National Academy of Sciences* 109.37 (2012), pp. 14802–14807.
- [19] Y H Lee, J R Pierce, and P J Adams. "Representation of nucleation mode microphysics in a global aerosol model with sectional microphysics". *Geoscientific Model Development* 6.4 (2013), pp. 1221–1232.
- [20] J Liggió and S M Li. "A new source of oxygenated organic aerosol and oligomers". *Atmospheric Chemistry and Physics* 13.6 (2013), pp. 2989–3002.
- [21] Eric M Lipsky and Allen L Robinson. "Effects of Dilution on Fine Particle Mass and Partitioning of Semivolatile Organics in Diesel Exhaust and Wood Smoke". *Environmental Science & Technology* 40.1 (Jan. 2006), pp. 155–162.
- [22] Rafael Lozano et al. "Global and regional mortality from 235 causes of death for 20 age groups in 1990 and 2010: a systematic analysis for the Global Burden of Disease Study 2010." *The Lancet* 380.9859 (Dec. 2012), pp. 2095–2128.
- [23] C Marcolli et al. "Internal mixing of the organic aerosol by gas phase diffusion of semivolatile organic compounds". *Atmospheric Chemistry and Physics* 4.11/12 (2004), pp. 2593–2599.
- [24] Ryan C Moffet et al. "Chemically segregated optical and microphysical properties of ambient aerosols measured in a single-particle mass spectrometer". *Journal of Geophysical Research* 113.D12 (June 2008), p. D12213.
- [25] David FS Natusch and John R Wallace. "Urban aerosol toxicity: the influence of particle size". *Science* 186.4165 (1974), pp. 695–699.
- [26] S Nava et al. "Science of the Total Environment". *Science of the Total Environment, The* 408.6 (Feb. 2010), pp. 1403–1413.
- [27] James F Pankow. "An absorption model of gas/particle partitioning of organic compounds in the atmosphere". *Atmospheric Environment* 28.2 (1994), pp. 185–188.
- [28] R K Pathak et al. "Ozonolysis of  $\alpha$ -pinene: parameterization of secondary organic aerosol mass fraction". *Atmospheric Chemistry and Physics* 7.14 (2007), pp. 3811–3821.

- [29] J R Pierce et al. "Nucleation and condensational growth to CCN sizes during a sustained pristine biogenic SOA event in a forested mountain valley". *Atmospheric Chemistry and Physics* 12.7 (2012), pp. 3147–3163.
- [30] C Arden Pope III and Douglas W Dockery. "Health Effects of Fine Particulate Air Pollution: Lines that Connect". *Journal of the Air & Waste Management Association* 56.6 (June 2006), pp. 709–742.
- [31] C Arden Pope III, Majid Ezzati, and Douglas W Dockery. "Fine-particulate air pollution and life expectancy in the United States". *New England Journal of Medicine* 360.4 (2009), pp. 376–386.
- [32] Albert A Presto et al. "Intermediate-Volatility Organic Compounds: A Potential Source of Ambient Oxidized Organic Aerosol". *Environmental Science & Technology* 43.13 (July 2009), pp. 4744–4749.
- [33] Ryan Randazzo. *EPA approves plan to curtail operations at Navajo Generating Station*. July 2014. URL: <http://www.azcentral.com/story/money/business/2014/07/28/epa-approves-plan-curtail-operations-navajo-generating-station/13277331/>.
- [34] Allen L Robinson et al. "Updating the Conceptual Model for Fine Particle Mass Emissions from Combustion Systems Allen L. Robinson". *Journal of the Air & Waste Management Association* 60.10 (Oct. 2010), pp. 1204–1222.
- [35] Joel Schwartz et al. "The Effect of Dose and Timing of Dose on the Association between Airborne Particles and Survival". *Environmental Health Perspectives* 116.1 (Oct. 2007), pp. 64–69.
- [36] Maria Sehlstedt et al. *The Role of Particle Size and Chemical Composition for Health Risks of Exposure to Traffic Related Aerosols*. Tech. rep. Dec. 2007.
- [37] J H Seinfeld and S N Pandis. *Atmospheric Chemistry and Physics: From Air Pollution to Climate Change*. Wiley, 2012.
- [38] Randy Showstack. "The Perfect Haze: Scientists Link 1999 U.S. Pollution Episode to Midwest Aerosol Plumes and Kennedy Plane Crash". *Eos, Transactions American Geophysical Union* 81.2 (Jan. 2000), pp. 13–14.
- [39] M. Shrivastava et al. "Reformulating the atmospheric lifecycle of SOA based on new field and laboratory data". *Atmospheric Chemistry and Physics Discussions* 11.7 (2011), pp. 20107–20139.
- [40] Constantinos Sioutas. *Physicochemical and Toxicological Assessment of the Semi-Volatile and Non-Volatile Fractions of PM from Heavy-Duty Vehicles Operating with and Without Emissions Control Technologies*. Tech. rep. PB2012-107458. California Air Resources Board Resources Agency, Oct. 2011.
- [41] S Solomon et al. "Climate change 2007: The physical science basis, contribution of working group 1 to the fourth assessment report of the Intergovernmental Panel on Climate Change" (2007).

- [42] Chen Song et al. "Effect of hydrophobic primary organic aerosols on secondary organic aerosol formation from ozonolysis of alpha-pinene". *Geophysical Research Letters* 34.20 (Oct. 2007), p. L20803.
- [43] Ross Strader, Fred Lurmann, and Spyros N Pandis. "Evaluation of secondary organic aerosol formation in winter". *Atmospheric Environment* 33.29 (1999), pp. 4849–4863.
- [44] Michael P Tolocka et al. "Formation of Oligomers in Secondary Organic Aerosol". *Environmental Science & Technology* 38.5 (Mar. 2004), pp. 1428–1434.
- [45] Sean Twomey. "The influence of pollution on the shortwave albedo of clouds". *Journal of the atmospheric sciences* 34.7 (1977), pp. 1149–1152.
- [46] Rainer Volkamer et al. "Secondary organic aerosol formation from anthropogenic air pollution: Rapid and higher than expected". *Geophysical Research Letters* 33.17 (2006), p. L17811.
- [47] Anthony S Wexler. "Atmospheric aerosol models for systems including the ions H<sup>+</sup>, NH<sub>4</sub><sup>+</sup>, Na<sup>+</sup>, SO<sub>4</sub><sup>2-</sup>, NO<sub>3</sub><sup>-</sup>, Cl<sup>-</sup>, Br<sup>-</sup>, and H<sub>2</sub>O". *Journal of Geophysical Research* 107.D14 (2002), p. 4207.
- [48] Brent J Williams et al. "An In-Situ Instrument for Speciated Organic Composition of Atmospheric Aerosols: Thermal Desorption Aerosol GC/MS-FID (TAG)". *Aerosol Science and Technology* 40.8 (June 2006), pp. 627–638.
- [49] C S Zerefos et al. "Further evidence of important environmental information content in red-to-green ratios as depicted in paintings by great masters". *Atmospheric Chemistry and Physics* 14.6 (2014), pp. 2987–3015.

# Chapter 2

## Background and Related work

### 2.1 Representations of phase-separation in organic aerosol models

As stated in Chapter 1, the majority of regional and global models that treat PM do so by assuming a single, well-mixed organic phase. The veracity of this assumption, due to both the aforementioned thermodynamic and kinetic considerations, should be questioned. According to Hoyle et al. (2011), partitioning of biogenic oxidation products from atmospheric reactions into POA is one of the main mechanisms that anthropogenic emissions can effect biogenic aerosol. They label this added SOA mass as “eBSOA,” enhanced biogenic SOA, and has been observed in the field (e.g. Shilling et al., 2013).

Indeed, when the pseudo-ideal mixing assumption is relaxed, and organic aerosol classes are allowed (or constrained) to phase separate, it can have significant impacts on both composition and mass. Figure 2.1 demonstrates this nicely: PM 2.5 mass is modeled for the eastern US domain in two ways (B. Murphy, personal communication, 2011). In 2.1a, all OA classes—anthropogenic SOA, POA, bSOA—are considered well-mixed, while in 2.1b they form separate organic phases. The mass is  $\sim 2x$  higher for the well-mixed case. Koo, Ansari, and Pandis (2003) found a 10x mass enhancement of SOA when including POA as an absorbing material. Bowman and Karamalegos (2002) simulate phase separation between SOA and POA by exploring a range of activity coefficients for SOA in POA. For the most chemically-dissimilar SOA and POA, SOA concentrations were reduced by 45% compared to the ideal-mixing base case. Simulating the urban outflow of Mexico City, Dzepina et al. (2009) found little effect on mass when modeling all organics in a single phase versus two phases, with a 15% reduction in mass for

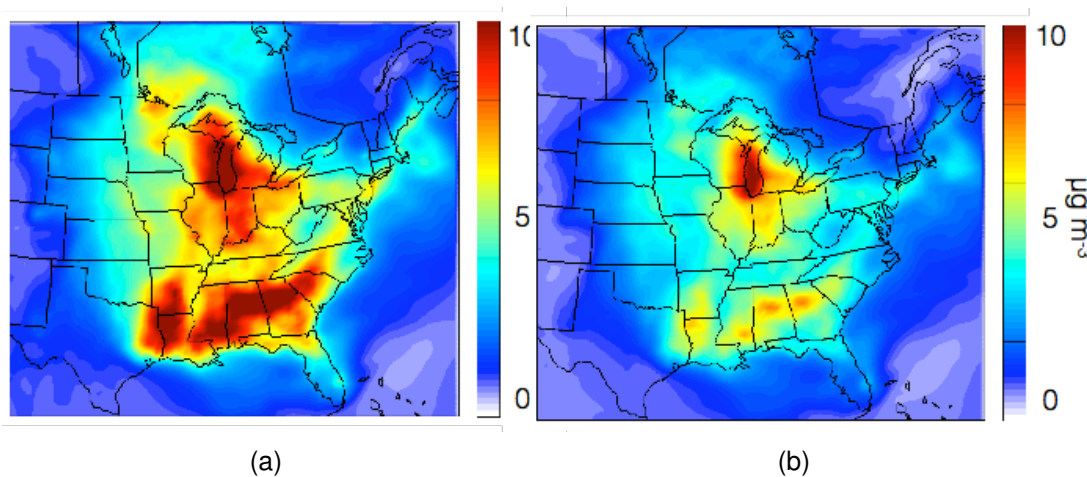


Figure 2.1: Organic aerosol mass concentration over eastern United States under two different thermodynamic treatments of different OA types: **A.** pseudo-ideal mixing, and **B.** all OA types phase separated (B. Murphy, personal communication, 2011).

three organic phases. They write that the reduction in mass quickly “self compensates,” as organics are driven into the gas-phase where they are quickly oxidized, quickly reducing the activity coefficients between the different phase-separated OA types as they converge towards similar composition.

While the preceding is not an exhaustive list of modeling studies dealing with organic-organic phase-separation, it illustrates the importance of how the condensed phase is treated, both for particle mass and composition.

## 2.2 Experimental studies of organic aerosol phase-separation

An even smaller number of studies have investigated organic phase-separation for atmospheric aerosols experimentally. One reason for this is that observing phase-separation in submicron particles is analytically challenging. Direct observations of externally-mixed populations require single-particle measurements, and phase-separation within particles requires even finer measurements. Thus, most of the studies to-date rely on indirect evidence to infer the presence or absence of multiple

phases.

Song et al. (2007) were the first to explore SOA/POA mixing using SOA yields as a proxy indicator for whether the POA mass was absorbing or not. In a typical smog chamber SOA experiment, the mass yield of OA from a gas-precursor increases with the total OA mass present, where yield is defined as the mass of SOA formed per mass of precursor reacted. This follows from equation 1.1, as the fraction of compound  $i$  in the condensed phase increases with higher  $C_{OA}$ . Song et al. (2007) found no increase in the SOA yield of  $\alpha$ -pinene + O<sub>3</sub> when hydrophobic particles (dioctyl phthalate, a surrogate for highly-reduced POA) were used as condensational surface area compared to control experiments using inorganic seed particles. In a subsequent study, using hydrophilic seed particles, Song et al. (2011) found that fulvic and adipic acid seeds showed no SOA enhancement, while citric acid did, implying that the latter formed a well-mixed solution with SOA while the others did not. In a similar SOA yield study, Hildebrandt et al. (2011) found enhanced yields of biogenic SOA (from  $\alpha$ -pinene + O<sub>3</sub>) when using anthropogenic SOA particles as seeds.

Size-distribution analysis is another means of (indirectly) inferring phase-separation in mixed-OA systems. Zelenyuk et al. (2012) use particle sphericity to infer the presence of pyrene nodules on the surface of SOA particles. Size-classified SOA, without the presence of pyrene, is spherical; but when pyrene is coated onto SOA and then classified, the particles are highly non-spherical, implying that the pyrene is not only not mixing into the SOA, but forming “islands” on the particle surface instead of a uniformly thick coating. Asa-Awuku et al. (2009) use the temporal evolution size-distributions of different mass spectral fragments to identify diesel exhaust particles dissolving into SOA in a smog chamber mixing experiment. Using fragments unique to each aerosol, the authors inferred that diesel exhaust was evaporating and then absorbing into the existing SOA particles,

through a redistribution of the diesel mass fragments across particle size.

In some of these studies (e.g. pyrene and SOA), mixing should not be expected, as the activity coefficients for each material in the other are so high that they dictate two stable phases. However, when two initially phase-separated organics are expected to collapse into a uniform mixture but don't, these studies can reveal kinetic limitations to the mixing process. When mixing "should" occur thermodynamically but does not, there are two possibilities that can significantly retard the process: 1) low volatility, and 2) condensed-phase mass transfer limitations. If the volatility of an aerosol is extremely low, the mixing timescale may be longer than the observational timescale (Marcolli et al., 2004). If volatility is not limiting the kinetics, condensed-phase mass transfer limitations can also stand in the way (e.g. low diffusivity in the particle bulk). Thus, it is extremely important to know the expected thermodynamics, to draw any conclusions about the kinetics (or visa versa).

### 2.3 Experimental & modeling studies of diffusivity in organic aerosol

It has recently been reported that SOA may exist in a highly-viscous semi-solid phase state, which may present a significant impediment to mixing. Viscosity and molecular diffusivity are related through the Stokes-Einstein relationship:

$$D = \frac{kT}{6\pi\eta r} \quad (2.1)$$

where  $D$  is diffusivity,  $k$  is Boltzmann's constant,  $T$  is temperature,  $r$  is the apparent radius of the diffusing molecule, and  $\eta$  is dynamic viscosity. Further, a characteristic time of diffusion can be calculated, according to:

$$\tau = \frac{d_p^2}{4\pi^2 D} \quad (2.2)$$

For solids, with viscosities of order  $10^{12}$  or greater, this translates to a diffusion coefficient of  $1\text{e-}21\text{ cm}^2\text{ s}^{-1}$  and timescales of months for a 100 nm particle (Koop et al., 2011). While viscosity of particles is in itself interesting, the diffusion coefficient is the fundamental quantity of interest to mixing. Obviously, such timescales would make the mixing process irrelevant to the real atmosphere where particles have a lifetime on the order of a week.

Recently, there has been a spate of research related to particle viscosity and diffusivity. Qualitatively, particle bounce has been used to infer a solid (and thus highly viscous) phase-state for SOA (Virtanen et al., 2010; Saukko, Kuuluvainen, and Virtanen, 2012), with increasing bounce for more oxidized particles (Saukko et al., 2012). Slow evaporation of SOA in vapor-free experiments have been used to infer diffusive limitations within particle bulk (Zelenyuk et al., 2012; Abramson et al., 2013), though other studies suggest that observed slow evaporation could instead be the result of low-volatility (Saleh, Donahue, and Robinson, 2013) and should not be conflated with condensed-phase mass transfer limitations. Other techniques, such as the particle “poke-flow” (Renbaum-Wolff and Grayson, 2013) and partitioning studies (Perraud et al., 2012), have also concluded that diffusive limitations in particles may lead to extremely long mixing timescales.

Very few of these studies provide quantitative estimates of the diffusion coefficient. For SOA particles (from the canonical  $\alpha$ -pinene +  $\text{O}_3$  system), the literature values range from  $10^{-19}\text{ m}^2\text{ s}^{-1}$  (Zhou et al., 2013) to  $10^{-23}\text{ m}^2\text{ s}^{-1}$  (Renbaum-Wolff and Grayson, 2013). These translates to a range of diffusion timescales spanning minutes to years. Further work is clearly needed to address this discrepancy.

## Bibliography

- [1] Evan Abramson et al. “Experimental determination of chemical diffusion within secondary organic aerosol particles”. *Physical Chemistry Chemical Physics* 15.8 (2013), p. 2983.
- [2] A Asa-Awuku et al. “Mixing and phase partitioning of primary and secondary organic aerosols”. *Geophysical Research Letters* 36.15 (Aug. 2009).
- [3] Frank M Bowman and Ana M Karamalegos. “Estimated Effects of Composition on Secondary Organic Aerosol Mass Concentrations”. *Environmental Science & Technology* 36.12 (June 2002), pp. 2701–2707.
- [4] Katja Dzepina et al. “Evaluation of recently-proposed secondary organic aerosol models for a case study in Mexico City”. *Atmospheric Chemistry and Physics* 9.15 (2009), pp. 5681–5709.
- [5] Lea Hildebrandt et al. “Evaluating the Mixing of Organic Aerosol Components Using High-Resolution Aerosol Mass Spectrometry”. *Environmental Science & Technology* 45.15 (Aug. 2011), pp. 6329–6335.
- [6] C R Hoyle et al. “A review of the anthropogenic influence on biogenic secondary organic aerosol”. *Atmospheric Chemistry and Physics* 11.1 (2011), pp. 321–343.
- [7] Bonyoung Koo, Asif S Ansari, and Spyros N Pandis. “Integrated approaches to modeling the organic and inorganic atmospheric aerosol components”. *Atmospheric Environment* 37.34 (Nov. 2003), pp. 4757–4768.
- [8] Thomas Koop et al. “Glass transition and phase state of organic compounds: dependency on molecular properties and implications for secondary organic aerosols in the atmosphere”. *Physical Chemistry Chemical Physics* 13.43 (2011), p. 19238.
- [9] C Marcolli et al. “Internal mixing of the organic aerosol by gas phase diffusion of semivolatile organic compounds”. *Atmospheric Chemistry and Physics* 4.11/12 (2004), pp. 2593–2599.
- [10] V. Perraud et al. “Nonequilibrium atmospheric secondary organic aerosol formation and growth”. *Proceedings of the National Academy of Sciences* 109.8 (2012), pp. 2836–2841.
- [11] L Renbaum-Wolff and J W Grayson. “Viscosity of alpha-pinene secondary organic material and implications for particle growth and reactivity”. *Proceedings of the ...* 2013.
- [12] Rawad Saleh, Neil M Donahue, and Allen L Robinson. “Time Scales for Gas-Particle Partitioning Equilibration of Secondary Organic Aerosol Formed from Alpha-Pinene Ozonolysis”. *Environmental Science & Technology* (May 2013), p. 130517130052009.

- 
- [13] E Saukko, H Kuuluvainen, and A Virtanen. "A method to resolve the phase state of aerosol particles". *Atmospheric Measurement Techniques* 5.1 (2012), pp. 259–265.
- [14] E Saukko et al. "Humidity-dependent phase state of SOA particles from biogenic and anthropogenic precursors". *Atmospheric Chemistry and Physics* 12.16 (2012), pp. 7517–7529.
- [15] J E Shilling et al. "Enhanced SOA formation from mixed anthropogenic and biogenic emissions during the CARES campaign". *Atmospheric Chemistry and Physics* 13.4 (2013), pp. 2091–2113.
- [16] Chen Song et al. "Effect of Hydrophilic Organic Seed Aerosols on Secondary Organic Aerosol Formation from Ozonolysis of  $\alpha$ -Pinene". *Environmental Science & Technology* 45.17 (Sept. 2011), pp. 7323–7329.
- [17] Chen Song et al. "Effect of hydrophobic primary organic aerosols on secondary organic aerosol formation from ozonolysis of alpha-pinene". *Geophysical Research Letters* 34.20 (Oct. 2007), p. L20803.
- [18] Annele Virtanen et al. "An amorphous solid state of biogenic secondary organic aerosol particles". *Nature* 467.7317 (Oct. 2010), pp. 824–827.
- [19] Alla Zelenyuk et al. "Synergy between Secondary Organic Aerosols and Long-Range Transport of Polycyclic Aromatic Hydrocarbons". *Environmental Science & Technology* 46.22 (Nov. 2012), pp. 12459–12466.
- [20] Shouming Zhou et al. "Kinetic limitations in gas-particle reactions arising from slow diffusion in secondary organic aerosol". *Faraday Discussions* 165 (2013), p. 391.

# Chapter 3

## Organic Aerosol Mixing Observed by Single-Particle Mass Spectrometry

*We present direct measurements of mixing between separately prepared organic aerosol populations in a smog chamber using single particle mass spectra from the High-Resolution Time-of-Flight Aerosol Mass Spectrometer (HR-ToF-AMS). Docosane and  $D_{46}$ -docosane (22 carbon linear solid alkane) did not show any signs of mixing, but squalane and  $D_{62}$ -squalane (30 carbon branched liquid alkane) mixed on the timescale expected from a condensational-mixing model. Docosane and  $D_{46}$ -docosane were driven to mix when the chamber temperature was elevated above the melting point for docosane. Docosane vapors were shown to mix into  $D_{62}$ -squalane, but not the other way around. These results are consistent with low diffusivity in the solid phase of docosane particles. We performed mixing experiments on secondary organic aerosol (SOA) surrogate systems finding that SOA derived from  $d8$ -toluene (a surrogate for anthropogenic SOA (aSOA)) does not mix into squalane (a surrogate for hydrophobic primary organic aerosol (POA)), but does mix into SOA derived from  $\alpha$ -pinene (a biogenic SOA (bSOA) surrogate). For the aSOA/POA, the volatility of either aerosol does not limit gas-phase diffusion, indicating that the two particle populations do not mix simply because they are immiscible. In the aSOA/bSOA system, the presence of  $d8$ -toluene derived SOA molecules in the  $\alpha$ -pinene derived SOA provides evidence that the diffusion coefficient in  $\alpha$ -pinene derived SOA is high enough for mixing on the timescale of 1 minute. The observations from all of these mixing experiments are generally invisible to bulk aerosol composition measurements, but are made possible with single-particle composition data.*

---

This chapter was originally published as Robinson, Saleh, and Donahue, 2013

### 3.1 Introduction

We care about fine particles (aerosol) in the atmosphere for three main reasons: they kill people, they have strong but uncertain climate effects, and they can make it very hard to see. Fine particles are central to three of the top 10 leading causes of mortality in the global burden of disease (Lozano et al., 2013), and roughly 50,000 people per year die in the US from inhalation of excessive levels of fine particles in ambient air (Pope, Ezzati, and Dockery, 2009). The aerosol indirect effect couples particles to climate via cloud droplet numbers (Twomey, 1977; Albrecht, 1989). The associated changes to cloud droplet number, and thus cloud albedo, from pre-industrial times are one of the largest climate forcing uncertainties (Solomon et al., 2007). Additionally, direct scattering of light by fine particles also has a significant climate effect. Finally, haze is simply difficult to see through. By obscuring the horizon it poses a threat to pilots; this may have been the cause of the small plane crash that claimed the lives of John F. Kennedy Jr and his companions in 1999 (Showstack, 2000).

Aerosol is a suspension of particles and vapor, and tropospheric aerosol is a complex mix of inorganic and organic components whose physical and chemical characteristics depend strongly on source, location, and atmospheric age, among many other factors (Jimenez et al., 2009). The organic fraction, which comprises a large percentage of aerosol mass, between 20-90% (Kanakidou et al., 2005), is poorly understood relative to the inorganic fraction. Organic species in atmospheric aerosol cover a wide range of molecular weights, polarities, and volatilities (Goldstein and Galbally, 2007). Due to the large number and variety of molecules in tropospheric organic aerosol (OA), thermodynamic predictions of individual equilibrium vapor pressures and miscibilities in this complex mixture are for practical purposes impossible.

The partitioning of organic constituents plays a crucial role in determining the chemical composition and physical characteristics of particles, as well as the evolving gas-phase chemistry, an important mechanism for chemical aging in OA (Donahue et al., 2011). Whether there exists a single organic phase or multiple organic phases should have dramatic consequences for the partial pressures of any organic molecules in the system, as species in a mixture have greatly reduced equilibrium vapor pressures compared to their pure reference phase, via Raoult's Law. Thus it is extremely important in predictions of aerosol mass and composition to know how many organic phases are present in aerosol systems found in the atmosphere.

Most regional-scale modeling studies assume an internally-mixed aerosol. This assumption means that all particles of the same size have the same composition. Furthermore, if models treat semi-volatile organics, most assume that those organics form a single phase, which is typically treated as distinct from a second inorganic (sometimes called aqueous) phase. That organic condensed phase is assumed to be in equilibrium with the gas phase. Implicit in this assumption is that diffusion into the condensed organic phase is fast compared to gas-phase diffusion. Recent experimental studies call into question whether this can be true (Renbaum-Wolff and Grayson, 2013; Vaden et al., 2011; Perraud et al., 2012), and thus whether an internally-mixed aerosol can be assumed for atmospheric models. The process of mass exchange between two organic aerosol populations can shed light on the diffusion timescales within aerosol particles. If mixing is observed on a rapid timescale, then, unambiguously, significant diffusion limitations are not present in the system. Conversely, when mixing does not occur, it may point to mass transfer barriers, including, but not limited to, low condensed-phase diffusivity.

In this work, we describe experimental techniques for performing aerosol mixing experiments, and demonstrate the use of single-particle mass spectrometry

for determining whether two aerosol populations mix. This technique is applied first to mixing experiments between single-component aerosol populations that cleanly demonstrate both the vapor pressure-driven mixing process, as well as observations of phase-separation in OA systems. The technique is then applied to atmospherically-relevant mixing situations, to determine the mixing behavior between biogenic secondary organic aerosol (SOA) with both anthropogenic SOA and primary organic aerosol (POA).

### **3.2 Background**

There have been numerous studies experimentally addressing the question of whether mixed-OA systems have single or multiple phases. A wide range of conclusions has been drawn from those studies about general particle behavior in the atmosphere based either on explicit modeling of the results or on inferences invoked to explain discrepancies between expectations and observations. Song et al. (2007) used yield data from SOA formation on organic seed particles to infer whether there was a single organic phase, or a core-shell phase-separated morphology in their smog chamber experiments. They concluded that SOA derived from  $\alpha$ -pinene oxidation did not mix with dioctyl phtalate (DOP). Hildebrandt et al. (2011) used a similar experimental design to conclude that SOA from  $\alpha$ -pinene oxidation and SOA from toluene oxidation do mix to form a single phase. Vaden et al. (2010), using the more direct method of single-particle mass spectrometry, observed phase separation in an  $\alpha$ -pinene SOA/DOP system. Asa-Awuku et al. (2009) found that initially phase-separated SOA from  $\alpha$ -pinene oxidation and diesel exhaust OA collapsed into a single organic phase in a smog chamber experiment, inferred from size-distribution measurements of tracer fragments in the High-Resolution Time-of-Flight Aerosol Mass Spectrometer (HR-ToF-AMS). Using a thermodenuder, Cappa and Wilson (2011) identified lubricating oil particles

coated with  $\alpha$ -pinene SOA as a two-phase system, having “side-by-side” morphologies.

Most of the OA mixing studies described above relied on inference to identify the number of organic phases present, with the exception of Vaden et al.’s single-particle measurements. Observing sub-micron phase separation directly is analytically very challenging, but the measurements are of utmost importance. Measuring OA mixing is highly related to another research question as well, regarding the condensed-phase diffusivity of molecules in OA particles. Recent research has questioned whether the dynamics of OA mixing would allow it to take place on atmospheric timescales, even when the constituents favor a single phase at equilibrium (Vaden et al., 2011; Koop et al., 2011; Perraud et al., 2012). If OA exists as a glassy solid, with a high internal viscosity and low internal molecular diffusivity, the timescale for mixing might be long relative to the average atmospheric lifetime of an OA particle. Thus, any observations of OA mixing are potentially related to the phase state of OA particles as well.

Two processes can move material between organic particles: coagulation and condensation (gas-phase diffusion). Coagulative mixing is straight-forward: as shown in Figure 3.1a, the collision between two different particles (yellow and purple) will result in one “new” particle with a mixed composition. This new particle will of necessity be larger than either of the two original particles. However, at the number concentrations of the experiments we shall describe here (as well as much of the atmosphere), coagulation is not a significant mixing process. If the aerosol is semi-volatile, then condensational mixing must be considered as well. When semi-volatile organics are associated initially with two different particle populations that are later brought together, if those compounds favor a single condensed phase at equilibrium they will tend to mix within every particle across both (initially dissimilar) populations (Marcolli et al., 2004). This “Marcolli mixing” occurs through gas-phase

diffusion, and could rapidly blur the distinction between particles emitted from various organic-rich sources (wood burning, vehicles, cooking, etc) while at the same time redistributing secondary organics among the particle population.

Mixing can mean many things for particles. Particle populations can be said to be “well mixed” if particles have similar compositions, and particles of the same size are “internally mixed” if their compositions are all identical. However, well-mixed particle populations can still contain particles with complex morphologies and multiple distinct phases in each particle. A common example is the existence of distinct “organic” and “aqueous” phases (liquid-liquid phase separation) for particles containing organic compounds that are not above some critical oxidation threshold (Smith, Bertram, and Martin, 2012; Bertram et al., 2011; Marcolli and Krieger, 2006).

Here we are interested in the mixing of different organic constituents within and among particles. Many organic compounds associated with aerosols are thought to be semi volatile, meaning significant fractions are found in both the condensed and vapor phases at equilibrium (Donahue et al., 2006; Robinson et al., 2007; Odum et al., 1996) This applies to both SOA (Presto and Donahue, 2006) and POA (Grieshop et al., 2009). SOA is often initially formed via gas-phase oxidation and subsequent condensation of oxidation products to particles (Kroll et al., 2009); thus whether or not different secondary compounds form a single phase at equilibrium, they will tend to wind up on all particles present when they are being formed.

Exp.	10 m <sup>3</sup> Smog Chamber	100 L Sample Bag	Mixing?
1	Docosane	d46-Docosane	N
2	d46-Docosane	Docosane	Y (w/ heating)
3	SOA (d8-Toluene + OH, AS seed)	Squalane	N
4	d62-Squalane	Squalane	Y
5	—	SOA ( $\alpha$ -Pinene + O <sub>3</sub> )	—
6	SOA (d8-Toluene + OH, AS seed)	SOA ( $\alpha$ -Pinene + O <sub>3</sub> )	Y

Table 3.1: List of mixing experiments

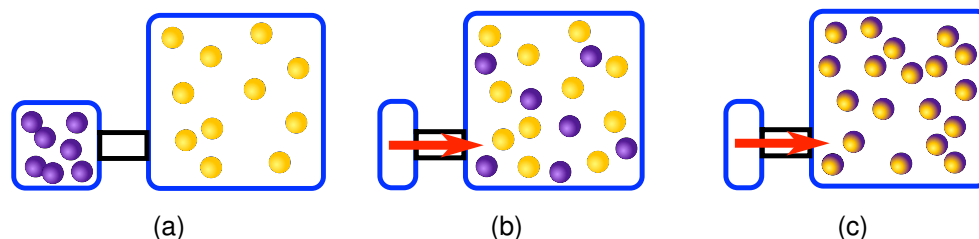


Figure 3.1: Schematic for mixing experiments. **(A)** Aerosol populations are prepared in separate chambers prior to the mixing event. Extreme cases of mixing behavior, where the two populations exist as completely **(B)** separate phases (no mixing), or **(C)** the two populations mix via gas-phase exchange (complete mixing).

### 3.3 Methods

#### 3.3.1 Overview of environmental chamber mixing experiments

We conducted a series of mixing experiments, all following a common design depicted in Figure 3.1. Experimental details are listed in Table 3.1. For each mixing experiment, two aerosol populations were prepared separately, each in a chamber isolated from the other. As shown in Figure 3.1a, one aerosol population was formed in a 100-L teflon sample bag, and the other was formed in a 10 m<sup>3</sup> teflon chamber. This is similar to the procedure used by Asa-Awuku et al. (2009) and different from other SOA mixing studies where there is some sort of sequential aerosol preparation in the same volume (Song et al., 2007; Hildebrandt et al., 2011). This accomplished the following goals: first, in the case of SOA, the SOA precursor was given enough time to completely react with its oxidation source prior to the event of mixing. Second, all aerosols, both pure-component and SOA, were given time to reach thermodynamic equilibrium so that they were no longer growing by condensation. Only after each population was determined to be in equilibrium were the contents of the smaller chamber transmitted (via compression) into the larger chamber. Further changes in the system after this transfer can thus be attributed to mixing.

In all experiments presented here, one of the aerosol sources (either the pure-component aerosol or the SOA precursor) was prepared from a fully-deuterated compound. This ensures separability in the mass spectra between the two organic aerosols in each mixing experiment, and provides unique tracer mass fragments that can be used to determine the source of any particle. Hildebrandt et al., 2011

### 3.3.2 Aerosol preparation

Aerosol preparation and characterization procedures used in this study are similar to those used in previous smog-chamber experiments conducted at Carnegie Mellon University (CMU) (Weitkamp et al., 2007). Prior to each experiment, all chambers were flushed continuously for >12 hours with clean, dry air (cleaned with HEPA, silica-gel, and activated-carbon filters in series) to ensure low background particle, organic vapor, and water concentrations. All experiments were performed at low (<5%) relative humidity and room temperature (298K). Background particle concentrations were less than 10 particles  $\text{cm}^{-3}$  for each experiment.

SOA was formed by either the ozonolysis of  $\alpha$ -pinene or the photo-oxidation of deuterium-substituted toluene ( $\text{D}_8$ -toluene) with added OH.  $\alpha$ -Pinene SOA was formed in the 100-L chamber by injecting a liquid aliquot of the precursor into a heated tube fit with an air-tight septum. Clean, dry air carried the vaporized  $\alpha$ -pinene into the 100-L chamber, which was previously charged with excess ozone. No seed particles were used in the  $\alpha$ -pinene SOA experiments because the nucleated particles reached a sufficient size (vacuum aerodynamic diameter ( $D_{va}$ ) >180 nm) to be seen with the light scattering laser in the AMS. For  $\text{D}_8$ -toluene SOA formation, nitrous acid (HONO) was used as an OH source for photo-oxidation.  $\text{D}_8$ -toluene was added to the 10  $\text{m}^3$  chamber using a septum injector, and swept into the chamber with clean, dry air. HONO was added to the chamber by bubbling filtered air through a nitrous acid solution for 15 minutes. Ultraviolet lights

were turned on to initiate D<sub>8</sub>-toluene photo-oxidation, but were turned off prior to the mixing event to cease OH production. Ammonium sulfate seeds were used for all D<sub>8</sub>-toluene SOA experiments to provide surface area for condensable organic vapors. Initial ammonium sulfate concentrations for experiments with seed particles were 2,000 cm<sup>-3</sup> and had a count median diameter of approximately 100 nm. This ensured that D<sub>8</sub>-toluene SOA particles would be large enough for detection by the light scattering module. Seed particles were generated through atomization of 1 g/L (NH<sub>4</sub>)<sub>2</sub>SO<sub>4</sub> solution, followed by a silica-gel diffusion dryer and a 2 mC neutralizer before the particles entered the chamber.

Pure-component organic particles were prepared by flash vaporization. A small, resistive metal heater enclosed in a stainless-steel sheath was used to flash the organic material into the chamber, where aerosol particles were formed by homogenous nucleation. To perform this flash vaporization, an aliquot of the organic material was placed on the stainless steel surface before the heater was inserted into the chamber on the end of a long tube. With a flow of clean, dry dispersion air used to mix the chamber, the heater was power-cycled until the organic material completely evaporated. The resulting vapor plume cooled rapidly via mixing in the chamber, developing a sufficient supersaturation to drive nucleation and rapid growth of pure particles.

### 3.3.3 Measurement suite for mixing Experiments

Ensemble particle volume and number concentrations were measured with a Scanning Mobility Particle Sizer (SMPS, TSI classifier model 3080, CPC model 3772 or 3010). Ensemble particle composition and mass were measured with a High-Resolution Time-of-Flight Aerosol Mass Spectrometer (HR-ToF-AMS) operated in the single-reflection V-mode. Single-particle mass spectra were taken with an HR-ToF-AMS operated in Light Scattering Single Particle (LSSP) mode. The experi-

mental setup for these studies is shown in Figure 3.2. We discuss briefly the use of LS-mode for this application below.

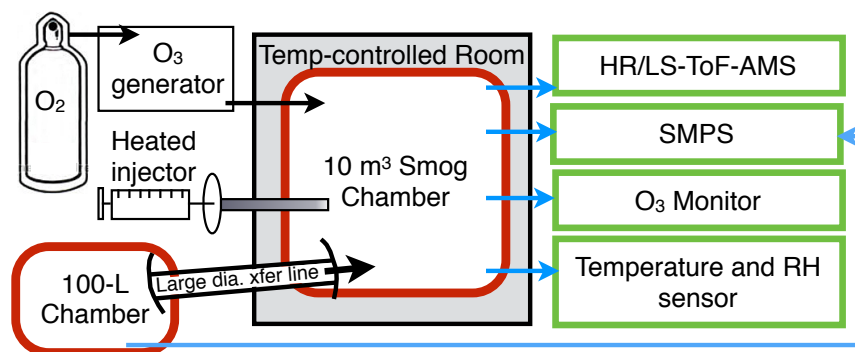


Figure 3.2: Experimental setup for mixing experiments. Blue outlines show measurement suite, red outlines show the two-chamber design, and black outlines show chamber inputs. In some experiments, a flash vaporizer (not shown in this picture) was used for aerosol formation instead of the heated injector.

### 3.3.4 Operation of HR-ToF-AMS in single-particle mode

Single particle mass spectra for particles with  $D_{va}$  greater than 180 nm were acquired by operating the HR-ToF-AMS in LSSP mode. For all experiments, the HR-ToF-AMS was operated according to the following procedure: The HR-ToF-AMS alternated between V-mode, which provides ensemble average mass spectra (MS) and size-resolved composition data (PToF, particle time of flight), and LSSP-mode, which provides single-particle sizing and composition information, for 60s each.

The construction and operation of the light scattering module for the ToF-AMS has been fully described elsewhere (Cross et al., 2009; Liu et al., 2013). Briefly, the instrument consists of a continuous-wave laser (405 nm, 50-mW; CrystaLaser, LC BCL-050-405) that crosses the collimated particle beam at a right angle within the time-of-flight region of the instrument. During LSSP and PToF operation, a chopper at just after the aerosol lens constitutes the beginning of the PToF region. During the large majority of chopper cycles, either zero or one particle traverses the

PToF region. In LSSP-mode, scattered light from sampled particles is collected by an ellipsoidal mirror with one focus at the particle-laser intersection point and the other at the photocathode of a photomultiplier tube. The scattering signal provides two important pieces of information: first, pulse timing measures the flight time between the chopper and the laser providing the particle vacuum aerodynamic diameter. Second, the pulse also triggers the collection of individual mass spectra over the entire chopper cycle. This is necessary because data cannot be acquired and processed continuously and triggering on light scattering reduces the data rate to a manageable load.

Data from LSSP-mode were processed using custom software.<sup>1</sup> The software classifies particles based on how they interact with the vaporizer, sorting particles into “prompt,” “delayed,” and “null” events. Prompt particles are operationally defined as those particles whose signal arrives within 20% of the predicted time based on the velocity calculated from the chopper-to-laser distance and the measured light scattering pulse. Delayed particles are all particles whose MS signals deviate by more than 20% of the predicted arrival time, and null particles are those with a scattered light signal but no (below threshold) detectable MS signal (Liu et al., 2013).

We used the following parameters for data processing: a scattering threshold (signal-to-noise) of five to reject events with low scattered light intensity (Liu et al., 2013), and an operationally-defined MS threshold of 15 collected ions for each particle to be considered for MS analysis. Before sorting particles into “prompt,” “delayed,” and “null” events. Our results were not sensitive to our MS threshold, though it should be noted that this value is in-between the two MS thresholds used in Liu, et al (Liu et al., 2013) (6 ions for CE calculations, and 40 ions for clustering).

---

<sup>1</sup>Sparrow 1.04A, written by D. Sueper, Aerodyne Research Inc. and University of Colorado at Boulder; available at <http://cires.colorado.edu/jimenez-group/ToFAMSResources/ToFSoftware/index.html>Analysis4

Particle coincidence—i.e. multiple particles entering the ToF region of the instrument per chopper cycle—at the number concentrations of these experiments was minimal, but can be identified from the scattered light signal. All coincident particles were filtered by the software, and not considered in the analysis.

Our analysis and separation of single particle mass spectra relies on using the cosine similarity between two vectors (each of which represent a mass spectrum):

$$\cos(\theta) = \frac{\vec{A} \cdot \vec{B}}{\|\vec{A}\| \|\vec{B}\|} \quad (3.1)$$

This correlation coefficient ranges from zero to one, where values close to one represent vectors with a small angle between them, or a high degree of similarity. Values close to zero represent vectors with a high angle of separation and low similarity. For the mass spectra of single particles, this quantity reflects whether particles in an ensemble are chemically similar to a chosen reference spectrum (or not). We have selected chemicals for our mixing experiments that exploit the use of cosine similarity. Because there exists a high degree of separability between isotopically- and non-labeled aerosol, (Hildebrandt et al., 2011) cosine similarity is able to completely segregate into groups the different particles in these mixing experiments.

## 3.4 Results and Discussion

### 3.4.1 Observations of external mixtures

The mixing behavior between aerosol populations of docosane (prepared in the 10 m<sup>3</sup> smog chamber) and D<sub>46</sub>-docosane (prepared in the 100-L sample bag) is shown in Figure 3.3a. The top panel of Figure 3.3 shows the time series for two tracer mass spectral fragments unique to each type of particle: *m/z* 50 (C<sub>3</sub>D<sub>7</sub><sup>+</sup>) for D<sub>46</sub>-docosane and *m/z* 43 fragment (C<sub>3</sub>H<sub>7</sub><sup>+</sup>) for docosane. All measurements were

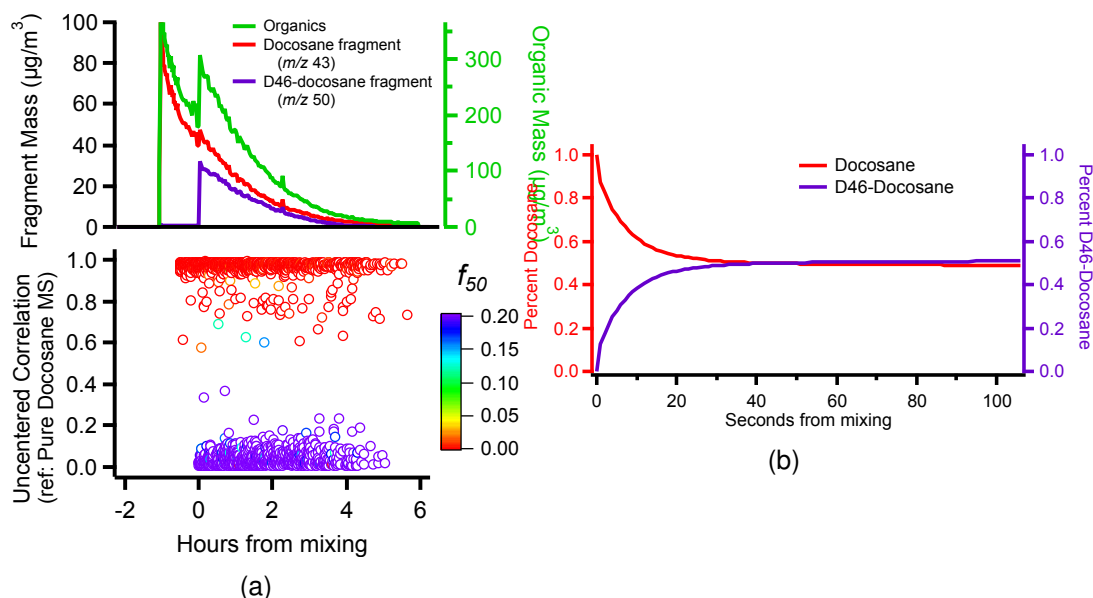


Figure 3.3: Time-evolution of mixing state between aerosol populations of docosane and  $D_{46}$ -docosane. **(A)** Top panel shows the time-series of marker mass spectral fragments  $m/z$  43 (docosane) and  $m/z$  50 ( $D_{46}$ -docosane), and the total organic mass from the time of the mixing event from the HR-ToF-AMS running in V-mode. Bottom panel shows uncentered correlation coefficients for all prompt single-particle mass spectra. Reference mass spectrum is  $D_{46}$ -docosane. The plot shows two chemically distinct populations that do not mix after 5 hours of being in the same chamber. **(B)** Simulation of condensational mixing between docosane/ $D_{46}$ -docosane, showing the mass fraction of each compound in the initially-docosane particle population versus time.

from the  $10 \text{ m}^3$  smog chamber (the “mixing chamber”). Roughly one hour before mixing the two populations, docosane particles were formed in the mixing chamber via flash vaporization, shown by appearance of  $m/z$  43 in the top panel of Figure 3.3a.  $D_{46}$ -docosane particles were then introduced into the mixing chamber from the smaller bag, shown by the appearance of  $m/z$  50. The particles were then left undisturbed in the mixing chamber for five hours.

The bottom panel of Figure 3.3a shows the correlation coefficient of each prompt single-particle MS compared to the reference spectrum of  $D_{46}$ -docosane, plotted as a function of time, calculated using equation 3.1. Particles are colored by the fraction of a tracer ion to the total ion number according to the following

equation:

$$f_{m/z_i} = \frac{\# \text{ of ions at } m/z_i}{\text{total } \# \text{ of ions}} \quad (3.2)$$

(e.g.  $f_{43}$  = # of ions at  $m/z$  43 / total # of ions for a single-particle). Only particles with 150 ions or more are shown on this plot for clarity, though this filter does not affect our result. Prior to mixing, the particles all have very low correlation coefficients. At  $t = 0$ , a new population of particles is visible, with very high correlation to the  $D_{46}$ -docosane reference. Two very distinct populations remain present in the chamber until the end of the experiment. All mixing experiments follow this same experimental and presentation scheme.

There were no changes in the correlation coefficients of the two populations, meaning that no significant mixing occurred. Similarly, when we manually separate the two groupings and look at their average mass spectra at the end of the experiment (Figure 3.4), there are no changes with time; no marker fragments from either aerosol are seen in the other grouping's mass spectra.

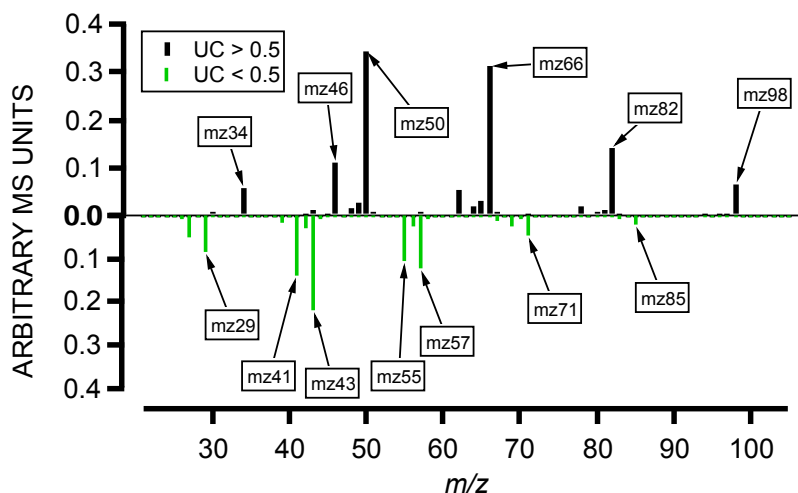


Figure 3.4: Average mass spectra for each particle population at  $t=4$  hours that shows particles with uncentered correlation (UC) coefficient  $>0.5$  are initially pure  $D_{46}$ -docosane, and particles with  $UC < 0.5$  are initially pure docosane. The mass spectra of each population has almost no fragments in common with the other.

Figures 3.3 and 3.4 are empirical evidence that coagulation is not a significant mixing process in these experiments. However, we ran simulations to confirm this assertion: using a sectional coagulation model, we compared the amount of particles coagulating into a given size bin with the total number of particles in that bin as a function of time. Figure 3.5 shows this comparison using particle size-distribution data from the docosane/D<sub>46</sub>-docosane experiment. The number of particles coagulating into the bin is so small compared to the total number of particles in the bin, that coagulation can be ignored as a significant mixing process. This is confirmed by the complete lack of any significant evolution in the mass spectra for the two populations during this experiment. This is true for the rest of the experiments presented as well, which have similar number concentrations.

That docosane and D<sub>46</sub>-docosane do not show mixing is perhaps surprising. The docosane/D<sub>46</sub>-docosane system should have near ideal-solution behavior, as the two constituents are functionally identical. Mixing is thus driven purely by entropy. We have simulated this experiment using a coupled aerosol- and gas-phase model, which is presented in Figure 3.3b. The timescale for condensational mixing for docosane, assuming ideal mixing with D<sub>46</sub>-docosane and no condensed-phase barriers to mass transfer, should be on the order of minutes. The saturation concentration of solid docosane at  $T = 293.15$  K is estimated to be  $C^{sat} = 25 \mu\text{g m}^{-3}$  for the conditions of these experiments (Pankow and Asher, 2008).

We hypothesize that the mixing barrier in this case is either low molecular diffusivity in the condensed phase or low mass accommodation, due to the solid phase of docosane (and D<sub>46</sub>-docosane) at the temperature of this experiment. Accommodation coefficients,  $\alpha$ , of several orders of magnitude below unity have been reported for crystalline solids (Somorjai and Lester, 1967). In fact,  $\alpha \leq 10^{-4}$  is required to explain the observation here. To test this hypothesis, the experiment was repeated with an additional step where the smog chamber temperature was in-

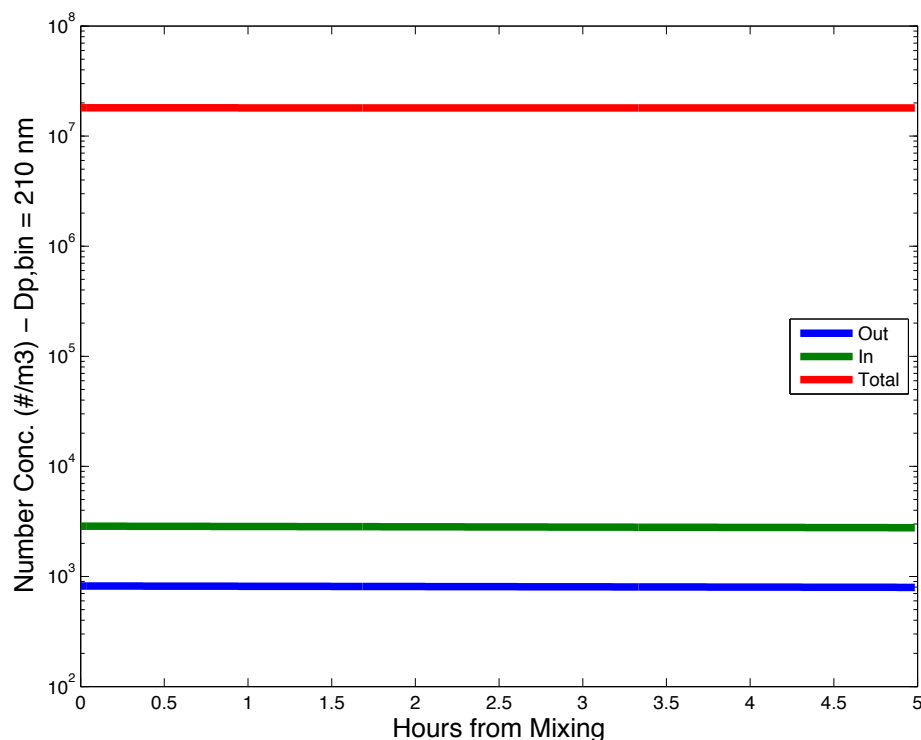


Figure 3.5: Simulated time series of number concentration for SMPS size bin with midpoint  $D_p=210$  nm for docosane/ $D_{46}$ -docosane mixing experiment. Figure shows the total number of particles in the given size bin (red), and the number of particles coagulating both into (green) and out of the size bin (blue) as a function of time from the mixing event. Because the number of particles moving to and from the size bin is small compared to the total number of particles, coagulation is shown to be of minimal importance as a mixing process for the number concentrations of these experiments.

creased from 25 °C to 46 °C two hours after the mixing event. The melting point of docosane is 44 °C. Figure 3.6 shows a sharp transition from two separate particle populations to a single population of mixed composition when the smog chamber reaches its maximum temperature. While the entropic driving force is high for vapors of one compound to condense into particles of the other in both of these experiments, the solid phase makes the particles unavailable to accept vapors on the timescale of the experiment. The same barrier is not present when the particles are liquid, and in this case we do see mixing. These data emphasize the value of

single-particle composition data, as this result would otherwise have been invisible to bulk composition measurements.

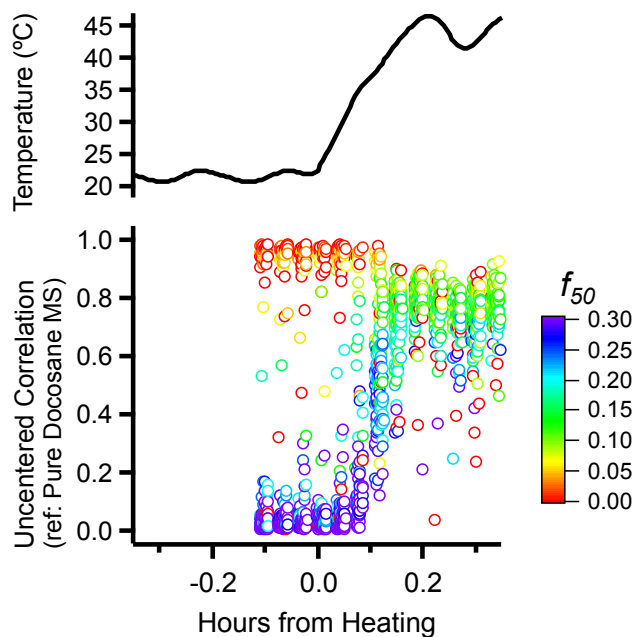
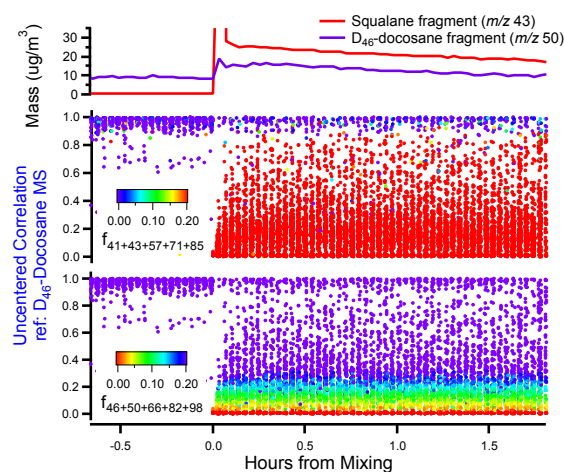
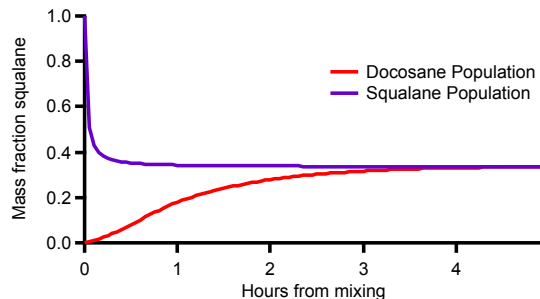


Figure 3.6: Time-evolution of mixing between docosane and  $D_{46}$ -docosane with smog chamber heating. With the increase of temperature at  $t = 0$  the two distinct populations rapidly mix into a single phase.

We also validated this hypothesis with a mixing experiment between squalane and  $D_{46}$ -docosane (presented in Figure 3.7).  $D_{46}$ -docosane particles were prepared initially in the larger smog chamber, and squalane particles were moved from the 100-L bag into the smog chamber to initiate the mixing experiment.  $D_{46}$ -docosane vapors were taken up rapidly at 25 °C by squalane particles, which presented no diffusion limitation to absorption due to their liquid phase-state. Squalane vapors were not observed to move into the solid docosane particles even though our condensational-mixing model predicts that they should if the accommodation coefficient were high (see Figure S4). This further supports our conclusion that docosane is volatile enough to mix through the gas phase under typical ambient conditions, but that mass transfer or diffusion limitations prevent solid docosane



(a)



(b)

Figure 3.7: Time-evolution of mixing state between aerosol populations of squalane and  $D_{46}$ -docosane. **(A)** Top panel shows the single-particle data colored by the fraction of the sum of prominent marker fragments for each pure component. Prominent squalane fragments are the colorscale for the middle panel, while prominent  $D_{46}$ -docosane markers are the colorscale for the bottom panel. Reference mass spectrum is  $D_{46}$ -docosane. The data show squalane absorbing material from  $D_{46}$ -docosane, but not the other way around. **(B)** Simulation of squalane/ $D_{46}$ -docosane condensational mixing, showing the mass fraction of squalane in each particle population versus time.

particles from absorbing molecules from the gas phase.

We also observe a persistent external mixture in a similar mixing experiment between SOA formed via oxidation of  $D_8$ -toluene (Hildebrandt et al., 2011) and pure squalane particles, the results of which are shown in Figure 3.8. Both of these aerosol types are often used as atmospheric surrogates in smog chamber studies. SOA formed from toluene oxidation SOA is commonly used as a laboratory sur-

rogate for anthropogenic SOA (Pandis et al., 1992), while squalane is extremely low vapor pressure oil, and is used to represent hydrophobic POA (Song et al., 2007). Because the liquid squalane particles will take up vapors rapidly if thermodynamics favors it (as with docosane), this suggests that the limitation comes from the toluene-derived SOA. Either the SOA simply has very low volatility and thus no vapors to add to the squalane particles, or mixing is simply not favored.

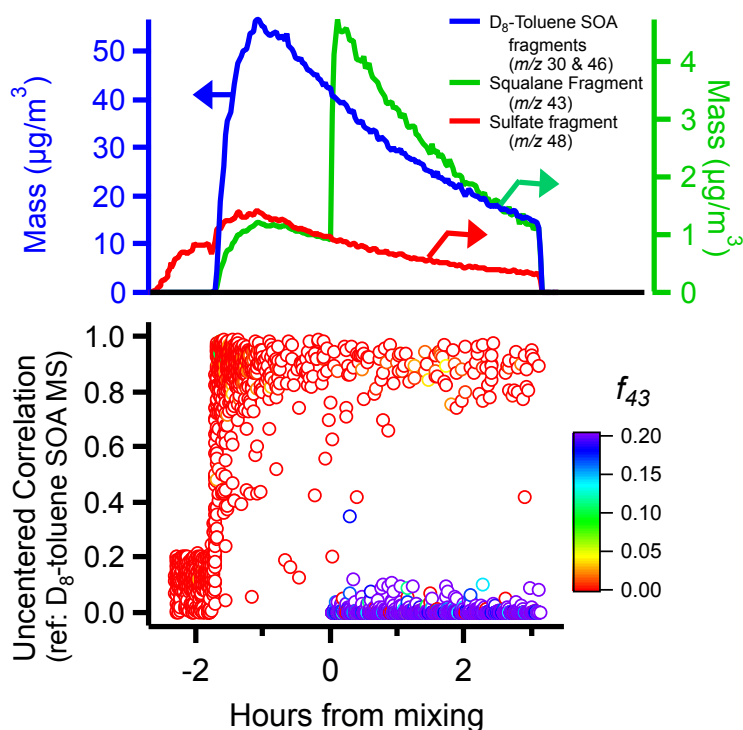


Figure 3.8: Time-evolution of mixing state between aerosol populations of squalane and D<sub>8</sub>-toluene secondary organic aerosol with single particle data colored by  $f_{43}$ . Reference mass spectrum is D<sub>8</sub>-toluene SOA. The two particle populations remain distinct over the course of the experiment.

The correlation coefficients (reference D<sub>8</sub>-toluene SOA) for the two populations remain completely segregated hours after they are combined, meaning there is no significant mixing between the two condensed phases (bottom panel of Figure 3.8). Note also that the correlation coefficients of the ammonium sulfate seed particles are low compared to the SOA formed from D<sub>8</sub>-toluene oxidation reference

spectrum. These low-coefficient particles begin to disappear as soon as the D<sub>8</sub>-toluene oxidation is initiated, providing single-particle evidence of organic oxidation products coating the salt seed particle. We also calculated coagulation to be insignificant for this experimental timescale.

Unlike the docosane/D<sub>46</sub>-docosane experiment, this result is completely expected. Squalane, a long-chain branched alkane, is very likely immiscible with the oxidation products comprising the SOA from D<sub>8</sub>-toluene, functionalized molecules such as epoxides and diols (Baltaretu et al., 2009). These results are consistent with those reported by Song et al. (2007), who saw no yield enhancement for biogenic SOA ( $\alpha$ -pinene + O<sub>3</sub>) in the presence of surrogate POA seed (dioctylphthalate, a compound similar to squalane), evidence they used to conclude that SOA and POA form separate phases. Our result indicates that anthropogenic SOA and hydrophobic POA do not mix, though whether this should be extrapolated from the laboratory to the atmosphere is unclear. Regardless, these data demonstrate that smog chamber mixing experiments with single-particle data can be used to answer such questions of atmospheric significance.

### 3.4.2 Observations of vapor pressure-driven mixing

We performed an identical mixing experiment with populations of squalane and D<sub>62</sub>-squalane particles, the results of which are shown in Figure 3.9a. Unlike the docosane mixing experiment, we see clear evidence of mixing between squalane and D<sub>62</sub>-squalane, even though the vapor-pressure driving force for squalane ( $C^{sat} = 8 \times 10^{-2} \mu\text{g m}^{-3}$  at  $T = 293.15 \text{ K}$  (Pankow and Asher, 2008)) is much lower than even the solid phase of docosane. There is clear evolution in the chemical composition of the two visible particle populations over the course of the experiment, as shown in Figure 3.9a. Only particles with 150 ions or more are shown on this plot for clarity, though this filter does not affect our result.

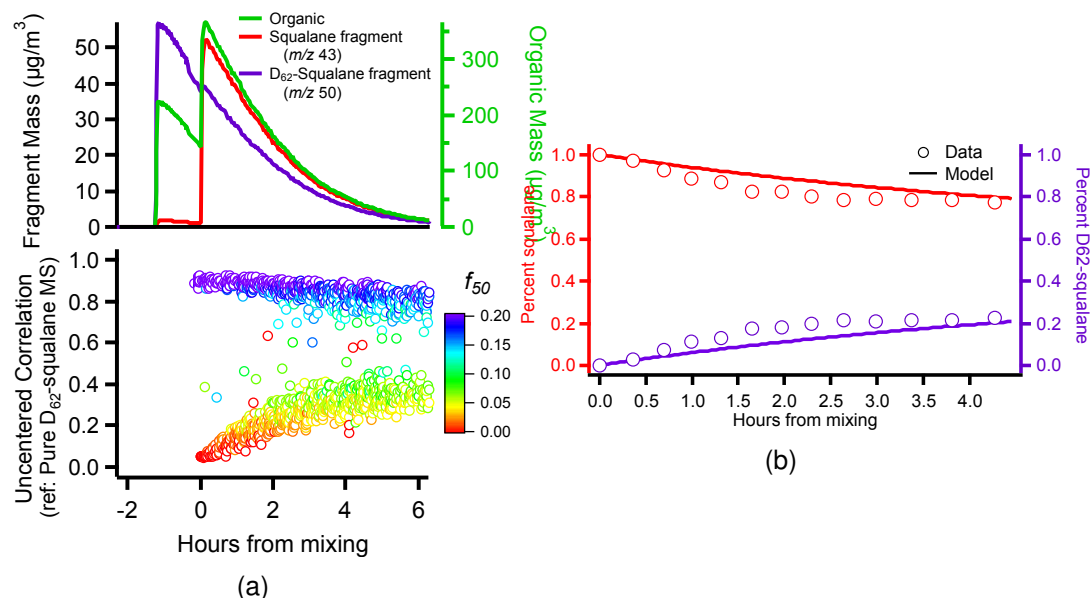


Figure 3.9: Time-evolution of mixing state between aerosol populations of squalane and  $\text{D}_{62}$ -squalane. (a.) Reference mass spectrum is  $\text{D}_{62}$ -squalane. (b.) Time-series of mass percent of squalane and  $\text{D}_{62}$ -squalane for the particle population that was initially pure squalane.

We manually separated the two particle groupings into different categories (one with a correlation coefficient less than 0.5, the other greater than 0.5). The average mass spectra for each grouping is calculated for the first 30 minutes after the aerosol populations are mixed together and at  $t=4$  hours, shown in Figure 3.10. These average single particle mass spectra closely resemble the pure mass spectra of  $\text{D}_{62}$ -squalane and squalane collected with standard V-mode operation of the HR-ToF-AMS in calibration experiments (see Figure S5). At  $t=4$  hours, the prominent peaks in each grouping at  $t = 0$  have grown into the mass spectrum of the opposite grouping (for instance,  $m/z$  50 ( $\text{C}_3\text{D}_7^+$ ) is initially absent in the squalane grouping, but is significant at  $t=4$  hours). With this manual method, we are thus able to quantify the extent to which the two populations have mixed as a function of time. Using a simple chemical mass balance approach, we calculate the mass

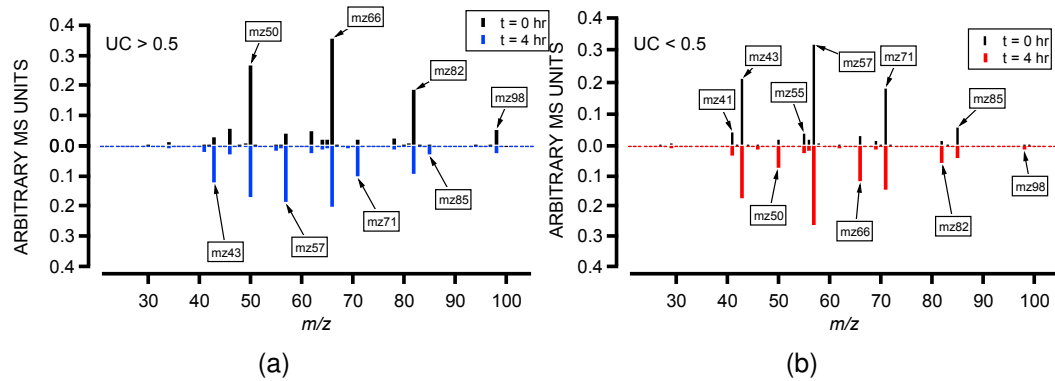


Figure 3.10: Average mass spectra for each particle population at  $t=0$  and  $t=4$  hours. **(A)** Particles with  $UC > 0.5$  (initially pure  $D_{62}$ -squalane). **(B)** Particles with  $UC < 0.5$  (initially pure squalane). The MS at  $t=4$  hours for each **(A)** and **(B)** show tracer fragments unique to the other pure component showing up in the average mass spectrum.

percent of the two chemicals in each aerosol population:

$$\text{Percent A} = \frac{f_{m/z_i}}{f_{m/z_i, \text{pure}, t=0}} \quad (3.3)$$

By the end of the experiment (4.5 hours from the mixing event), the initially pure-squalane particles are 78% percent squalane and 22%  $D_{62}$ -squalane by mass while the “ $D_{62}$ -squalane particles” are 58% percent squalane and 42% percent  $D_{62}$ -squalane. This time evolution of the mass percent of each compound in the initially-pure particles is presented in Figure 3.9b. The same condensational-mixing model is applied to this squalane mixing experiment, which is also plotted in Figure 3.9b. The agreement between the model and the data indicate that squalane exhibits ideal mixing, with no accommodation limitations, as expected.

Though the mixing is “expected” based on our modeling, it is worth noting how counterintuitive this is. Squalane is a 30-carbon molecule with a saturation concentration of roughly  $10^{-2} \mu\text{g m}^{-3}$  and yet within a few hours these molecules will wander from particle to particle under ambient conditions. This serves to emphasize just how sticky a molecule must be to remain more or less firmly on or in

ambient particles; it must be much less volatile than glucose or paraffin wax (Donahue et al., 2011). This is also why the vast majority of primary aerosol emissions from combustion sources such as internal combustion engines, open burning, and cooking are in fact quite volatile (Robinson et al., 2010). The gas phase, in turn, is a dangerous place for large hydrocarbons and they are oxidized rapidly (Donahue et al., 2013). Compounds used as molecular markers of specific sources, such as levoglucosan used to identify wood burning, decay rapidly due to gas-phase attack by hydroxyl radicals (Hennigan et al., 2010). This oxidation in turn often produces lower volatility products that are sticky enough to remain (at least partly) in the condensed phase and thus form secondary (oxidized) organic aerosol (Robinson et al., 2007; Presto et al., 2010).

The squalane experiment is a clear demonstration of both the process and timescale of condensational mixing. However, it is also a situation where single-particle composition data are the only type of data that can reveal this process, as the size-distributions for squalane and  $D_{62}$ -squalane are completely coincident. Asa-Awuku et al. (2009) use non-coincident mass distributions (from PToF-mode) to reveal that diesel-exhaust POA can dissolve into  $\alpha$ -pinene SOA. Their analysis, however, relies on the distributions being initially distinct in size, so that movement of material from one mode to another can be seen. In the above experiment, due to the coincidence of the size distributions, this mixing behavior is thus invisible, and no conclusions about mixing can be made. In such situations, only single-particle mass spectra can elucidate mixing behavior using data from an AMS.

Correlation plots can also be used to visualize mixing dynamics in these chamber studies. Figure 3.11 shows the correlation of mass spectral tracer fragments for each aerosol population colored by time from the mixing event. In the docosane case (Figure 3.11a), there is a high degree of anti-correlation between each tracer, which persists for the entire experiment. On the other hand, for squalane (Fig-

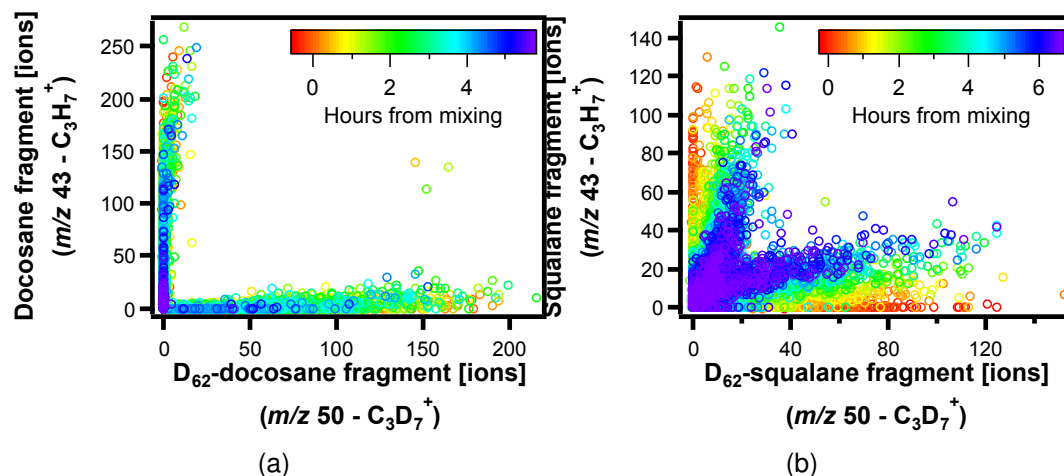


Figure 3.11: Correlation plots between marker mass spectral fragments with color-scale indicating time in the experiment (red=beginning, purple=end). **(A)** Docosane ( $m/z\ 43$  marker) and  $D_{46}$ -docosane ( $m/z\ 50$  marker) mixing experiment. **(B)** Squalane and  $D_{62}$ -squalane mixing experiment. Note particles are gaining signal from the opposite marker with time.

ure 3.11b) we see the two distinct vectors converging over time as each aerosol population picks up molecules of the other from the shared vapor phase.

### 3.4.3 Observation of mixing between $\alpha$ -pinene-derived SOA and toluene-derived SOA

Having established our ability to observe the presence and absence of mixing in several systems, we now turn to the mixing behavior of SOA derived from two important precursors associated with anthropogenic and biogenic emissions: toluene and  $\alpha$ -pinene, respectively. SOA from  $\alpha$ -pinene was prepared by ozonolysis in a 100-L sample bag. SOA from isotopically-labeled toluene was formed in a  $10\ m^3$  smog chamber by OH oxidation, similar to the previously described experiment.  $\alpha$ -pinene SOA was then added to the larger smog chamber. Single-particle mass spectra were correlated with a reference mass spectrum for SOA derived from  $D_8$ -toluene to assess mixing behavior. The system including the isotopic labels is

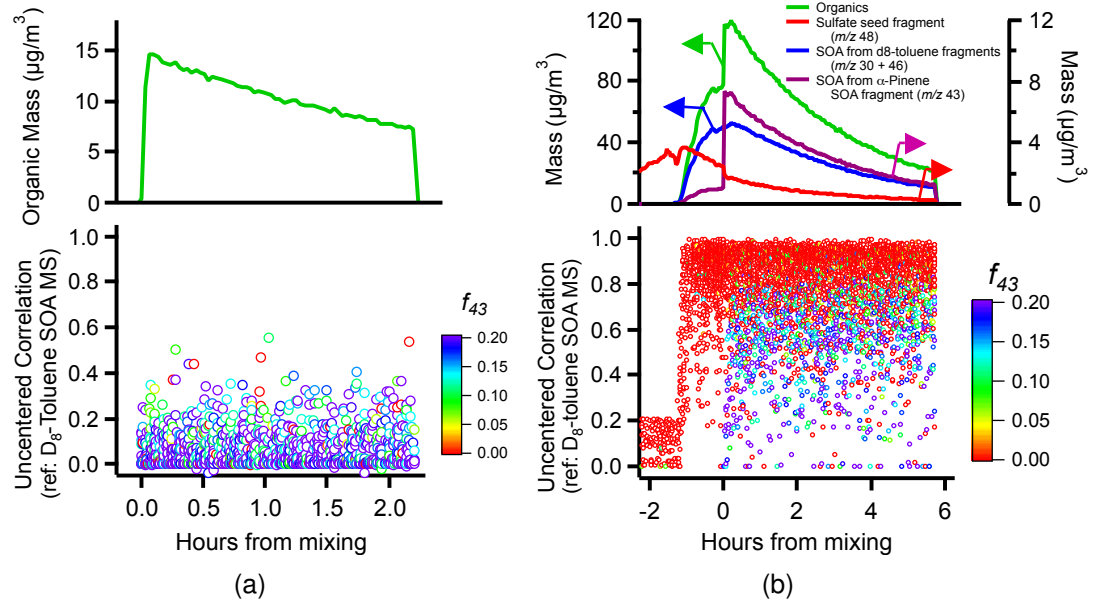


Figure 3.12: **(A)** Time series of  $\alpha$ -Pinene SOA control dilution experiment. Reference mass spectrum is  $\text{D}_8$ -toluene SOA. **(B)** Time series of mixing experiment between  $\alpha$ -pinene SOA and  $\text{D}_8$ -toluene SOA. Reference mass spectrum is  $\text{D}_8$ -toluene SOA. Note that the particles containing high amounts of  $m/z$  43 are much more closely correlated with the  $\text{D}_8$ -toluene reference than  $\alpha$ -pinene SOA diluted into a clean chamber).

identical to the one described by Hildebrandt, et al (Hildebrandt et al., 2011), except those authors formed the two SOA in a single chamber, with one type serving as a condensation seed for the other. Here we formed the two populations separately and followed their mixing after chemistry reached its completion.

As a control, shown in Figure 3.12a, we first injected SOA derived from  $\alpha$ -pinene oxidation into a clean smog chamber. The lower panel plots the correlation coefficient of these particles with reference to SOA derived from  $\text{D}_8$ -toluene, which remains near zero throughout the 2 hour experiment. However, as shown in Figure 3.12b, when the same  $\alpha$ -pinene derived SOA particles were injected into a smog chamber containing SOA derived from toluene, the mass spectra of those  $\alpha$ -pinene particles rapidly developed a strong correlation with the reference spectrum. This indicates that a significant mass of condensable vapors from the  $\text{D}_8$  toluene mixed

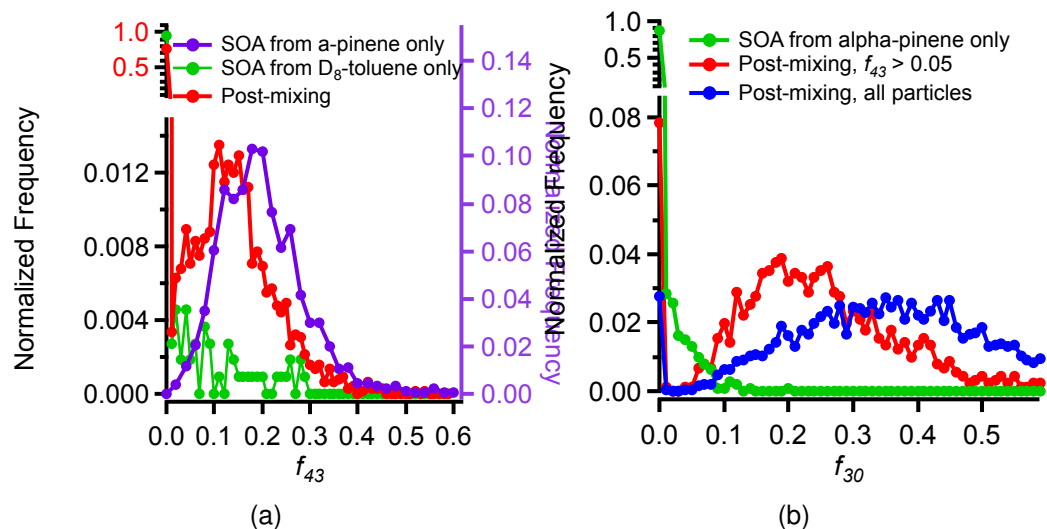


Figure 3.13: **(A)** Normalized histogram of distribution of  $f_{43}$  within single particles for the  $\alpha$ -pinene SOA and D<sub>8</sub>-toluene SOA mixing experiment, and a pure  $\alpha$ -pinene SOA dilution experiment. The fraction of the  $\alpha$ -pinene marker fragment shifts to lower values with the incorporation of non- $\alpha$ -pinene SOA molecules entering the particles. **(B)** Normalized histogram of distribution of  $f_{30}$  for: pure  $\alpha$ -pinene SOA particles from a control experiment, as well as single particles from the  $\alpha$ -pinene SOA and D<sub>8</sub>-toluene SOA mixing experiment. Separate traces are shown for all single particles in the mixing experiment, as well as single particles with significant  $m/z$  43 (originally  $\alpha$ -pinene SOA).

into the particles derived from  $\alpha$ -pinene.

The histogram in Figure 3.13a shows the distribution of  $f_{43}$  for these two experiments. In Figure 3.13a, there is a clear reduction in the fraction of  $m/z$  43, as toluene molecules have condensed onto these particles and now contribute new fragments to the single particle MS. There is no contribution of  $m/z$  43 to the SOA derived from toluene oxidation, shown by the green trace in Figure 3.13a, so all particles with significant  $f_{43}$  are SOA particles originally from  $\alpha$ -pinene oxidation. When those  $\alpha$ -pinene derived particles enter a chamber containing toluene-derived SOA, the peak in the histogram shifts from 0.2 to 0.12. This indicates that approximately 40% of the mass in the particles comes from toluene oxidation products, indicating a high degree of mixing throughout most of the volume of these particles. A similar histogram showing the distribution of  $f_{30}$  confirms that D<sub>8</sub>-toluene oxida-

tion product fragments (for which  $m/z$  30 is a unique tracer) condense onto SOA from  $\alpha$ -pinene oxidation (Figure 3.13b). SOA from  $\alpha$ -pinene oxidation in our control experiment shows practically no signal from  $m/z$  30. However, there is significant  $m/z$  30 in the  $\alpha$ -pinene SOA (determined by filtering the single particle mass spectra for  $f_{43}>0.05$ ) after the mixing event.

Because the mass size distributions for the two SOA populations have unique mass spectral fragments that distinct in size, we are able to use PToF data to confirm our conclusions (as in Asa-Awuku et al., 2009). Figure 3.14 shows a toluene fragment ( $m/z$  30) condensing onto the originally- $\alpha$ -pinene derived SOA particles.

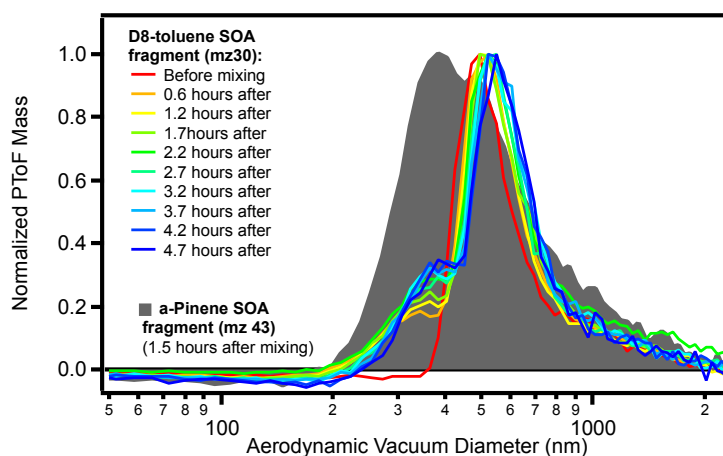


Figure 3.14: Time-evolution of normalized mass distributions for  $m/z$  30, a marker fragment for  $D_8$ -toluene SOA.  $\alpha$ -pinene SOA marker fragment ( $m/z$  43) is plotted in the background to show how  $D_8$ -toluene SOA molecules are condensing onto the  $\alpha$ -pinene SOA mode.

The presence of  $D_8$ -toluene oxidation products within the SOA from  $\alpha$ -pinene oxidation must be from absorption of those vapors into the particles. Coagulation is ruled out, as previously explained for above experiments, as an important mixing process for its long timescale (see Figure 3.5). Adsorption is ruled out because there is no driving force for residual vapors to adsorb onto the SOA from  $\alpha$ -pinene, as there is not a super-saturation of  $D_8$ -toluene oxidation products in the chambers. Thus, the presence of oxidized  $D_8$ -toluene molecules at the mass fraction of  $\sim 40\%$ ,

very strongly indicates that there is absorption into the  $\alpha$ -pinene SOA particles.

Interestingly, almost no mixing occurs in the other direction. As shown by the strong band of particles with high correlation to the D<sub>8</sub>-toluene SOA reference, few of these toluene particles receive  $\alpha$ -pinene SOA molecules. The majority (over 70 %) of particles with correlation >0.8 have no  $m/z$  43 in them at all. It is possible that there were few if any  $\alpha$ -pinene SOA vapors available for condensation into the D<sub>8</sub>-toluene SOA. Other studies have shown diluted  $\alpha$ -pinene SOA to evaporate slowly, on multi-hour timescales, due either to (1) very low internal diffusivities for organic molecules trying to escape the condensed phase and reach the new equilibrium dictated by the dilution (Vaden et al., 2011), or (2) some other long timescale process, such as the decomposition of oligomeric species (Grieshop, Donahue, and Robinson, 2007). We can say with confidence that some fraction (if not all) of an  $\alpha$ -pinene SOA particle does not have extremely low internal diffusivity, characteristic of crystalline solids or glasses. We draw this conclusion because D<sub>8</sub>-toluene SOA molecules are able to enter the  $\alpha$ -pinene-derived SOA particles rapidly (in minutes). It remains possible that some fraction of the  $\alpha$ -pinene SOA particles do not absorb toluene oxidation product vapors, but our measurements do not allow us to answer this question nor diagnose a particle morphology.

### 3.5 Conclusions

Particle mixing dynamics are critically important to the evolution of organic aerosols in the atmosphere. The data presented here show that single particle mass spectra from LSSP operation of the HR-ToF-AMS are extremely effective at elucidating the mixing dynamics of aerosol populations. Indeed, we present experiments where any mixing behavior happening would be invisible to the normal ensemble measurement techniques.

Distinct particle populations will mix when there is a thermodynamic driving

force to do so. This happens at a rate no faster than a maximum determined by the volatility of constituents comprising the particles. The rate may be slower if there are substantial barriers to mass transfer, such as accommodating into crystal lattices or diffusing through a highly viscous condensed phase. It is important to distinguish between thermodynamic versus kinetic reasons for non-mixing. That is, particle populations that slowly mix (or don't mix at all) because they are immiscible must be distinguished from those that mix slowly because other mass transfer limitations. Thus, when experiments reveal relatively rapid mixing there is little or no ambiguity about potential mass transfer limitations. When mixing is slow, one can conclude that condensed phase mass-transfer limitations exist only when volatility limitations to mixing have been ruled out. We have shown examples of each situation.

By employing single-component particle populations containing isotopically labeled molecules of known volatility, we have been able to identify systems that mix according to expectation and others that show clear limitations to mass transfer. Populations comprised of hydrogenated and deuterated squalane (30 carbon liquid oil) mix with each other slowly over the course of many hours, at a rate consistent with the (extremely low) saturation mass concentration of the squalane. This serves to illustrate just how low saturation vapor pressures must be for molecules to stay in particles under ambient conditions. Conversely, populations of particles containing much lower molecular weight hydrogenated and deuterated docosane (22 carbon paraffin wax) fail to show any signs of mixing for many hours at room temperature. This is true even though the saturation concentration of docosane vapors above solid docosane is much higher than that of squalane vapors over liquid squalane. When heated above the melting point of the docosane, however, the hydrogenated and deuterated docosane particle populations mix rapidly. Because docosane vapors also mix into liquid squalane particles at room temperature, this

indicates clearly that mass-transfer limitations do exist for uptake of docosane vapors into crystalline docosane particles.

In the atmosphere, particle populations are complex mixtures, and in many cases they contain highly oxidized secondary organic constituents. It is these oxidized molecules that have most frequently been associated with highly viscous glassy states in particles (Zobrist et al., 2008; Koop et al., 2011; Vaden et al., 2011); SOA derived from  $\alpha$ -pinene has been identified as slow to evaporate (Vaden et al., 2011) and by implication glassy.

Here we have shown that particle populations comprised of biogenic SOA derived from ozonolysis of  $\alpha$ -pinene and anthropogenic SOA derived from OH oxidation of (deuterated) toluene are able to mix quickly. Specifically, vapors derived from deuterated toluene are able to mix into particles derived from  $\alpha$ -pinene very quickly. Those same toluene-derived vapors show no sign of mixing into particles of pure squalane, suggesting that the lack of mixing in the presence of toluene-derived vapors indicates a thermodynamic inhibition (they are simply immiscible), rather than a mass-transfer limitation to uptake. There is thus no evidence that these  $\alpha$ -pinene derived SOA particles had any substantial mass-transfer limitations delaying vapor uptake.

The same mixing experiments that revealed rapid mixing of toluene-derived vapors into  $\alpha$ -pinene derived SOA particles did not show mass transfer going the other way. There was no uptake of  $\alpha$ -pinene derived vapors into particles derived from toluene oxidation. The reasons for this remain unknown. It may be that the vapor concentration of the diluted  $\alpha$ -pinene ozonolysis products are simply too low (possibly because the  $\alpha$ -pinene derived particles are not volatile enough to produce them), or it may be because the toluene-derived particles raise barriers to the uptake of those vapors. Recent experimental (Saleh, Donahue, and Robinson, 2013) and modeling (Trump and Donahue, 2014) work from our group suggest

that the volatility distribution of  $\alpha$ -pinene derived SOA may be lower than reported previously from SOA formation studies (Pathak et al., 2007). Whether the lack of penetration into the D<sub>8</sub>-toluene derived SOA by molecules from  $\alpha$ -pinene oxidation is due to low volatility, diffusion-limitations or mass transfer barriers, or is simply an issue of miscibility, is a question being pursued in future work.

The experiments described here reveal that answers to questions such as “are SOA particles glassy?” or “does ambient organic aerosol reach equilibrium rapidly in the atmosphere?” are complex and the answers likely depend on the specific characteristics of the mixtures in question. We must take great care to avoid generalizations about either the presence or absence of equilibrium behavior and take great pains to understand these systems under conditions that come as close as possible to those found in the real atmosphere. The biogenic  $\alpha$ -pinene SOA system is a de facto model for SOA in both experimental studies and chemical transport models, and the experiments described here reveal that these particles can rapidly uptake vapors from an external source. While not a direct measurement of equilibrium, these data do show that diffusion in SOA from  $\alpha$ -pinene ozonolysis should not impede equilibrium partitioning. Other recent studies (Saleh, Donahue, and Robinson, 2013; Yatavelli et al., 2013) that do measure equilibrium timescales in SOA systems show that they are short. There is thus no compelling reason to rush to judgement that all organic aerosol systems are necessarily slow to equilibrate under ambient conditions, but there is certainly a compelling reason to continue to probe the question of when systems are likely to move slowly toward equilibrium and how the equilibrium timescale significantly influences important aerosol properties, like mixing.

## Bibliography

- [1] Bruce A Albrecht. "Aerosols, cloud microphysics, and fractional cloudiness". *Science* 245.4923 (1989), pp. 1227–1230.
- [2] A Asa-Awuku et al. "Mixing and phase partitioning of primary and secondary organic aerosols". *Geophysical Research Letters* 36.15 (Aug. 2009).
- [3] Cristian O Baltaretu et al. "Primary Atmospheric Oxidation Mechanism for Toluene". *The Journal of Physical Chemistry A* 113.1 (Jan. 2009), pp. 221–230.
- [4] A K Bertram et al. "Predicting the relative humidities of liquid-liquid phase separation, efflorescence, and deliquescence of mixed particles of ammonium sulfate, organic material, and water using the organic-to-sulfate mass ratio of the particle and the oxygen-to-carbon elemental ratio of the organic component". *Atmospheric Chemistry and Physics* 11.21 (2011), pp. 10995–11006.
- [5] C D Cappa and K R Wilson. "Evolution of organic aerosol mass spectra upon heating: implications for OA phase and partitioning behavior". *Atmospheric Chemistry and Physics* 11.5 (2011), pp. 1895–1911.
- [6] ES Cross et al. "Single particle characterization using a light scattering module coupled to a time-of-flight aerosol mass spectrometer". *Atmospheric Chemistry and Physics* 9 (2009), pp. 7769–7793.
- [7] N M Donahue et al. "A two-dimensional volatility basis set: 1. organic-aerosol mixing thermodynamics". *Atmospheric Chemistry and Physics* 11.7 (2011), pp. 3303–3318.
- [8] N M Donahue et al. "Coupled Partitioning, Dilution, and Chemical Aging of Semivolatile Organics". *Environmental Science & Technology* 40.8 (Apr. 2006), pp. 2635–2643.
- [9] N M Donahue et al. "Why do organic aerosols exist? Understanding aerosol lifetimes using the two-dimensional volatility basis set". *Environmental Chemistry* 10.3 (2013), p. 151.
- [10] Allen H Goldstein and Ian E Galbally. "Known and unexplored organic constituents in the earth's atmosphere". *Environmental Science & Technology* 41.5 (2007), pp. 1514–1521.
- [11] A P Grieshop, N M Donahue, and A L Robinson. "Is the gas-particle partitioning in alpha-pinene secondary organic aerosol reversible". *Geophysical Research Letters* 34.10.1029 (2007).
- [12] Andrew P Grieshop et al. "Constraining the Volatility Distribution and Gas-Particle Partitioning of Combustion Aerosols Using Isothermal Dilution and Thermodesorber Measurements". *Environmental Science & Technology* 43.13 (July 2009), pp. 4750–4756.

- [13] Christopher J Hennigan et al. "Levoglucosan stability in biomass burning particles exposed to hydroxyl radicals". *Geophysical Research Letters* 37.9 (May 2010), p. L09806.
- [14] Lea Hildebrandt et al. "Evaluating the Mixing of Organic Aerosol Components Using High-Resolution Aerosol Mass Spectrometry". *Environmental Science & Technology* 45.15 (Aug. 2011), pp. 6329–6335.
- [15] J L Jimenez et al. "Evolution of Organic Aerosols in the Atmosphere". *Science* 326.5959 (Dec. 2009), pp. 1525–1529.
- [16] M Kanakidou et al. "Organic aerosol and global climate modelling: a review". *Atmospheric Chemistry and Physics* 5.4 (Mar. 2005), pp. 1053–1123.
- [17] Thomas Koop et al. "Glass transition and phase state of organic compounds: dependency on molecular properties and implications for secondary organic aerosols in the atmosphere". *Physical Chemistry Chemical Physics* 13.43 (2011), p. 19238.
- [18] Jesse H Kroll et al. "Measurement of fragmentation and functionalization pathways in the heterogeneous oxidation of oxidized organic aerosol". *Physical Chemistry Chemical Physics* 11.36 (2009), p. 8005.
- [19] S Liu et al. "Organic particle types by single-particle measurements using a time-of-flight aerosol mass spectrometer coupled with a light scattering module". *Atmospheric Measurement Techniques* 6 (2013), pp. 187–197.
- [20] Rafael Lozano et al. "Global and regional mortality from 235 causes of death for 20 age groups in 1990 and 2010: a systematic analysis for the Global Burden of Disease Study 2010". *The Lancet* 380.9859 (2013), pp. 2095–2128.
- [21] C Marcolli et al. "Internal mixing of the organic aerosol by gas phase diffusion of semivolatile organic compounds". *Atmospheric Chemistry and Physics* 4.11/12 (2004), pp. 2593–2599.
- [22] Claudia Marcolli and Ulrich K Krieger. "Phase Changes during Hygroscopic Cycles of Mixed Organic/Inorganic Model Systems of Tropospheric Aerosols". *The Journal of Physical Chemistry A* 110.5 (Feb. 2006), pp. 1881–1893.
- [23] Jay R Odum et al. "Gas/particle partitioning and secondary organic aerosol yields". *Environmental Science & Technology* 30.8 (1996), pp. 2580–2585.
- [24] Spyros N Pandis et al. "Secondary organic aerosol formation and transport". *Atmospheric Environment. Part A. General Topics* 26.13 (1992), pp. 2269–2282.
- [25] JF Pankow and WE Asher. "SIMPOL. 1: a simple group contribution method for predicting vapor pressures and enthalpies of vaporization of multifunctional organic compounds". *Atmospheric Chemistry and Physics* 8.10 (2008), pp. 2773–2796.

- [26] R K Pathak et al. "Ozonolysis of  $\alpha$ -pinene: parameterization of secondary organic aerosol mass fraction". *Atmospheric Chemistry and Physics* 7.14 (2007), pp. 3811–3821.
- [27] V. Perraud et al. "Nonequilibrium atmospheric secondary organic aerosol formation and growth". *Proceedings of the National Academy of Sciences* 109.8 (2012), pp. 2836–2841.
- [28] C Arden Pope III, Majid Ezzati, and Douglas W Dockery. "Fine-particulate air pollution and life expectancy in the United States". *New England Journal of Medicine* 360.4 (2009), pp. 376–386.
- [29] Albert A Presto and Neil M Donahue. "Investigation of alpha-Pinene + Ozone Secondary Organic Aerosol Formation at Low Total Aerosol Mass". *Environmental Science & Technology* 40.11 (June 2006), pp. 3536–3543.
- [30] Albert A Presto et al. "Secondary Organic Aerosol Formation from High-NO<sub>x</sub> Photo-Oxidation of Low Volatility Precursors: n-Alkanes". *Environmental Science & Technology* 44.6 (Mar. 2010), pp. 2029–2034.
- [31] L Renbaum-Wolff and J W Grayson. "Viscosity of alpha-pinene secondary organic material and implications for particle growth and reactivity". *Proceedings of the . . .* 2013.
- [32] A L Robinson et al. "Rethinking Organic Aerosols: Semivolatile Emissions and Photochemical Aging". *Science* 315.5816 (Mar. 2007), pp. 1259–1262.
- [33] Allen L Robinson et al. "Updating the Conceptual Model for Fine Particle Mass Emissions from Combustion Systems Allen L. Robinson". *Journal of the Air & Waste Management Association* 60.10 (Oct. 2010), pp. 1204–1222.
- [34] Rawad Saleh, Neil M Donahue, and Allen L Robinson. "Time Scales for Gas-Particle Partitioning Equilibration of Secondary Organic Aerosol Formed from Alpha-Pinene Ozonolysis". *Environmental Science & Technology* (May 2013), p. 130517130052009.
- [35] Randy Showstack. "The Perfect Haze: Scientists Link 1999 U.S. Pollution Episode to Midwest Aerosol Plumes and Kennedy Plane Crash". *Eos, Transactions American Geophysical Union* 81.2 (Jan. 2000), pp. 13–14.
- [36] M L Smith, A K Bertram, and S T Martin. "Deliquescence, efflorescence, and phase miscibility of mixed particles of ammonium sulfate and isoprene-derived secondary organic material". *Atmospheric Chemistry and Physics* 12.20 (2012), pp. 9613–9628.
- [37] S Solomon et al. "Climate change 2007: The physical science basis, contribution of working group 1 to the fourth assessment report of the Intergovernmental Panel on Climate Change" (2007).
- [38] G A Somorjai and J E Lester. "Evaporation mechanism of solids". *Progress in Solid State Chemistry* 4 (1967), pp. 1–52.

- [39] Chen Song et al. "Effect of hydrophobic primary organic aerosols on secondary organic aerosol formation from ozonolysis of alpha-pinene". *Geophysical Research Letters* 34.20 (Oct. 2007), p. L20803.
- [40] E R Trump and N M Donahue. "Oligomer formation within secondary organic aerosols: equilibrium and dynamic considerations". *Atmospheric Chemistry and Physics* 14.7 (2014), pp. 3691–3701.
- [41] Sean Twomey. "The influence of pollution on the shortwave albedo of clouds". *Journal of the atmospheric sciences* 34.7 (1977), pp. 1149–1152.
- [42] T.D. Vaden et al. "Atmospheric Chemistry Special Feature: Morphology of mixed primary and secondary organic particles and the adsorption of spectator organic gases during aerosol formation". *Proceedings of the National Academy of Sciences* 107.15 (Apr. 2010), pp. 6658–6663.
- [43] T.D. Vaden et al. "Evaporation kinetics and phase of laboratory and ambient secondary organic aerosol". *Proceedings of the National Academy of Sciences* 108.6 (2011), pp. 2190–2195.
- [44] Emily A Weitkamp et al. "Organic Aerosol Formation from Photochemical Oxidation of Diesel Exhaust in a Smog Chamber". *Environmental Science & Technology* 41.20 (Oct. 2007), pp. 6969–6975.
- [45] R L N Yatavelli et al. "Semi-continuous measurements of gas/particle partitioning of organic acids in a ponderosa pine forest using a MOVI-HRToF-CIMS". *Atmospheric Chemistry and Physics Discussions* 13.6 (2013), pp. 17327–17374.
- [46] B Zobrist et al. "Do atmospheric aerosols form glasses?" *Atmospheric Chemistry and Physics Discussions* 8.3 (2008), pp. 9263–9321.

# Chapter 4

## Probing the morphology and diffusivity of mixed SOA/Squalane particles using size-resolved composition and single-particle measurements

*An analysis of the formation and evaporation of mixed-particles containing squalane and SOA is presented. First, we use a two-population smog chamber experiment to test the phase-behavior between isotopically-labeled squalane ( $D_{62}$ -squalane) and SOA (from  $\alpha$ -pinene +  $O_3$ ). Next, we present mixed-particle experiments where one particle-type (squalane or SOA) was prepared first to serve as surface area for condensation of the other material, forming the mixed-particles. The mixed-particles were then subjected to a heating-ramp from 22 to 44 °C in the chamber. From these experiments, we were able to determine that: 1) squalane and SOA phase separate; 2) the vast majority of squalane is able to evaporate from the mixed particles on the same timescale regardless of the order of preparation; 3) almost all of the SOA mass is comprised of material less volatile than squalane; 4) AMS collection efficiency in these mixed-particle systems is highly variable over the course of these experiments where particle phase is (likely) dynamic, but can be parameterized as a function of the mass fraction of squalane, and 5) the evaporation profile of squalane can be used for estimate the diffusion coefficient ( $D_{org}$ ) of squalane through SOA at these elevated temperatures.*

### 4.1 Introduction

Atmospheric aerosol particles negatively influence human health and have a large, yet highly uncertain impact on the climate (Solomon et al., 2007). The organic fraction of atmospheric particulate matter (PM) comprises 20-90% of the submicron

---

Originally prepared for publication as: Robinson, E.S., Saleh, R., and Donahue, N.M.: Probing the morphology and diffusivity of mixed SOA/Squalane particles using size-resolved composition and single-particle measurements. *Env. Sci. & Tech.*, 2014. *in preparation*

PM mass, and is a complex mixture of myriad different species emitted either directly as particles (primary organic aerosol (POA)) or transferred to the condensed phase through oxidative chemistry (secondary organic aerosol (SOA)) (Jimenez et al., 2009). Owing largely to this chemical complexity, the processes surrounding the formation, growth, and chemical evolution of OA in the atmosphere are currently poorly understood, as evinced by a persistent gap between measured atmospheric OA and the predictions of regional chemical transport models (Volkamer et al., 2006).

Most predictive models assume all classes of OA (e.g. biogenic SOA, hydrophobic POA) form a single, pseudo-ideal condensed phase (e.g. Strader, Lurmann, and Pandis, 1999). This requires that all OA types are miscible in one-another and exhibit no barriers to mass transfer that would cause the mixing process to play out over multiple timesteps within the model. These models also assume that equilibration with a changing gas-phase happens on timescales shorter than the model timesteps. It has been recently proposed that these assumptions may not hold under certain circumstances for many types of OA, and may significantly contribute to the discrepancy between models and measurements.

First, multiple recent smog chamber studies present convincing evidence for phase-separation between different classes of OA (e.g. different varieties of SOA and POA (Song et al., 2007; Asa-Awuku et al., 2009; Robinson, Saleh, and Donahue, 2013)). Very likely there are multiple organic phases present in the atmospheric OA ensemble, especially in urban areas with diverse sources of particles (Moffet et al., 2008). Second, recent experimental studies argue that SOA can remain out of equilibrium with its gas-phase on long timescales: Vaden et al. (2011) reported evaporation rates of SOA in a vapor-free environment that were much slower than predicted based on previously reported volatility distributions. These data were used to conclude that there are diffusive limitations to mass transfer

within the particle bulk. Perraud et al. (2012) reported differences between measured particle-phase concentrations of organic nitrates in SOA and their expected concentrations assuming ideal activity coefficients, implicating either variable activity coefficients as a function of OA concentrations for organic nitrates in SOA, or mass transfer limitations. In evaporation studies using pyrene as a chemical tracer for diffusion within SOA, Abramson et al. (2013) and Zelenyuk et al. (2012) both reported evaporation rates for pyrene embedded in SOA slower than for pure pyrene, which is again used to conclude that molecular diffusion of organics within SOA is very slow.

There exists a small number of studies that attempt to quantify the diffusivity of organics within an SOA matrix (and at the publication date of this thesis, the following is a comprehensive list). Using evaporative perturbation techniques at dry (RH < 5%, Abramson et al. (2013) report  $D_{org}$  for pyrene within SOA to be  $2.5 \times 10^{-17}$  cm<sup>2</sup>/s, and Loza et al. (2013) report  $D_{org}$  within SOA to be  $1 \times 10^{-17}$  cm<sup>2</sup>/s. Zhou et al. (2013) also measure the  $D_{org}$  value of pyrene through SOA from  $\alpha$ -pinene + O<sub>3</sub>, but do so by measuring the decay of pyrene via heterogenous reaction. They report  $D_{org} = 2 \times 10^{-14}$ ,  $8 \times 10^{-14}$  (in cm<sup>2</sup>/s), and  $> 1 \times 10^{-12}$  for RH = 5%, 50%, and 70%, respectively. Similarly, Renbaum-Wolff and Grayson (2013) report  $D_{org}$  as a function of RH, though using dissimilar methods—mechanical measurements of viscosity. They report a range of almost ten orders of magnitude ( $D_{org} < 10^{-17}$  cm<sup>2</sup>/s at RH < 30% and  $D_{org} \sim 10^{-9}$  cm<sup>2</sup>/s at RH < 30%). Clearly, the plasticizing effect of water plays a role in organic diffusivity within SOA, but also (likely) the organic molecule moving through the SOA matrix (e.g. pyrene).

Simultaneously, recent work (Ehn et al., 2015; Kokkola et al., 2014) shows that some SOA types are likely much less volatile than previous studies had suggested (Pathak et al., 2007). A much lower volatility distribution for SOA would potentially explain the slow evaporation seen in previous studies, without invoking mass trans-

fer limitations to explain the data (Saleh, Donahue, and Robinson, 2013). Similarly, non-mixing between different types of OA has recently been cited as evidence for slow diffusivity within SOA (Loza et al., 2013), though low volatility and/miscibility limitations could potentially explain these data as well. In general, a thorough understanding of a given system's expected phase behavior and volatility distribution(s) are required to make conclusions about mass transfer within particles, and all of these aspects are important for how OA dynamics are conceptualized in regional models.

The experiments presented here add to our understanding of mixing, mass transfer, and volatility of SOA. We present experiments in which particles with two phases are sequentially prepared (e.g. SOA formation onto squalane seeds), and then subjected to elevated temperatures. Depending on the morphology of these mixed-particles (e.g. SOA shell on a squalane core), these experiments provide a direct test of organic diffusivity within SOA during the temperature-ramp perturbation. We find that squalane is able to evaporate from these mixed particles on short timescales, and are also able to estimate the fraction of the SOA with volatility lower than that of squalane. We also present mixing experiments between separate populations of SOA and  $D_{62}$ -squalane particles that directly demonstrate the phase-separation behavior between the two aerosol types.

## 4.2 Methods

We performed variations on two basic experiments: 1) separately preparing two aerosol populations and combining them into a common volume, and 2) preparing an aerosol population of uniform (nominally core-shell) composition. All experiments were conducted in dry smog chamber conditions ( $RH < 5\%$ ). Both experimental procedures and the measurement suite used are detailed in the following section.

#### 4.2.1 Two-population experiments

We have reported the concept and procedure for similar two-population experiments in detail previously (Robinson, Saleh, and Donahue, 2013). In brief, two aerosol populations are prepared in separate chambers, and then combined into a shared volume. By using single-particle mass spectrometry, we can track the composition of each population and attribute further compositional changes to mixing.

In this mixing experiment, we prepared SOA from the reaction of  $\alpha$ -pinene and  $O_3$  in a 50-L sample bag. The bag was charged with excess ozone, into which 1.2  $\mu\text{L}$  of  $\alpha$ -pinene was injected through a heated tube fitted with an airtight septum. After 15 minutes, the contents of the sample bag were then diluted by a factor of  $\sim 200$  into a 10  $\text{m}^3$  smog chamber, and left for one hour for characterization. The reason for preparing the SOA this way, as opposed to in the smog chamber directly, was to ensure that particles were large enough to be measured by the light-scattering single-particle (LSSP) module of the AMS, which has a lower optical detection limit of  $d_{va} = 180$  nm. It should be noted that the SOA in these experiments was formed at high concentration (mass yield curves suggest  $C_{OA} \sim 6$   $\text{mg m}^{-3}$ ) but then diluted to a much lower value ( $C_{OA} \sim 30$   $\mu\text{g m}^{-3}$ ). In a separate 50-L sample bag, we prepared  $D_{62}$ -squalane particles by flash vaporization. A small aliquot of  $D_{62}$ -squalane was placed onto the tip of a heated stainless steel surface and then inserted into the sample bag for *in situ* vaporization, after which homogeneously-nucleated  $D_{62}$ -squalane particles formed. The contents of this bag were also then diluted into the larger smog chamber. This experiment was performed to establish whether or not SOA and  $D_{62}$ -squalane should be expected to form a single phase or remain phase-separated.

#### 4.2.2 Mixed-particle experiments

We performed two types of mixed-particle experiments: 1.) SOA particles were used as seeds for condensation of D<sub>62</sub>-squalane, and 2.) D<sub>62</sub>-squalane particles were used as seeds for condensation of SOA. In all cases, the SOA was formed from the reaction of  $\alpha$ -pinene + O<sub>3</sub>.

For experiments using D<sub>62</sub>-squalane as seed particles, D<sub>62</sub>-squalane was flash vaporized directly into the 10 m<sup>3</sup> smog chamber. High heat and low (3 lpm) flow of dispersal air was used to ensure a high super-saturation in the vapor plume which led to large, homogeneously-nucleated particles (number mode diameter,  $d = 160$  nm; condensation sink,  $CS = 0.34 \text{ min}^{-1}$ ). After formation and characterization of the D<sub>62</sub>-squalane particles, the smog chamber was charged with ozone ( $\sim 1$ -2 ppm), and then a 1.2  $\mu\text{L}$  aliquot of  $\alpha$ -pinene was injected into the chamber through a heated tube fitted with a septum. Clean, dry air was used to carry  $\alpha$ -pinene vapor into the smog chamber. In some cases, limited SOA nucleation was observed in addition to condensation onto the pre-existing seed particles, and in others no nucleation occurred and all SOA condensed onto the pre-existing seed particles.

In the reverse experiment, where SOA was used as a seed for condensation of D<sub>62</sub>-squalane, SOA was formed under the same conditions described in the previous section (SOA from 1.2  $\mu\text{L}$   $\alpha$ -pinene + excess O<sub>3</sub> was prepared in and then diluted from a 50-L sample bag into the 10 m<sup>3</sup> smog chamber). Following SOA characterization in the 10 m<sup>3</sup> smog chamber, D<sub>62</sub>-squalane was flash-vaporized directly into the chamber. In all of these experiments, there were no homogeneously-nucleated D<sub>62</sub>-squalane particles—all of the D<sub>62</sub>-squalane condensed onto existing SOA particles. This was confirmed by a large increase in particle volume without any accompanying increase in particle number concentration, as measured by the SMPS. The flash vaporization was conducted with low-heat and a high (15 lpm)

flow of dispersal air, to dilute the high-concentration  $D_{62}$ -squalane plume as much as possible. This reduced the supersaturation of the squalane, preventing any new particle formation.

After preparation and characterization of the mixed-particles, the smog chamber temperature was then elevated from 22 °C to 44 °C, perturbing the equilibrium of the system, and prompting evaporation.

#### 4.2.3 Instrument suite

Relative humidity and temperature in the smog chamber were monitored using a commercial humidity monitor (Vaisala HNP-233). Ozone was generated by flowing oxygen through a corona-discharge ozone generator (Azco, HTU500AC) and measured using a UV photometric ozone monitor (Dasibi 1008-PC). Ensemble particle volume and number concentrations were measured using a Scanning Mobility Particle Sizer (SMPS; TSI, Inc.). Organic aerosol composition and mass were measured with the High-Resolution Aerosol Mass Spectrometer (HR-ToF-AMS; Aerodyne, Inc.) operated in single-reflectron V-mode, fully described by DeCarlo et al. (DeCarlo et al., 2006). Data collected in MS/PToF modes were analyzed using a custom software packages SQUIRREL<sup>1</sup> and PIKA<sup>2</sup>. Single-particle mass spectra were acquired using the light-scattering single-particle (LSSP) module coupled to the HR-ToF-AMS (Cross et al., 2009). Single-particle data analysis was performed using the SPARROW software package<sup>3</sup>. An operationally-defined threshold of 6 ions was used to distinguish null particle events from particles giving meaningful chemical mass signals (Liu et al., 2013).

<sup>1</sup>SQUIRREL 1.51, written by D. Sueper, Aerodyne Research Inc. and University of Colorado at Boulder; available at <http://tinyurl.com/tofams?analysis>

<sup>2</sup>PIKA 1.12C, written by D. Sueper, Aerodyne Research Inc. and University of Colorado at Boulder; available at <http://tinyurl.com/tofams?analysis>

<sup>3</sup>Sparrow 1.04A, written by D. Sueper, Aerodyne Research Inc. and University of Colorado at Boulder; available at <http://cires.colorado.edu/jimenez-group/ToFAMSResources/ToFSoftware/index.htmlAnalysis4>

## 4.3 Results

### 4.3.1 Two-population SOA/Squalane mixing

Previously, we have shown that squalane OA is capable of mixing through gas-phase exchange on the timescales of smog chamber experiments, by conducting a two-population experiment with labeled/unlabeled squalane (Robinson, Saleh, and Donahue, 2013). We have also shown that labeled squalane OA and SOA formed from toluene oxidation do not mix together, despite the lack of a diffusive barrier to absorption of toluene-SOA vapors into liquid squalane particles, and the availability of semi-volatile squalane vapors that could partition into the toluene-SOA mass. The reason for the lack of mixing is simply that thermodynamics does not favor it—squalane and SOA from toluene oxidation are immiscible.

Extending this previous work, here we present results from a two-population experiment using D<sub>62</sub>-squalane particles and SOA particles (from  $\alpha$ -pinene ozonolysis), shown in Figure 4.1a. We see the persistence of two chemically-distinct aerosol populations over the course of  $\sim 2$  hours after the particle populations are combined, with no sign of convergence, indicative of non-mixing. The time series in the top panel shows the total organic mass (green), and mass spectral fragments highly specific to each particle type ( $m/z$  43, largely C<sub>2</sub>H<sub>3</sub>O<sup>+</sup>, for SOA; and  $m/z$  66, C<sub>4</sub>D<sub>9</sub><sup>+</sup>, for squalane). The mass concentrations in the top panel decrease due to particle losses to walls. The bottom panel shows the uncentered correlation coefficients of individual particles, a common measure of similarity between mass spectra and a reference spectrum (Ulbrich et al., 2009) (in this case, the reference is the average MS for SOA from LSSP-mode). Data points are colored by the fraction of  $m/z$  43 in each single-particle MS. At  $t = 0$ , D<sub>62</sub>-squalane particles are added to the SOA-filled chamber (shown by the red trace in top panel, and red particles in lower panel). Were squalane particles absorbing vapors from the SOA, we would

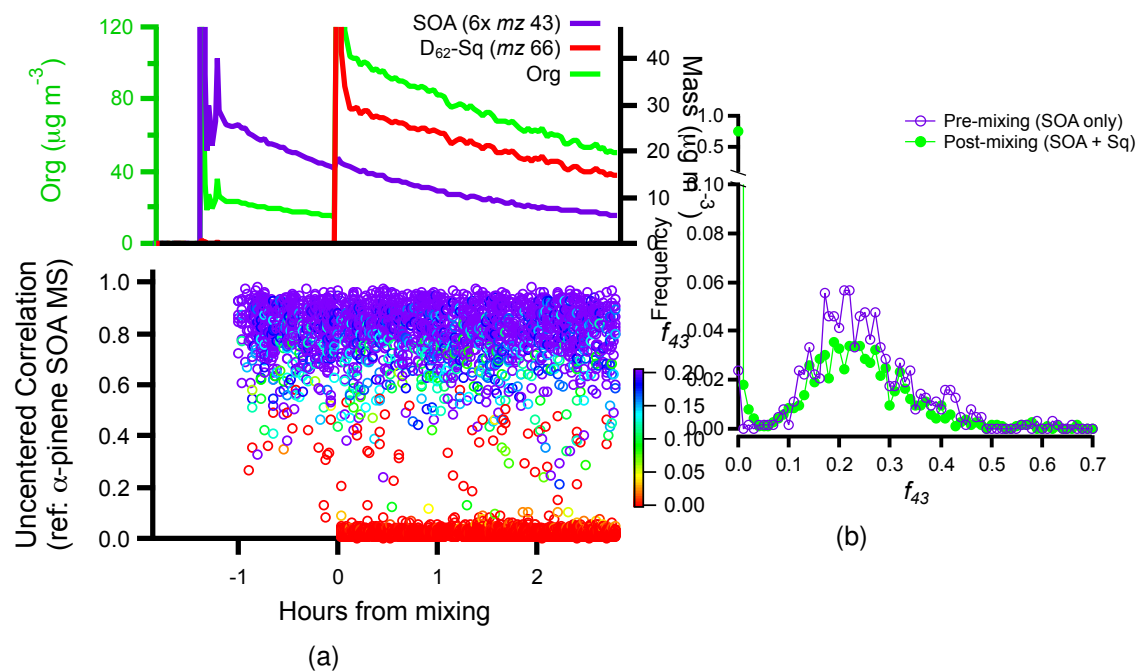


Figure 4.1: **(A)** Time series of a two-population experiment demonstrating that SOA from  $\alpha$ -pinene +  $\text{O}_3$  and squalane OA do not mix. Prior to  $t = 0$ , only SOA is present in the chamber (marked by  $m/z$  43). At  $t = 0$ ,  $D_{62}$ -squalane particles are added to the chamber (marked by  $m/z$  66). The bottom panel shows the uncentered correlation coefficients of all prompt particles with SOA as the reference MS. Data points are colored by the fraction of  $m/z$  43 in each particle. **(B)** Histogram of prompt, single-particle  $f_{43}$  values for two time periods: pre-mixing (SOA only) and the end of the experiment (both populations). The characteristic  $f_{43}$  value for “pure” SOA is not changed in the post-mixing period by the dilution of squalane material in those particles, but a large number ( $\sim 60\%$ ) of particles lacking any  $m/z$  43 are present.

see  $m/z$  43 in their mass spectra and an increase in their correlation coefficients, neither of which are present. Additionally, we see no absorption of  $m/z$  66 into the SOA particles, which would dilute the amount of SOA mass in the SOA particles, decreasing  $f_{43}$  (see Figure 4.1b). From these single-particle data, we can conclude that there is no gas-phase exchange between the particle populations, and rule out the possibility that squalane and SOA would be well-mixed, even if present within a single aerosol particle. This result is expected, and agrees with the previous results of Vaden et al that indicated phase separation in mixed SOA/dioctyl phthalate

(DOP) particles (Vaden et al., 2011) and our own results for squalane and toluene-derived SOA (Robinson, Saleh, and Donahue, 2013). Like squalane, DOP is used as a surrogate for hydrophobic POA in smog chamber experiments. Our experiment provides further evidence of immiscibility between squalane, a hydrophobic laboratory surrogate for POA, and SOA from  $\alpha$ -pinene ozonolysis.

#### 4.3.2 Evaporation dynamics of mixed SOA/Squalane particles

After establishing the immiscibility between these two materials, we proceeded to conduct mixed-particle experiments, where one constituent (D<sub>62</sub>-squalane or SOA) served as a surface for condensable vapors from the other. Figure 4.2a shows a representative time-series for an experiment where D<sub>62</sub>-squalane particles served as seeds for SOA formation. Like Figure 4.1, we use the same color scheme: red corresponds to the squalane fragment ( $m/z$  66) and purple corresponds to the SOA fragment ( $m/z$  43), plotted on the left y-axis (log scale). This figure importantly highlights the small (but non-zero) amount of  $m/z$  43 in D<sub>62</sub>-squalane. There were no new particles formed upon SOA formation, so all of the SOM condensed onto the pre-existing squalane seeds. On the right axis, we plot the mass fraction of D<sub>62</sub>-squalane to the total OA, which is calculated using following equation:

$$\text{Mass fraction squalane} = \frac{f_{66, t}}{f_{66, t < 0}} \quad (4.1)$$

where the signature value of  $f_{66}$  in pure squalane is 0.4. This equation assumes that there is no chemistry on-going in the chamber after SOA formation. Upon formation of the SOM, the mass fractions of each component to the total OA are roughly equal.

At  $t = 1.5$  hours, we heated the smog chamber from 22 °C to 44 °C. There is a sharp decrease of  $m/z$  66 and a more mild decrease of  $m/z$  43 (Figure 4.2a).

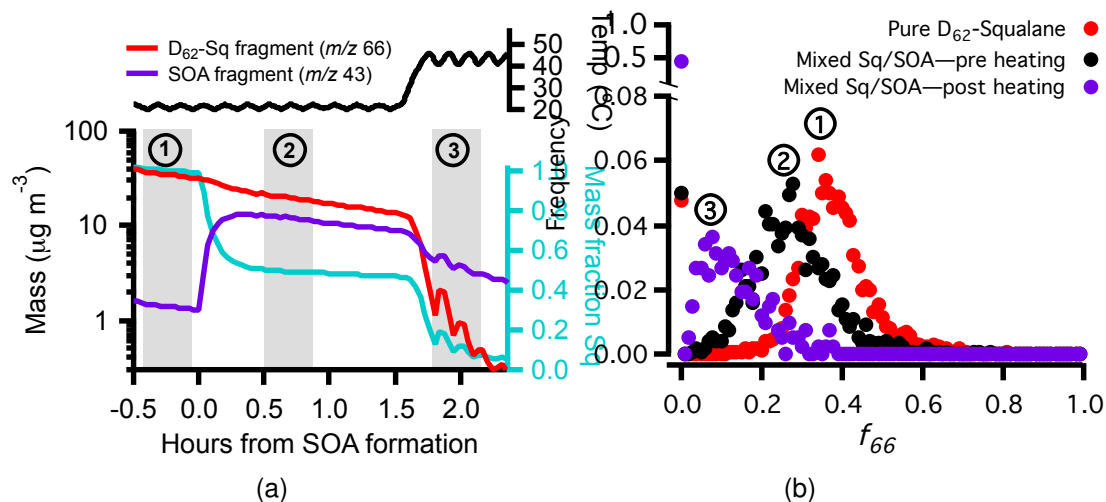


Figure 4.2: **(A)** Time series of a mixed-particle experiment where  $\text{D}_{62}\text{-Squalane}$  particles served as seeds for the condensation of SOM from  $\alpha$ -pinene ozonolysis, followed by a heating ramp. This plot illustrates the relative volatility of the two OA types and the ability of squalane to evaporate from these mixed particles. AMS mass fragments mostly unique to each aerosol type are shown on the left y-axis versus time from SOA formation:  $m/z$  66 ( $\text{D}_{62}\text{-squalane}$ ) and  $m/z$  43 (SOA). Mass-fraction of squalane to the total OA is shown on the right y-axis. At  $t \sim 1.5$  hr the chamber temperature is ramped from  $22^{\circ}\text{C}$  to  $44^{\circ}\text{C}$ . Upon heating, the majority of the squalane mass evaporates, and the OA becomes almost entirely comprised of SOA. Numbers 1-3 show time periods used for **(B)**: histograms of prompt, single-particle  $f_{66}$  values. The evolution of the three  $f_{66}$  histograms illustrates the inherent spread of single-particle MS even for pure compounds, the addition of SOM to the squalane seeds on a single-particle basis, and the significant evaporation of squalane (and enrichment of SOA) across all particles, respectively.

Neither of these traces are corrected for any changes in collection efficiency that occur during the heat ramp. The mass fraction of squalane decreases from 0.45 to 0.05. This indicates that 1.) squalane is clearly evaporating from the mixed-particles, as 90% of the squalane is gone after heating, and that 2.) squalane is more volatile than a significant fraction of the SOA. Squalane has a saturation concentration of approximately  $8 \times 10^{-2} \mu\text{g/m}^{-3}$  at  $22^{\circ}\text{C}$  (Pankow and Asher, 2008). For this experiment, we calculate that there is very little, if any, evaporation of SOA (see Figure 4.6), meaning that almost all of the SOA mass is less volatile than squalane. We base this on the mass fraction remaining of SOA after heating compared to the mass fraction of squalane remaining after heating. There are

further details in section 4.3.4 about calculating SOA MFR.

Figure 4.2b illustrates how the single-particle mass spectra change before and after SOA formation, and after increasing the temperature of the smog chamber. (averaging periods 1, 2, and 3, respectively, shown by shaded areas in grey in Figure 4.2a). The signature value of  $f_{66} = 0.4$  in pure squalane is shown for averaging period 1 (red trace). Here we see the inherent spread of single-particle mass signals: while the average value of the distribution agrees with the bulk measurement, any given particle may fall within a value quite different from the bulk average. This reflects the small number of ions in electron impact ionization. After SOA is formed, and condensible products are added to the seed particles, the  $f_{66}$  distributions shifts to smaller values (black trace). The shift between the red and black traces indicate that individual particles are indeed gaining SOA mass (squalane is “diluted” on a fractional basis of the total mass for a given particle). Again, given the results from the experiment shown in Figure 4.1, we expect these particles to contain two organic phases. Note that the number of single-particles with measured  $f_{66} = 0$  is non-zero for pure D<sub>62</sub>-squalane (averaging period 1), but does not increase with the addition of SOA (averaging period 2). An increase in the frequency of  $f_{66} = 0$  events would serve as an indication of nucleation, but here the lack of such an increase further shows that the condensing OM is going to the pre-existing seeds and forming particles with mixed-composition. After the chamber is heated, there is a further shift towards lower  $f_{66}$  values (averaging period 3). Many of the single-particles lose so much squalane that it is no longer measurable (note the appearance of a large number of  $f_{66} = 0$  events on the split y-axis). Figure 4.2b shows that mixed squalane/SOA particles were formed, and that, upon heating, the squalane preferentially evaporates. This is fully consistent with the bulk measurements in Figure 4.2a, and more importantly verifies our data analysis on the basis of individual particles.

Because these smog-chamber particles are polydisperse and we expect two separate organic phases, the condensation of SOM will not be uniform across the squalane seeds—we expect the amount of condensed SOM to be a strong function of size (Donahue et al., 2014). Indeed, using size-resolved composition data from AMS PToF mode, we find that the mass fraction of squalane is lower (thus, SOA mass fraction is higher) for small particles as condensation favors particles with higher surface area-to-volume. This is another consistency check that two phases are being formed, as particle composition is non-uniform as a function of diameter—if the two materials formed a single phase, the activities for each would be non-uniform as a function of size and would thus be out of equilibrium. Figure 4.3 shows how the squalane mass fraction evolves for the three averaging periods as a function of particle size (top panel), along with the normalized PToF distributions for mass fragments specific to each material (middle and bottom panels). The PToF data are normalized such that the value at the mode diameter matches the overall mass fraction of each material in a given averaging period. Interestingly, it appears that there is a maximum in squalane mass fraction at roughly 300 nm. This is likely an artifact—recent work in our group (referring here to Chapter 3 in this thesis) has shown that SOA from  $\alpha$ -pinene ozonolysis exhibits delayed vaporization, which causes an artificial broadening of the mass distribution at large sizes (Cross et al., 2009). Indeed, the mass fraction squalane as calculated by single-particle data show higher values than the PToF data at these large particle sizes, as shown in the top panel of Figure 4.3. Because single-particle size is optically-determined (and not determined by arrival as the MS), there is no artifact associated with delayed vaporization. Thus, the true mass fraction of squalane at large diameters is greater than the plot suggests.

Nonetheless, these data allow us to answer the following question: is squalane evaporating from particles across the size-range, or only for some particle sizes?

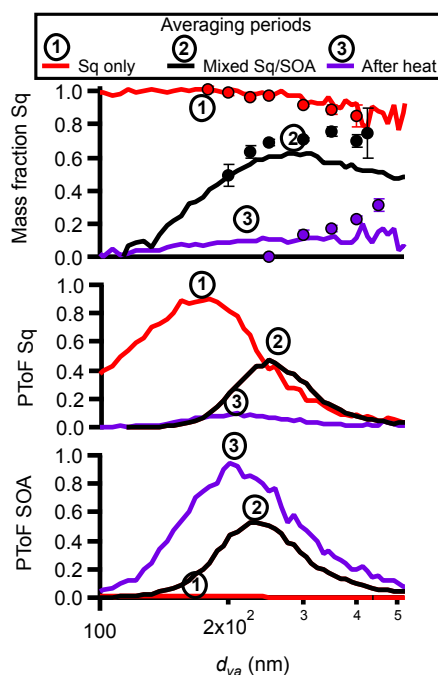


Figure 4.3: Size-resolved composition for a mixed-particle experiment where squalane particles serve as seeds for SOM condensation. The three shaded averaging periods are the same as those from Figure 2:  $D_{62}$ -squalane only (red), post-SOA formation and condensation onto seed particles (black), and after heating the smog chamber (purple). These plots demonstrate the size-dependence of SOM condensation on the squalane seeds, and that squalane is evaporating across all sizes with heating. Top panel shows the mass fraction of  $D_{62}$ -squalane to the total OA versus size for all three intervals, as calculated from PToF-mode (lines) or single-particle-mode (circles) data. Middle and bottom panels show the normalized evolution of the PToF data for each marker fragment ( $m/z$  66, middle and  $m/z$  43, bottom). Each mass distribution was first normalized by dividing by the value of the mode, and then weighting the normalized distribution by the overall mass fraction of squalane or SOA.

Consider the following: perhaps the decrease in the bulk squalane mass fraction (blue trace, Figure 4.2a) largely is influenced by evaporation of the largest squalane particles, with the smallest relative amount of condensed SOA? The difference between the black and purple traces in Figure 4.3 shows that this is not the case, and that squalane evaporates significantly across the entire size distribution. For reference, if we assume a core-shell morphology (with SOA coating the squalane core), a 250 nm particle in this system has roughly a 40 nm thick SOA shell. Re-

searchers often assume that coating experiments produce particles with the second constituent forming a shell around a core made up of the first constituent. However, for two phase systems there is likely only one minimum free energy morphology. Here, we do not know whether the SOA or the squalane has a lower surface tension and thus do not know which morphology is preferred.

When we prepare the mixed-particles in reverse order—SOA seed particles serving as condensational surface area for flash vaporized squalane—we similarly see growth of particles to larger sizes without any nucleation. Consistent with our earlier diagnosis of phase-separation within individual particles, we see a size-dependence to the mass fraction of squalane across particle size, shown in Figure 4.4. Upon heating the smog chamber to 44 °C, we see significant evaporation of squalane across all particle sizes, with the bulk mass fraction of squalane decreasing from 0.75 to 0.1 before and after heating (Figure 4.4a). The evaporation profile of squalane is qualitatively the same regardless of the order in which the mixed-particles are made.

#### 4.3.3 Collection efficiency of mixed SOA/Squalane particles

We looked at particle collection efficiency (CE) as a potential probe for particle morphology in the mixed-particle experiments. Particle CE is governed largely by the propensity for a particle type to bounce (or not) from the AMS vaporizer before it is able to vaporize (Docherty et al., 2013), subsequently leading to ionization and detection. Sub-unit CE for OA has been attributed to solid or semi-solid particles with greater likelihood to bounce off the AMS vaporizer surface before vaporization/ionization can occur, compared to liquid particles, which are collected with a near-unit CE (Alfarra, 2004). Figure 4.5 shows CE as a function of squalane mass fraction. The accompanying cartoons indicate what a core-shell morphology would hypothetically look like if the layering follows the same order in which the mixed-

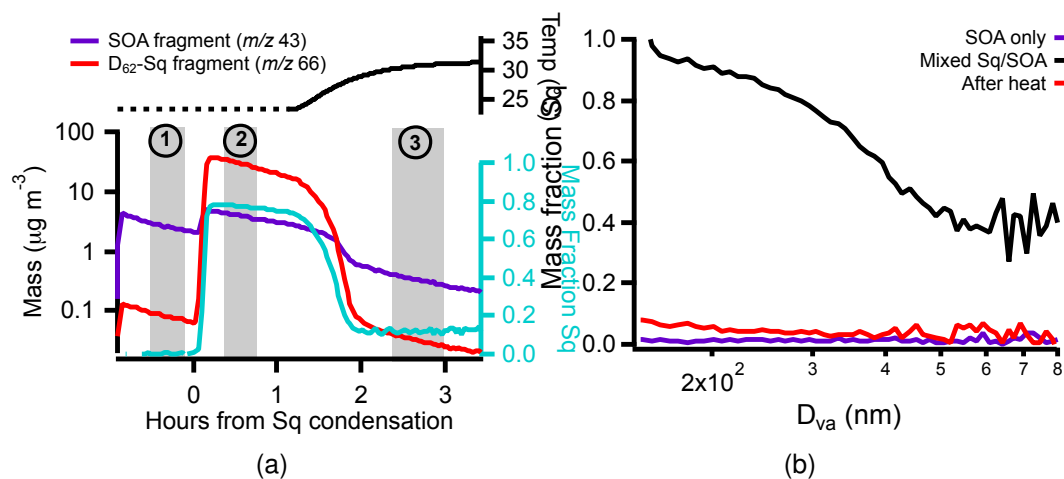


Figure 4.4: Mixed-particle experiment where SOA particles serve as seeds for squalane condensation, followed by a heating ramp. **(A)** Time-series showing mass of two AMS fragments that are tracers who each component:  $m/z$  43 for SOA (purple trace) and  $m/z$  66 (red trace). Mass fraction squalane, as calculated by equation (1), is shown in blue, and smog chamber temperature in black. The dotted line indicates that data was not digitized, but was confirmed to be  $\sim 23$  °C from a real-time display. **(B)** Mass fraction squalane as a function of particle size, as calculated from PToF data, similar to Figure 3.

particles were prepared. The numbers refer to each of the three stages of the experiment: seed particles only, seed particles with the condensed coating layer, and the particles after heating. Regardless of the ordering in which these mixed-particles were formed (SOA as seeds for squalane condensation, or squalane as seeds for SOA condensation), CE can be parameterized as a function of squalane mass fraction. Given that CE can be described solely as a function of squalane mass fraction, it is possible that a morphological reordering may have occurred in either or both experiments, and that the sampled particles have the same morphology regardless of the preparation order. On the other hand, particle bounce is a complex phenomenon governed by kinetic energy transfer from particle to vaporizer, and both the phases of the particle surface and the core are likely important. Thus, we can draw no definitive statements about morphology from these data, though this plot separately highlights the need to understand CE in AMS data where the phase-state of particles is dynamic over the course of a measurement

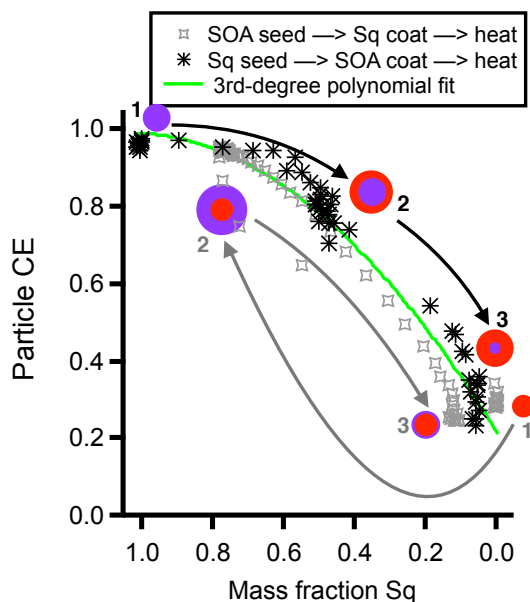


Figure 4.5: Particle collection efficiency as a function of squalane mass % for mixed-particle experiments followed by a heating ramp. Particles were prepared in two different ways: SOA seeds with squalane condensation (gray), and squalane seeds with SOA condensation (black). Cartoons illustrate what particles would look like if morphology is core-shell and follows the preparation sequence without any rearrangement of the two phases (where red represents SOA and purple represents squalane). Numbers demarcate each stage of the experiment seed particles only (1), mixed-particles (2), mixed-particles after heating (3). The CE parameterization as a function of squalane mass fraction is shown in green. A third-order polynomial of the following form was used to correct the AMS mass data for non-unit CE:  $CE = K_0 + K_1 \cdot \chi_{Sq} + K_2 \cdot \chi_{Sq}^2$ .

period.

#### 4.3.4 Comparative volatility analysis of mixed-particles

Figure 4.6 illustrates the process of using the CE parameterization to estimate the SOA mass fraction remaining (MFR) after the smog chamber is heated. The top panel shows the calculated CE to be used for all organic mass in the AMS, along with the smog chamber temperature. Panel two shows how the CE correction is applied to  $m/z$  43 (a tracer for SOA in this system). After applying the CE correction, a 1st-order exponential wall loss curve is fit to  $m/z$  43 to find the particle wall-loss

constant for the time-period after SOA formation and prior to heating. In panel three, MFR is plotted for SOA using  $m/z$  43 as a tracer with and without correcting for changing CE. MFR is calculated as follows:

$$\text{MFR} = \frac{m/z\ 43}{m/z\ 43_{fit}} \quad (4.2)$$

where the numerator is normalized by the extrapolated mass based on our wall-loss fit ( $m/z$  43<sub>fit</sub>). This approach of estimating MFR requires two assumptions. First, we assume that the mass of  $m/z$  43 decays according to first-order wall loss (e.g. Tkacik et al., 2012), and would continue to do so as extrapolated without any heating. Second, we assume that  $m/z$  43 is a perfect tracer for all components of the SOA over the entire heat range explored here. Previous studies have shown that the fraction of  $m/z$  43 for "pure" SOA ( $f_{43}$ ) decreases upon heating, meaning that at higher temperatures the OA is relatively enriched in molecules that contribute less to the  $m/z$  43 fragment than at the reference temperature. This would mean that our MFR measurements would be biased low, as  $m/z$  43 might underrepresent the total amount of SOA. Based on thermally-denuded SOA measurements by Lambe et al (Lambe et al., 2011), there is a very minimal decrease in  $f_{43}$  at temperatures similar to those in our smog chamber heat ramp (between 0 and 15% for MFR decrease from 1 to 0.5), we anticipate this bias to contribute at most 15% error to the SOA MFR.

We calculate the SOA MFR to be  $\sim 1$  in both of these mixed-particle experiments where SOA was formed on squalane seed particles. On the other hand, approximately 95% and 70% of the squalane evaporates (for a.) and b.), respectively). This comparative volatility analysis allows us to conclude that the overwhelming majority of this SOA is made of less-volatile compounds than squalane.

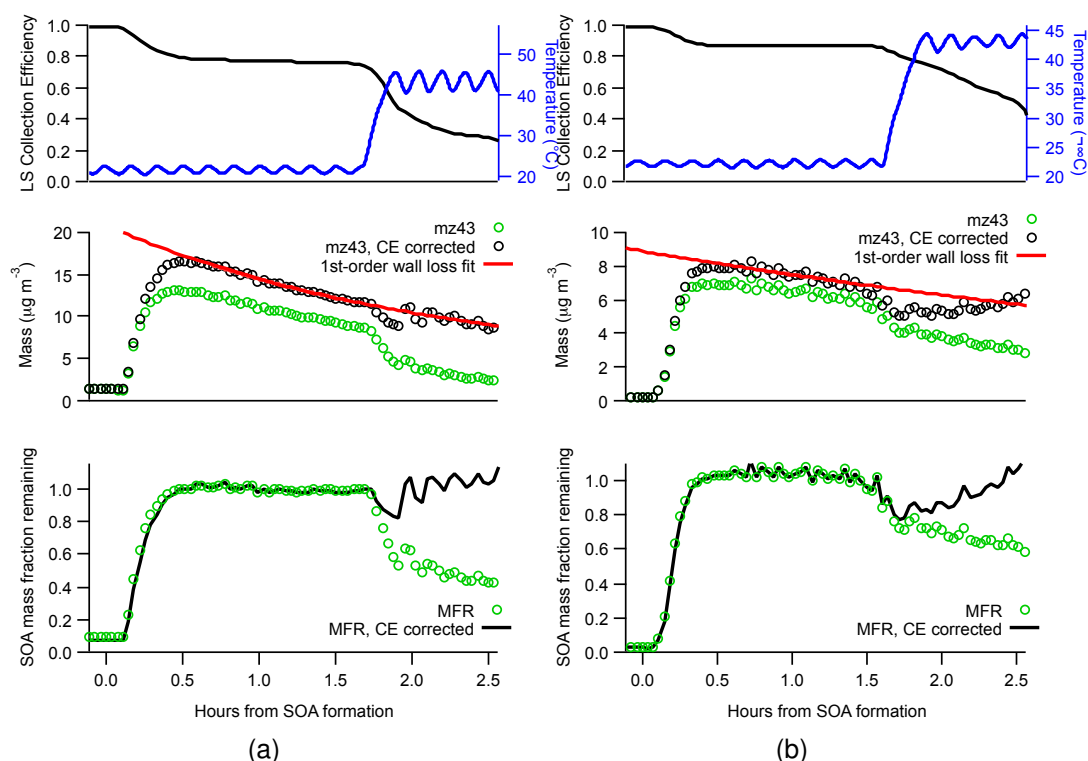


Figure 4.6: Time series illustrating steps to calculate the amount of SOA evaporated after smog chamber heating from 22 to 44 °C for two mixed-particle experiments. For both **(A)** and **(B)**, collection efficiency is parameterized according to the fitted equation from Figure 4.5 above, and follow a similar heat-ramp, shown by blue trace in top panel. The uncorrected and CE-corrected  $m/z$  43 masses are shown in the middle panel, along with the first-order exponential fit used to extrapolate the mass if there were no heating. The SOA mass fraction remaining (MFR) is calculated by dividing the measured mass with the wall loss fit, shown in the bottom panel. These corrections are necessary to estimate the MFR of SOA after heating because we know that CE is variable throughout this experiment. In both of these experiments, to first-order there is no substantial decrease in SOA mass after heating.

#### 4.4 Discussion

We have shown that when one sequentially prepares mixed squalane/SOA particles, and then heats them, squalane significantly, and preferentially, evaporates. This is illustrated by a bulk measurement of the mass fraction of squalane, but further supported by size-resolved mass distributions of marker mass spectral fragments and mass signals from individual particles. Remaining unanswered, how-

ever, is the following question: what is the particle morphology in this system? The answer has important implications for condensed-phase diffusivity.

Are the particles core-shell with squalane inside an SOA coating? This would be the naive explanation based on the order in which the particles were formed. Depth-profiling measurements of a very similar system (DOP seeds serving as condensational surface area for SOA) indicate that the morphology would be core-shell with squalane inside the SOA. Other morphologies should be considered as well. The full spectrum of possible morphologies is presented in Figure 4.7.

Perhaps there is a lens or partially-engulfed morphology, as has been demonstrated for liquid-liquid phase separated systems recently (Reid et al., 2011). Or perhaps the condensing SOA burrows into the squalane and the morphology is core-shell but reversed, with SOA as the core and squalane as the outer shell? The measurements we have presented here can only be used to infer possible morphologies—they can not definitively diagnose what the particles look like.

There must exist some lowest-energy configuration of two immiscible, condensed phases combined in a droplet suspended in air. Reid et al. present the general form of spreading coefficient ( $S_1$ ) of phase 1 on phase 2 for a droplet suspended in air (phase 3) for this system. For SOA in this mixed SOA/squalane system, the spreading coefficient is given by:

$$S_{SOA} = \sigma_{Sq,air} - (\sigma_{SOA,Sq} + \sigma_{SOA,air}) \quad (4.3)$$

where  $\sigma_{ij}$  is the surface tension at the interface of phase i and phase j. Likewise, we can write the spreading coefficient for squalane as:

$$S_{Sq} = \sigma_{SOA,air} - (\sigma_{Sq,SOA} + \sigma_{Sq,air}) \quad (4.4)$$

If  $S_{SOA}$  is negative, the the energy required to expand the area of the SOA-air

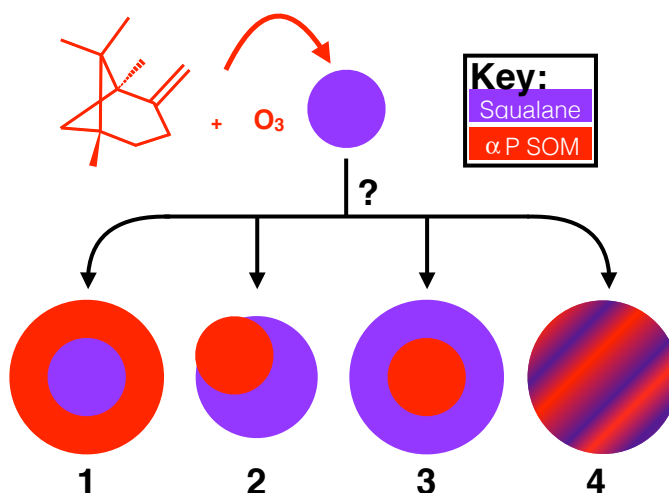


Figure 4.7: Cartoon depicting the formation process of mixed-particles prepared from SOM (from  $\alpha$ -pinene +  $O_3$ ) condensation on squalane seeds. Four possible morphologies are presented in cartoons labeled 1-4, which describe core-shell (SOM on top of squalane), partially-engulfed, core-shell (squalane on top of SOM), and well-mixed morphologies, respectively. The well-mixed morphology is ruled out by the two-population mixing experiment.

surface and SOA-Sq interface is too large to be recovered from the energy gained by the loss of the Sq-air surface. If  $S_{Sq}$  is also negative, then the squalane will not fully spread over the SOA, and a partially-engulfed structure emerges as the most stable configuration for the particle. If  $S_{Sq}$  is positive (while  $S_{SOA}$  is negative), then the spreading of the squalane over the SOA would lead to a core-shell structure with squalane on the outside. If  $S_{SOA}$  is positive and  $S_{Sq}$  is negative, then the stable configuration would be core-shell with SOA on the outside.

Squalane has a surface tension of  $26 \text{ mN m}^{-1}$  (Lafosse and Dreux, 1980) The surface tension of SOA, however, is unknown. A value of  $50 \text{ mN m}^{-1}$  has been used to model evaporation kinetics of SOA in a thermodenuder, but the results of these models are quite insensitive to the surface tension parameter (Lee et al., 2011). The surface tension of mixed-particles consisting of SOA (from  $\alpha$ -pinene +  $O_3$ ) and NaCl in cloud condensation spans a wide range ( $\sim 80 \text{ mN m}^{-1}$  down to

18 mN m<sup>-1</sup> for SOA dry volume fractions 0.6 to 0.88, respectively), and decreases with increasing SOA mass fraction, implying that the value for “pure” SOA might be quite low relative to water (Ruehl et al., 2012). Theoretically, the surface tension of any organic compound depends solely on its potential of ionization and molecular diameter, and is uncorrelated with polarity (Bormashenko, 2010). Thus, to what degree the SOA is comprised of oligomers should have a large impact on its surface tension. Regardless, the SOA surface tension is unknown. Additionally, the Sq-SOA interfacial tension is unknown, which could potentially have a large effect on the spreading coefficient values. Lastly, if a metastable core-shell configuration is formed (e.g. SOA shell, squalane core), but the opposite core-shell configuration is more energetically favorable (e.g. squalane shell, SOA core), it is conceivable that the shift to the stable configuration still might not occur. If some non-spherical geometry must be adopted to make the shift, then the energy required to reach the more stable state could make the shift unfavorable.

Both Vaden et al and Kolesar et al provide evidence for core-shell morphology in mixed-particles prepared from squalane seed particles serving as surface area for SOA condensation (Vaden et al., 2010; Kolesar et al., 2014). Vaden et al, using single-particle laser-ablation mass spectrometry, report a core-shell morphology for SOA-coated DOP in which the SOA remains on the outside the DOP core for the duration of their experiment (multiple hours). They infer this morphology using variable laser pulses designed to ablate only a fraction of the outer layer, and calibrate their technique using SOA/NaCl particles where SOA unequivocally is on the outside of the NaCl seeds. Kolesar et al invoke a core-shell morphology with SOA on the outside to explain the enhanced effective uptake coefficient with respect to squalane for SOA/squalane particles compared to bare squalane particles. These studies provide reason to believe that SOA forms a shell around a squalane core when the mixed-particles are prepared by condensing SOM on squalane seed par-

ticles.

The true particle morphology in this work has implications for the larger findings of this work. In our mixed-particle experiments, the majority (~60-95%) of the squalane mass rapidly evaporates into the gas-phase upon heating, while almost all of the SOA mass remains. Thus, if the morphology of these particles is core-shell with SOA on the outside, then there are very minimal diffusive limitations to the evaporation of squalane through the SOA layer at this elevated temperature. The majority of squalane mass would be moving, on the order of tens of minutes, through a substantial SOA coating (e.g. 40 nm thick SOA shell for a 250 nm particle). This data would be in disagreement with a number recent studies that make a case for organic diffusion coefficients in SOA being so low that equilibration might not be possible on atmospheric timescales (Perraud et al., 2012; Zelenyuk et al., 2012; Abramson et al., 2013).

If, on the other hand, the SOA trades places with the squalane, and the squalane forms the shell, or if the morphology is partially engulfed, then our data say nothing about organic diffusivity within the condensed SOA phase. In either of these cases, squalane would have an interface with air, and evaporation could simply proceed through this "window" to meet the new equilibrium saturation concentration at elevated temperature.

In summary, we find that studying the evaporation of mixed-particles has the potential to directly probe the diffusivity of SOA, though knowledge of particle morphology is crucial. Additionally, evaporation studies of mixed-particles can be used to constrain the fraction of the multi-component material (SOA in this case) with lower volatility than the pure-component material with known vapor pressure. We find that, to first order, all of the SOA has a volatility lower than that of squalane, and this comparative volatility analysis could be extended to other systems. We also provide further evidence that adds to previous work showing that hydrophobic

pure-component OA and SOA from  $\alpha$ -pinene + O<sub>3</sub> form separate phases (Song et al., 2007; Vaden et al., 2010). This exercise demonstrates that more studies on OA phase state and morphology are critical to fill our current gaps in knowledge of organic aerosol transformation in the atmosphere. Very clearly here, particle morphology is essential for determining the larger implications of this work.

#### 4.5 Conclusions and future work

In this study, we have shown five important things: First, we demonstrated that two-population mixing experiments inform phase-behavior for mixed-particle systems, and specifically that squalane and SOA (from  $\alpha$ -pinene + O<sub>3</sub>) do not mix. Second, we show that squalane can evaporate from mixed squalane/SOA particles on chamber-relevant timescales ( $\sim 1$  hour). Third, we demonstrate the utility of single-particle and bulk size-resolved composition data to show how squalane evaporates from particles across the entire size-range. We also present a parameterization of collection efficiency in this system that is independent of the order of preparation. Lastly, we present a comparative volatility analysis that demonstrates, to first order, that all of the SOA has volatility lower than that of squalane.

Remaining unresolved in this study is a quantification of squalane diffusivity through the SOA matrix ( $D_{org}$ ). In future work, we plan to simulate the movement of squalane through an SOA shell, using a kinetic layer model and comparing to data from these experiments. The kinetic layer model will resemble a simplified version of K2-SURF from Shiraiwa et al., 2012 (also used in Zhou et al., 2013). Size-distributions of the mixed-particles will provide particle size and SOA coating thickness as a starting point for the model. For mixed-particles prepared using squalane as seeds for SOA condensation, we will explore how closely the model, assuming this core-shell morphology, can recreate the observed evaporation profile of squalane. This will provide an estimate of  $D_{org}$  of squalane through SOA.

## Bibliography

- [1] Evan Abramson et al. "Experimental determination of chemical diffusion within secondary organic aerosol particles". *Physical Chemistry Chemical Physics* 15.8 (2013), p. 2983.
- [2] M Rami Alfarra. "Chapter Four: Laboratory Characterisation of the Aerodyne Aerosol Mass Spectrometer" (Nov. 2004), pp. 1–20.
- [3] A Asa-Awuku et al. "Mixing and phase partitioning of primary and secondary organic aerosols". *Geophysical Research Letters* 36.15 (Aug. 2009).
- [4] Edward Bormashenko. "Why do surface tensions of most of organic liquids demonstrate close values?" *arXiv* (May 2010), pp. 1–11.
- [5] ES Cross et al. "Single particle characterization using a light scattering module coupled to a time-of-flight aerosol mass spectrometer". *Atmospheric Chemistry and Physics* 9 (2009), pp. 7769–7793.
- [6] Peter F DeCarlo et al. "Field-Deployable, High-Resolution, Time-of-Flight Aerosol Mass Spectrometer". *Analytical Chemistry* 78.24 (Dec. 2006), pp. 8281–8289.
- [7] Kenneth S Docherty et al. "Collection Efficiency of the Aerosol Mass Spectrometer for Chamber-Generated Secondary Organic Aerosols". *Aerosol Science and Technology* 47.3 (Mar. 2013), pp. 294–309.
- [8] Neil M Donahue et al. "Volatility and aging of atmospheric organic aerosol" (2014), pp. 97–143.
- [9] Mikael Ehn et al. "A large source of low-volatility secondary organic aerosol". *Nature* 506.7489 (Apr. 2015), pp. 476–479.
- [10] J L Jimenez et al. "Evolution of Organic Aerosols in the Atmosphere". *Science* 326.5959 (Dec. 2009), pp. 1525–1529.
- [11] H Kokkola et al. "The role of low volatile organics on secondary organic aerosol formation". *Atmospheric Chemistry and Physics* 14.3 (2014), pp. 1689–1700.
- [12] Katheryn R Kolesar et al. "OH-Initiated Heterogeneous Oxidation of Internally-Mixed Squalane and Secondary Organic Aerosol". *Environmental Science & Technology* 48.6 (Mar. 2014), pp. 3196–3202.
- [13] M Lafosse and M Dreux. "Étude du mélange binaire squalane-stéaronitrile comme phase stationnaire: I. Comparaison des résultats provenant d'une étude par chromatographie en phase gazeuse avec ceux résultant des mesures de tension superficielle". *Journal of Chromatography A* 188.2 (1980), pp. 315–322.

- [14] A T Lambe et al. "Laboratory studies of the chemical composition and cloud condensation nuclei (CCN) activity of secondary organic aerosol (SOA) and oxidized primary organic aerosol (OPOA)". *Atmospheric Chemistry and Physics* 11.17 (2011), pp. 8913–8928.
- [15] Byong-Hyoek Lee et al. "Volatility of secondary organic aerosol from the ozonolysis of monoterpenes". *Atmospheric Environment* 45.14 (May 2011), pp. 2443–2452.
- [16] S Liu et al. "Organic particle types by single-particle measurements using a time-of-flight aerosol mass spectrometer coupled with a light scattering module". *Atmospheric Measurement Techniques* 6 (2013), pp. 187–197.
- [17] Christine L Loza et al. "On the Mixing and Evaporation of Secondary Organic Aerosol Components". *Environmental Science & Technology* (May 2013), p. 130531150231004.
- [18] Ryan C Moffet et al. "Chemically segregated optical and microphysical properties of ambient aerosols measured in a single-particle mass spectrometer". *Journal of Geophysical Research* 113.D12 (June 2008), p. D12213.
- [19] JF Pankow and WE Asher. "SIMPOL. 1: a simple group contribution method for predicting vapor pressures and enthalpies of vaporization of multifunctional organic compounds". *Atmospheric Chemistry and Physics* 8.10 (2008), pp. 2773–2796.
- [20] R K Pathak et al. "Ozonolysis of  $\alpha$ -pinene: parameterization of secondary organic aerosol mass fraction". *Atmospheric Chemistry and Physics* 7.14 (2007), pp. 3811–3821.
- [21] V. Perraud et al. "Nonequilibrium atmospheric secondary organic aerosol formation and growth". *Proceedings of the National Academy of Sciences* 109.8 (2012), pp. 2836–2841.
- [22] Jonathan P Reid et al. "The morphology of aerosol particles consisting of hydrophobic and hydrophilic phases: hydrocarbons, alcohols and fatty acids as the hydrophobic component". *Physical Chemistry Chemical Physics* 13.34 (2011), p. 15559.
- [23] L Renbaum-Wolff and J W Grayson. "Viscosity of alpha-pinene secondary organic material and implications for particle growth and reactivity". *Proceedings of the . . .* 2013.
- [24] Ellis Shipley Robinson, Rawad Saleh, and Neil M Donahue. "Organic Aerosol Mixing Observed by Single-Particle Mass Spectrometry". *The Journal of Physical Chemistry A* 117.51 (Dec. 2013), pp. 13935–13945.
- [25] C R Ruehl et al. "Strong evidence of surface tension reduction in microscopic aqueous droplets". *Geophysical Research Letters* 39.23 (Dec. 2012), n/a–n/a.

- [26] Rawad Saleh, Neil M Donahue, and Allen L Robinson. "Time Scales for Gas-Particle Partitioning Equilibration of Secondary Organic Aerosol Formed from Alpha-Pinene Ozonolysis". *Environmental Science & Technology* (May 2013), p. 130517130052009.
- [27] M. Shiraiwa et al. "Kinetic multi-layer model of gas-particle interactions in aerosols and clouds (KM-GAP): linking condensation, evaporation and chemical reactions of organics, oxidants and water". *Atmospheric Chemistry and Physics* 12.5 (2012), pp. 2777–2794.
- [28] S Solomon et al. "Climate change 2007: The physical science basis, contribution of working group 1 to the fourth assessment report of the Intergovernmental Panel on Climate Change" (2007).
- [29] Chen Song et al. "Effect of hydrophobic primary organic aerosols on secondary organic aerosol formation from ozonolysis of alpha-pinene". *Geophysical Research Letters* 34.20 (Oct. 2007), p. L20803.
- [30] Ross Strader, Fred Lurmann, and Spyros N Pandis. "Evaluation of secondary organic aerosol formation in winter". *Atmospheric Environment* 33.29 (1999), pp. 4849–4863.
- [31] Daniel S Tkacik et al. "Secondary Organic Aerosol Formation from Intermediate-Volatility Organic Compounds: Cyclic, Linear, and Branched Alkanes". *Environmental Science & Technology* 46.16 (Aug. 2012), pp. 8773–8781.
- [32] I M Ulbrich et al. "Interpretation of organic components from Positive Matrix Factorization of aerosol mass spectrometric data". *Atmospheric Chemistry and Physics* 9.9 (2009), pp. 2891–2918.
- [33] T.D. Vaden et al. "Atmospheric Chemistry Special Feature: Morphology of mixed primary and secondary organic particles and the adsorption of spectator organic gases during aerosol formation". *Proceedings of the National Academy of Sciences* 107.15 (Apr. 2010), pp. 6658–6663.
- [34] T.D. Vaden et al. "Evaporation kinetics and phase of laboratory and ambient secondary organic aerosol". *Proceedings of the National Academy of Sciences* 108.6 (2011), pp. 2190–2195.
- [35] Rainer Volkamer et al. "Secondary organic aerosol formation from anthropogenic air pollution: Rapid and higher than expected". *Geophysical Research Letters* 33.17 (2006), p. L17811.
- [36] Alla Zelenyuk et al. "Synergy between Secondary Organic Aerosols and Long-Range Transport of Polycyclic Aromatic Hydrocarbons". *Environmental Science & Technology* 46.22 (Nov. 2012), pp. 12459–12466.
- [37] Shouming Zhou et al. "Kinetic limitations in gas-particle reactions arising from slow diffusion in secondary organic aerosol". *Faraday Discussions* 165 (2013), p. 391.

# Chapter 5

## Collection efficiency of $\alpha$ -pinene secondary organic aerosol particles explored via light-scattering single-particle aerosol mass spectrometry

*Collection and vaporization efficiencies for secondary organic aerosol (SOA) particles made from  $\alpha$ -pinene +  $O_3$  were investigated using the single-particle capabilities of the Aerosol Mass Spectrometer (AMS). Ensemble mass distributions for this SOA derived from  $\alpha$ -pinene ozonolysis were found to have artificially long tails at large sizes, an artifact of delayed vaporization, where particles do not vaporize immediately upon impacting the vaporizer. Count-based collection efficiency ( $CE_p$ ) for SOA across these experiments ranged from 0.26 to 0.42. Between roughly a quarter to half of the chemically-detected particles exhibited delayed vaporization. This delayed vaporization and low collection efficiency is attributable to the low volatility and/or the phase state of the SOA. Using the coupled optical and chemical detection of the light scattering single-particle (LSSP) module of the AMS, we provide clear evidence that “delayed vaporization” is somewhat of a misnomer for these particles: the SOA promptly vaporizes, but not on the primary impact with the vaporizer, rather a subsequent impact with a hot surface in the vaporization region. We also find that the ionization efficiency (defined as ions per particle) decreases with delayed arrival time. Though the  $CE_p$  was found not to be a function of particle size (for the mobility diameter range 170-460 nm), we see a decrease in  $CE_p$  with thermodynamic temperature, implying that oxidation state and/or volatility can determine  $CE_p$ . These results demonstrate the utility of LSSP to best understand AMS collection efficiency for laboratory aerosols.*

---

Originally prepared for publication as: Robinson, E.S. and Donahue, N.M.: Collection efficiency of  $\alpha$ -pinene secondary organic aerosol particles explored via light-scattering single-particle aerosol mass spectrometry. Atmos. Meas. Tech., 2014. *in preparation*

## 5.1 Introduction

Organic aerosol (OA) comprises a significant fraction of submicron atmospheric particulate mass, ranging from 20-90% (Kanakidou et al., 2005; Jimenez et al., 2009). OA has been shown to have negative impacts on human health (Lozano et al., 2013) and remains highly uncertain in its effect on radiative climate forcing (Solomon et al., 2007). The physical and chemical characteristics of OA can vary dramatically, and depend strongly on source, location, atmospheric age, and other factors. Despite the ubiquity and importance of OA, real-time measurements are technically challenging due to the wide range of chemical composition, particle size, and volatility represented by organic aerosols in the atmosphere.

The Aerosol Mass Spectrometer (AMS, Aerodyne Research, Inc.) has recently been widely used in both ambient and laboratory measurements of OA, and led to significant increases in our understanding of how organic aerosols form (Craven et al., 2012), age (Donahue et al., 2012), and mix, (Asa-Awuku et al., 2009; Robinson, Saleh, and Donahue, 2013) by providing real-time measurements of size-resolved composition and mass for submicron, non-refractory particulate matter (NR-PM<sub>1</sub>). However, a lingering challenge with full quantification in the AMS is the mass collection efficiency (Canagaratna et al., 2007), which is the ratio of the measured AMS mass signal to the actual NR-PM<sub>1</sub> concentration. To obtain quantitative agreement between the AMS and other collocated instruments in field campaigns, a mass collection efficiency (CE<sub>m</sub>) is usually applied to correct for the consistently lower AMS-measured mass. CE<sub>m</sub> can be written as:

$$CE_m = \frac{\text{AMS mass}}{\text{Ext mass}} \quad (5.1)$$

where "Ext mass" is the mass of another (perfectly calibrated) instrument. Impor-

tantly, this calculation assumes ideal operating conditions for both instruments and the application of all other appropriate correction factors. For example, Drewnick et al. (2003), in an sulfate aerosol intercomparison study, applied a scaling factor of 2.41 ( $CE_m = 0.41$ ) to the AMS-measured sulfate to achieve good agreement with a collocated particle into liquid sampler (PILS) instrument. Middlebrook et al. (2012) recently reported parameterizations of  $CE_m$  for ambient sulfate-containing particles that could be used to predict  $CE_m$  based on particle acidity and mass fraction of ammonium nitrate. High  $CE_m$  values were consistent with predicted liquid phase state at 298 K.  $CE_m$  should be thought of as a sensitivity factor that varies for particle types of different composition and phase state.

Huffman et al. (2005) define the  $CE_m$  as the product of three, size-dependent terms:

$$CE_m(d_{va}) = E_L(d_{va}) \times E_S(d_{va}) \times E_B(d_{va}) \quad (5.2)$$

Where  $E_L(d_{va})$  is the lens transmission efficiency as a function of aerodynamic diameter, ( $d_{va}$ );  $E_S(d_{va})$  is the striking efficiency of particles on the AMS vaporizer that have made it through the lens and entered the time-of-flight chamber; and  $E_B(d_{va})$  is the vaporization efficiency of particles that strike the vaporizer surface, also known as "bounce" efficiency as particles can bounce from the vaporizer surface away from the ionization region and any chance of detection by the mass spectrometer. Any particle that enters the instrument, but is not detected by the mass spectrometer due to any of these three loss terms, contributes to the mass discrepancy between the AMS and another (perfectly-calibrated) mass measurement.

Previous measurements and models have characterized the loss of particles in the lens region and orifice, and have shown near-unit transmission efficiencies for particles in the size-range of 60-600 nm. However, for particle populations whose distribution is significantly outside of the transmission window, especially for larger

particles,  $E_L(d_{va})$  can contribute significantly (20%) to  $CE_m$  (Quinn et al., 2006).  $E_S(d_{va})$  is a measurement of the divergence of the particle beam upon expansion into the time-of-flight (ToF) chamber. While spherical particles can be narrowly focused on the 3.8 mm-wide vaporizer over the distance of the ToF chamber, particle non-sphericity can lead to divergence of the particle beam (Huffman et al., 2005). Studies show this term accounts for close to 0% of particle loss for ambient aerosol (Salcedo et al., 2007), and laboratory SOA and  $(NH_4)_2SO_4$  (Docherty et al., 2013).  $E_S(d_{va})$  can be well-characterized by the use of a beam-width probe (Huffman et al., 2005).

In the majority of cases, the largest uncertainty and largest contributor to sub-unit  $CE_m$  is the particle bounce term,  $E_B(d_{va})$ . Particle bounce has long been known to confound particle measurements, such as impactors and surface-desorption mass spectrometers (e.g. Myers and Fite, 1975; Virtanen et al., 2010). A limited number of studies have investigated the nature and root cause of particle bounce for laboratory aerosols in the AMS. Alfarra (2004) identified phase as a controller of particle bounce for a selection of laboratory organics, where particle phase state was inferred from the room temperature properties of the bulk materials. Liquid particles had near-unit  $CE_m$ , while solid particles had much lower efficiencies (20 to 50%). Matthew, Middlebrook, and Onasch (2008) found phase to govern particle bounce as well. Dry ammonium nitrate particles, thought to be metastable liquids at their experimental conditions (Lightstone et al., 2000), were measured with high  $CE_m$ , while dry ammonium sulfate particles had  $CE_m = 0.22$ , which increased to 0.73 when the particles were hydrated and deliquesced. Dry ammonium sulfate was also shown to be more efficiently collected (bounced less) with increasing thickness of a dioctyl sebacate coating layer. In some chamber experiments, Bahreini et al. (2005) showed this same increase in  $CE_m$  for dry ammonium sulfate particles with condensation of an SOA layer. However, for other SOA ex-

periments,  $CE_m$  for ammonium sulfate seed particles actually decreased with the condensation of SOA, implying that SOA phase was highly variable in their experiments and/or that other factors also govern particle bounce in the AMS, such as composition and volatility. Docherty et al. (2013) report an inverse relationship between  $CE_m$  for chamber-generated SOA and the  $f_{44}/f_{57}$  ratio (where  $m/z$  44 and  $m/z$  57 are comprised almost solely of signals from  $\text{COO}^+$  and  $\text{C}_4\text{H}_9^+$ , and  $f_{m/z_i}$  is the fraction of  $m/z_i$  to the total organic signal), implicating oxidation state as a factor influencing  $CE_m$ .

An even smaller number of studies have used the light scattering single-particle (LSSP) module of the AMS to investigate collection efficiency, despite its ability to provide a real-time, particle number-based measurement of  $E_B(d_{va})$ . We denote this collection efficiency as  $CE_p$  for "particle collection efficiency." Cross et al. (2007) first introduced LSSP as a method to resolve real-time densities of externally-mixed aerosols. Cross et al. (2009) later described the ability of LSSP to measure the  $CE_p$  of ambient particles from Mexico City, and found that a significant fraction of the optically-detected particles were either undetected by the mass spectrometer due to bounce ("null") or exhibited signal at a time much later than would be expected based on their *in situ* measured velocity ("delayed"). "Prompt" particles, those that gave an appreciable chemical ion signal when they were expected to, made up only 23% of the measured aerosol, with the delayed fraction at 26% and the null fraction at 51%. Liu et al. (2013) also report  $CE_p$  for measurements taken in Bakersfield, CA (Cal-Nex). They report a 46% prompt fraction, 6% delayed, and 48% null, and found a slight size-dependence in the campaign-average  $CE_p$ , which exhibited a maximum around  $d_{va} = 600$  nm (0.52) and a minimum (0.42) for large particles. Slowik et al. (2009) compared  $CE_m$  (density-corrected SMPS/AMS comparison) and  $CE_p$  for an ambient biogenic SOA event, and found them to be equal.

Here we further explore the use of LSSP to identify the nature of collection ef-

efficiency for lab and chamber-generated aerosols. We quantify particle bounce for ammonium nitrate, ammonium sulfate, squalane, and SOA from  $\alpha$ -pinene ozonolysis. We illustrate the difference between mass-based and number-based CE, which are not necessarily the same even for monodisperse aerosol, due to decreasing ionization efficiencies for delayed particles (defined as ions per particle or IPP). We show that IPP decreases with delay time, that  $CE_p$  is not a function of size for the SOA in this study, and that low volatility and/or high oxidation state decreases  $CE_p$ .

## 5.2 Methods

Organic aerosol preparation steps, measurements, and data analysis are detailed in the following section.

### 5.2.1 Particle generation and sampling

Inorganic aerosols (ammonium nitrate, ammonium sulfate) were prepared by atomizing dilute solution (1 g/L) using a constant output nebulizer (aerosol generator model 3076; TSI, Inc.). These particles were sent through a krypton neutralizer (10 mC) then size-selected using a differential mobility analyzer (classifier model 3080; TSI, Inc.) before sampling. Size-selected SOA was sampled in this same manner, but had a different preparation procedure. A 1.2  $\mu$ L aliquot of  $\alpha$ -pinene ( $\sim$  2 ppm) was injected into a clean 100-L Tedlar sample bag (SKC, Inc.), charged with excess ozone. It should be noted that the SOA produced in this way was formed at high OA concentration ( $C_{OA} \approx 1500 \mu\text{g m}^{-3}$ ). Doing so allowed us to study homogeneously nucleated SOA with the single-particle capability of the AMS, as the scattering laser requires large ( $d_{va} \geq 180 \text{ nm}$ ) particles. See Figure 5.1 for the general experimental schematic.

Squalane aerosols were produced directly in the 12 m<sup>3</sup> Carnegie Mellon Uni-

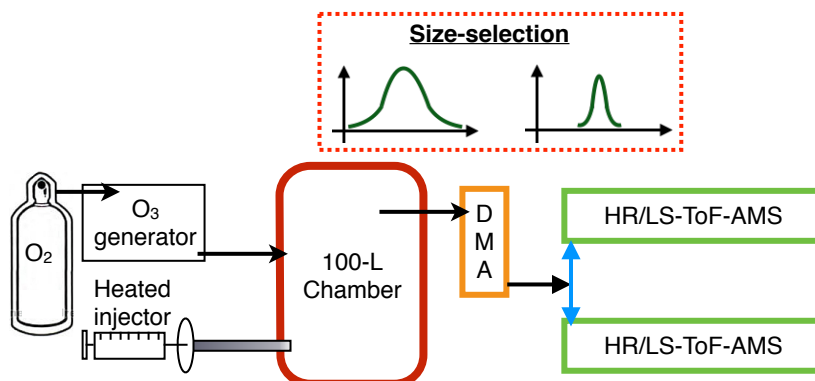


Figure 5.1: Experimental schematic for size-selected CE experiments. In all experiments, a DMA was used to size-select particles from an aerosol source (e.g. a small chamber filled with SOA in this case) before sampling with the SMPS and HR-ToF-AMS.

versity smog chamber, described elsewhere in greater detail. In brief, the smog chamber was flushed continuously for  $> 12$  h with clean, dry air (cleaned with HEPA, silica-gel, and activated-carbon filters in series) to ensure low background particle, organic vapor, and water concentrations. Squalane particles were prepared by flash vaporization using a small, resistive stainless-steel heater. A small aliquot of squalane ( $0.75 \mu\text{L}$ ) was placed on the heater surface, which was then inserted into the smog chamber. Clean dispersion air flowed through the heater to carry and mix the squalane plume into the chamber as the heater was power-cycled for 10 minutes. Pure squalane particles formed as the vapor plume cooled.

Ensemble particle volume and number concentrations were measured using a Scanning Mobility Particle Sizer (SMPS; TSI, Inc.). Ensemble composition and mass was measured with the High-Resolution Aerosol Mass Spectrometer (HR-ToF-AMS; Aerodyne, Inc.) operated in single-reflectron V-mode, fully described by DeCarlo et al. (2006). Single-particle mass spectra were acquired using the light-scattering single-particle (LSSP) module coupled to the HR-ToF-AMS.

### 5.2.2 Operation of light-scattering module

The LSSP module has been described in detail elsewhere in the literature. Briefly, the LSSP module consists of a continuous wave laser (405 nm, 50-mW; LC BCL-050-405; CrystaLaser) that crosses the collimated particle beam within the time-of-flight region of the AMS. Scattered light from sampled particles is collected by an ellipsoidal mirror that focuses the light onto a photomultiplier tube. This light scattering signal constrains the particle's velocity between the opening of the AMS chopper and the laser, allowing for the calculation of the vacuum aerodynamic diameter. It also prompts the saving of individual mass spectra over the entire chopper cycle (e.g. 200 spectra/chopper), allowing for the identification of signals from individual particles within the chopper cycle. Saving at this data rate without the laser triggering is not practically useful, as it results in an unmanageable data load. For example, when Drewnick et al. (2005) collected ToF-AMS single particle data without any triggering mechanism, of the 2.41 GB of data they collected, only 4 MB represented meaningful single-particle spectra after applying their thresholding algorithm. The LSSP allows for continuous single-particle detection at a high duty cycle for the long timescales of chamber studies or ambient sampling.

For data processing, we used an operationally-defined light-scattering threshold of five (signal-to-noise) to identify particle events, and a mass threshold of 6 ions to identify a detected particle to be further considered for particle classification, similar to Liu et al. (2013). At the number concentrations of the high- $C_{OA}$  SOA experiments, coincident particles—multiple particles sampled in a single chopper cycle—were present (12.66% of particles were coincident), but identifiable from the scattered light signal. For typical smog chamber number concentrations (e.g.  $\leq 2,000 \text{ cm}^{-3}$ ), the probability for coincidence is rare. We expect  $\sim 1$  particle per chopper cycle for a 1% chopper slit ( $\sim 70 \mu\text{s}$  wide). Coincident particles were

filtered out using custom LSSP software<sup>1</sup> and we did not consider them in our analysis or calculation of  $CE_p$ .

### 5.2.3 Calculation of collection efficiency

Individual particle events were classified based on how they interacted with the vaporizer, in terms of both ionization efficiency and vaporization quickness. As defined in Cross et al. (2009), particles defined as “prompt” arrived at the mass detector within a narrow time range after they would be expected to arrive based on their measured velocity in the ToF region and assuming instantaneous vaporization/ionization. The operationally-defined boundary between the prompt and delayed particles is when the actual arrival of the mass signal differs from the expected arrival time by 20% or more. In other words, we compared the measured arrival time at the detector ( $MS_{arrival}$ ) and the LS-estimated arrival time ( $LS_{arrival}$ ) based on the measured velocity between the chopper and laser to draw the boundary between prompt particles ( $MS_{arrival}/LS_{arrival} < 1.2$ ) and delayed particles ( $MS_{arrival}/LS_{arrival} > 1.2$ ).

LSSP provides an internal number-based measure of the AMS collection efficiency (Cross et al., 2009). The wide laser beam ( $\approx 2$  mm), relative to the width of the particle beam ( $\approx 0.5$  mm), allows for near complete optical detection of particles above the detection limit of the laser ( $d_{va} > 180$  nm). The LSSP-based  $CE_p$  is the comparison between the optically-detected particles (i.e. all particles that enter the TOF region and will hit the vaporizer surface) and particles that are chemically-detected (i.e. give signal in the mass spectrometer).

$$CE_p = \frac{N_{prompt} + N_{delayed}}{N_{prompt} + N_{delayed} + N_{null}} \quad (5.3)$$

<sup>1</sup>Sparrow 1.04A, written by D. Sueper, Aerodyne Research Inc. and University of Colorado at Boulder; available at <http://cires.colorado.edu/jimenez-group/ToFAMSResources/ToFSoftware/index.html> Analysis4

In this formulation, we consider both prompt and delayed particles as those that give meaningful chemical signals at the detector, though it may be of interest in other studies to look at the  $CE_p$  from e.g. only prompt particles. We are equating CE with  $E_B$ , a reasonable assumption for the aerosols studied here as they all fall within the lens transmission window ( $E_L = 1$ ) and are spherical and thus do not exhibit significant divergence from the particle beam ( $E_S = 1$ ). However, it is important to note this collection efficiency accounts only for whether or not a particle was observed in the mass spectrometer, and does not account at all for signal strength.

### 5.3 Results and Discussion

#### 5.3.1 Delayed vaporization PToF artifact

It is standard practice to present comparisons between the mass-weighted size distribution from the SMPS and the particle time-of-flight mass distribution from the AMS to compute density and collection efficiency (DeCarlo et al., 2004; Kostenidou, Pathak, and Pandis, 2007). The SMPS size-distribution is multiplied by the density such that the mode diameters align, according to,

$$d_{va} = \frac{\rho_p d_{ve}}{\rho_0 \chi} \quad (5.4)$$

where  $\rho_p$  is particle density,  $\rho_0$  is standard density ( $1 \text{ g cm}^{-3}$ ), and  $\chi$  is the dynamic shape factor, which is equal to one for spherical particles and is assumed to be true in the case of SOA from  $\alpha$ -pinene ozonolysis (Zelenyuk et al., 2008)). For spherical particles,  $d_{ve}$ , the volume equivalent diameter, is equal to mobility diameter. We estimate the density to be  $1.11 \text{ g/cm}^3$  from aligning the AMS and SMPS mode diameters, and the mass collection efficiency,  $CE_m$ , to be 0.46 from comparing the integrated PToF and SMPS mass distributions for one of our SOA experiments, shown in Figure 5.2. The particle collection efficiency for this experiment,  $CE_p$ ,

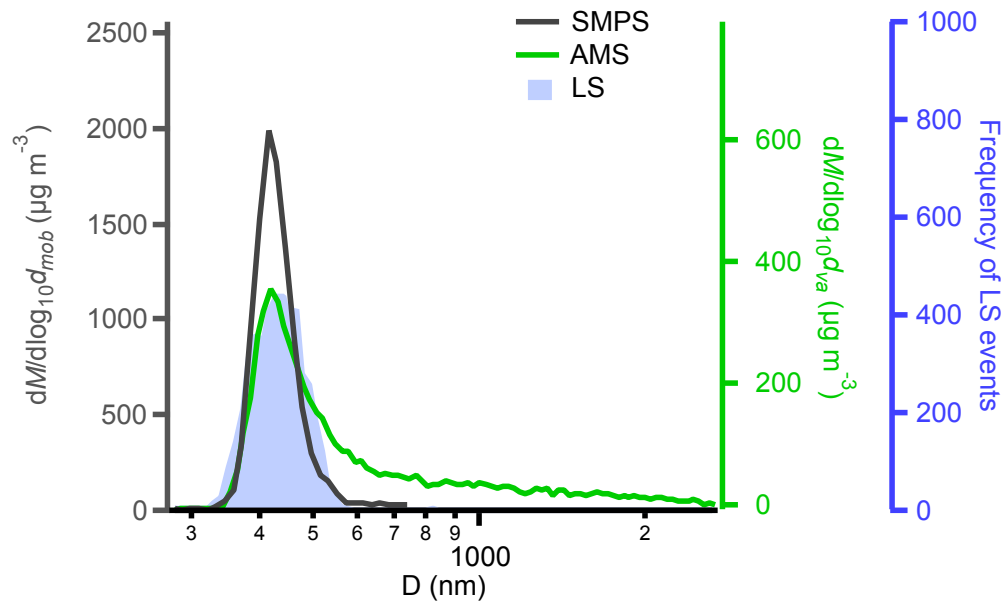


Figure 5.2: Ensemble mass distributions from SMPS (black) and AMS (green) of size-selected  $\alpha$ -pinene derived SOA particles with 370 nm mobility diameter. Frequency of optically-counted particles (from LSSP) as a function of size shown in blue.

is 0.42. The shaded blue area is the frequency of optically-counted particles as a function of size, as measured by light-scattering in the AMS. Like the SMPS distribution, this histogram is tight, as we expect it to be for size-selected particles. However, even after shifting the SMPS distribution by the density, the agreement between the two distributions degrades considerably at large diameters.

We explore the nature of this diverging agreement between the two size distributions at large diameters using data from LSSP mode, which provides single-particle light scattering and mass-spectral data. The flight path, and resulting data, for a single-particle in the AMS are shown in Figure 5.3. The scattered light pulse (magenta) triggers the saving of mass spectra over the entire chopper cycle. Individual extractions from the mass spectrometer, which are usually averaged together over tens of seconds to minutes, are resolved at  $\sim 10$  microseconds in single-particle mode. Using the distance between the chopper and the point of intersection be-

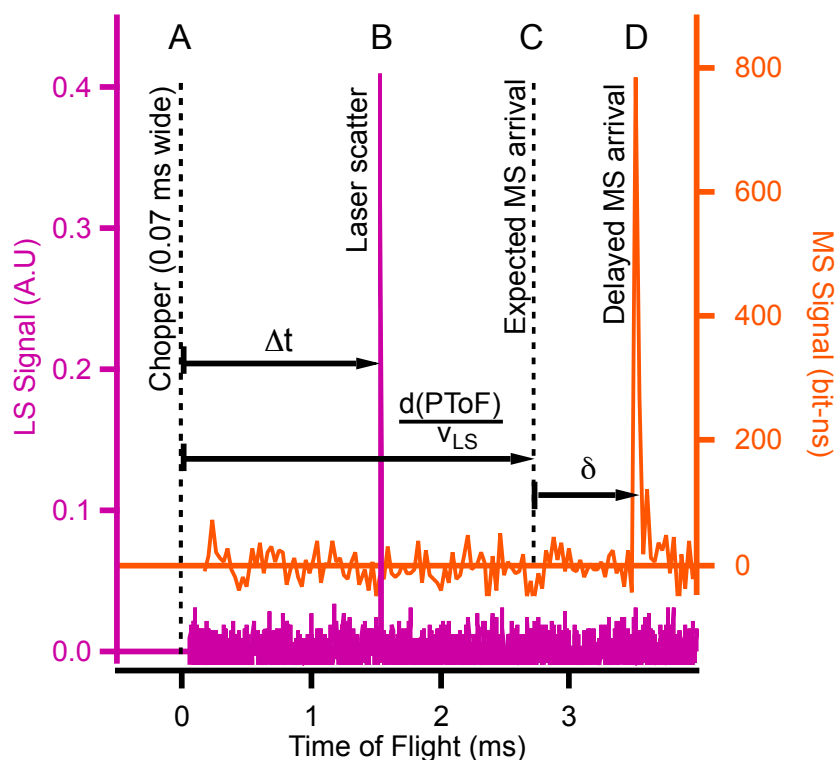


Figure 5.3: Scattered light (magenta) and mass spectrometer signal (orange) as a function of particle time-of-flight. The particle velocity ( $v$ ) is calculated by the measured time between the start of the chopper cycle (**A**) and detection of the scattered light peak (**B**). The velocity is used to estimate an expected arrival time of the chemical ion signal at the mass spectrometer (**C**) assuming prompt evaporation and ionization of the particle at the vaporizer. The difference between the expected (**C**) and actual (**D**) arrival times is denoted by  $\delta$ , and allows for the operational definition of prompt and delayed particle events.

tween the laser and particle beams, a flight velocity is calculated and used to predict the arrival of the particle's ions at the mass detector, assuming instantaneous vaporization and ionization. The mass signal as a function of time-of-flight is shown for the chopper cycle in orange. For some particles, the arrival of the ions at the detector is significantly offset ("delayed") from the predicted arrival time. This offset is used to categorize particles into prompt and delayed categories.

Figure 5.4 shows total ion signals from individual particles (grey circles) along

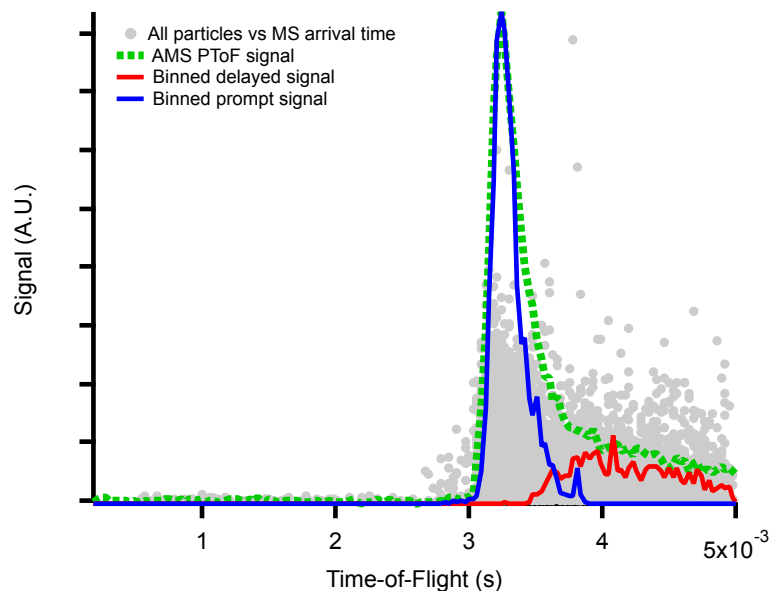


Figure 5.4: Particle signal versus particle time-of-flight from the chopper to the mass detector are shown for ensemble mode (green) and for all detected single particle events (gray circles). Flight times for each individual particle event are binned, and particle signals are sorted into their prompt (blue) and delayed (red) classifications, and then summed.

with total signals of prompt (blue) and delayed (red) particles. We see that the large-diameter PToF tail (green) matches the delayed particle distribution. Additionally, none of the prompt particles have measured times-of-flight greater than 4 milliseconds. As described in Cross et al. (2009), the physical basis for the broadened PToF distribution at large diameters is particles with delayed vaporization, which make up a significant fraction of the measured single-particles in this experiment (18.59% of all particles). However, the source of the delayed vaporization remains unknown.

### 5.3.2 Delayed particle signal strengths

Despite the number of prompt (16.8% of all particles) and delayed particles being nearly equal for this SOA, the two particle types do not contribute equally to the

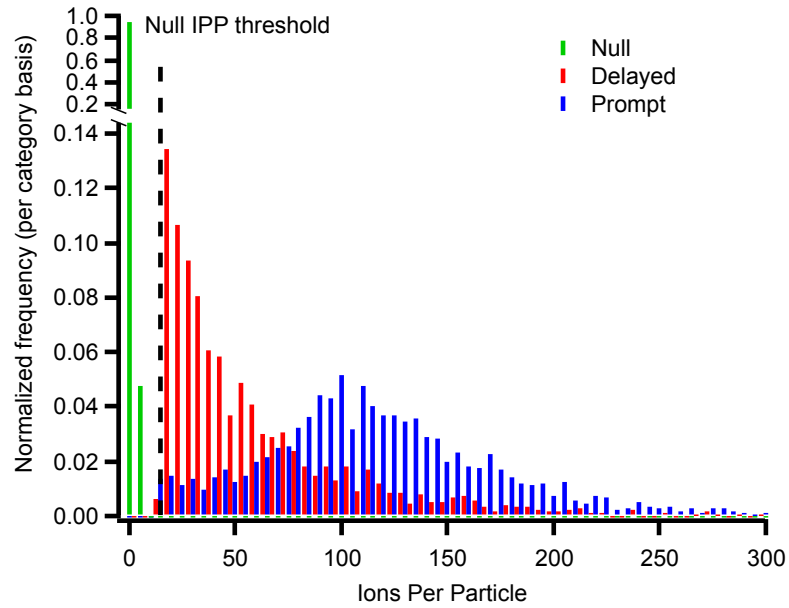


Figure 5.5: Histogram of ions per particle for null (green), delayed (red), and prompt (blue) particle categories. The y-axis is the frequency of single-particle events within a given category each category (in other words, all data for each category sum to one). The histogram bars for the delayed category is offset (by 5 ions) on the x-axis for clarity.

MS signal. As shown in Figure 5.5, prompt particles contribute significantly more signal per particle than delayed particles even though they are all the same size. We plot in Figure 5.5 a histogram of frequency vs ions per particle (IPP) on the x-axis. The sum of the bins for each category is one. In other words, the ionization efficiency for prompt particles is higher than that of delayed particles. If this were not the case, the delayed vaporization tail for SOA shown in Figure 5.2 would be even more pronounced.

The magnitude of particle delay time affects the single-particle mass signal (IPP) even within each category, possibly providing reason to redefine what it means to be “prompt” vs “delayed.” Figure 5.6 shows a steady decrease in the average IPP as a function of delay time. The error bars represent the standard error of the mean within each bin, while the gray shadow shows the standard de-

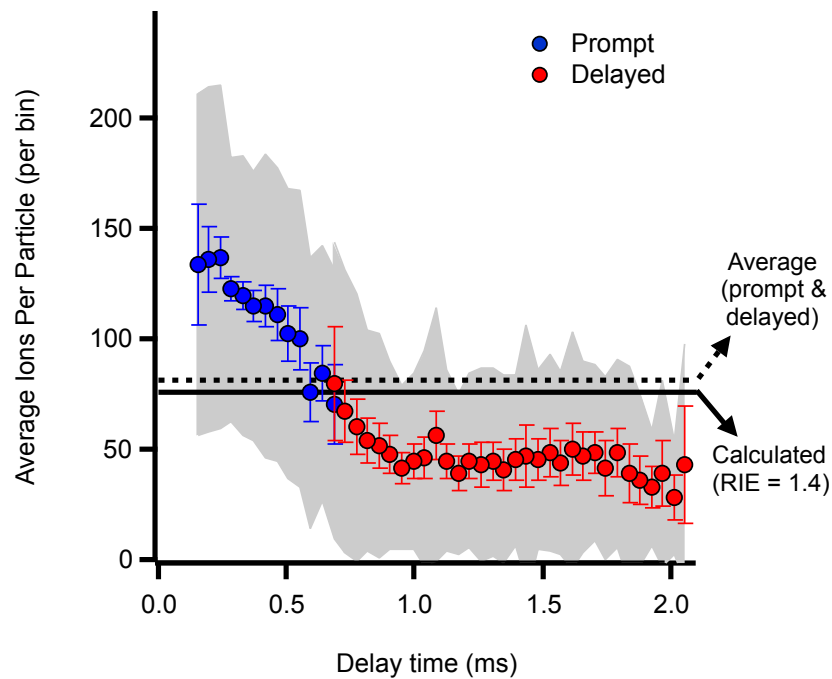


Figure 5.6: Ions per particle as a function of the delay time between the expected time of arrival for the chemical ion signal and the actual time of arrival. The data points are the arithmetic mean IPP value for a given delay time bin. Error bars are the standard error of the mean for each bin, which represent the precision of the average IPP values. The gray shadow behind is the standard deviation of ions per particle within each bin, which reflects the inherent spread of single particle signals. Dotted line shows the average IPP for the ensemble, while the solid line shows the calculated IPP based on an ionization efficiency (IE) of  $5 \times 10^{-7}$  and a relative IE (RIE) of 1.4 for organics compared to ammonium nitrate.

viation for each bin reflecting the inherent spread of single particle mass signals.

Plotting the accumulated particle counts as a function of delay time shows how single-particle information from LSSP mode can be used to best understand the response of the AMS to different particle types, each with its own sensitivity in the instrument (Figure 5.7a). The traces in Figure 5.7a are scaled by their measured  $CE_p$  values (from equation 5.3). The effect of delay time on IPP is absent for ammonium nitrate, the standard mass calibrant for the AMS, as all particles arrive

within the first few delay time bins. Squalane, a liquid at room temperatures with a near-unit  $CE_p$ , largely accumulates its signal at small delay times, but is noticeably slower to do so than ammonium nitrate. This suggests that, while the near-unit  $CE_p$  of ammonium nitrate is probably largely attributable to the metastable liquid phase state (even at the high vacuum conditions of the AMS), volatility also plays a large role in how promptly a particle vaporizes, as ammonium nitrate is more volatile than squalane ( $\sim 30 \mu\text{g m}^{-3}$  and  $\sim 0.1 \mu\text{g m}^{-3}$ , respectively). We estimate the squalane vapor pressure using SIMPOL (Pankow and Asher, 2008), and use the ammonium nitrate vapor pressure reported by Richardson and Hightower (1987)). On the other hand, the SOA exhibits delayed vaporization and low  $CE_p$ , not unlike crystalline ammonium sulfate, a possible indication of a solid or semi-solid phase state, extremely low-volatility material, or both. Figure 5.7b shows how the total mass signal from single particles accumulates faster than the particle counts as a function of delay time, as particles with low delay times contribute relatively more mass signal on average. Both traces are normalized by the  $CE_p$  value for the SOA from this experiment.

### 5.3.3 Nature of particle-vaporizer interactions

These results seem to indicate that when an aerosol type exhibits bounce, it also exhibits delayed vaporization and thus lower relative ionization efficiency for some fraction of particles. In investigating the offset between expected and actual arrival times, we tested two ideas about how the signal at the mass detector would arrive. If the particle impacts and sticks to the vaporizer surface, but does not promptly vaporize, it should show an accumulation of mass at the detector over time, beginning at the expected arrival time. It should sizzle. However, if the particle bounces off the vaporizer without any significant evaporation, and somehow returns to a hot surface at a later time, then the time-resolved arrival of ions should look similar to a

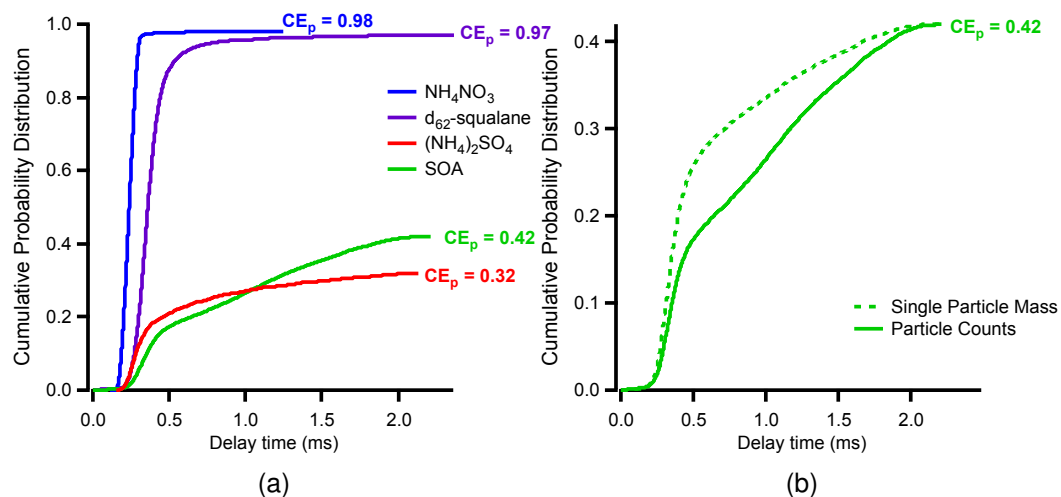


Figure 5.7: **(A)** Cumulative probability distributions of particle counts as a function of delay time for ammonium nitrate (blue),  $\text{D}_{62}$ -squalane (purple), ammonium sulfate (red), and SOA (from  $\alpha$ -pinene +  $\text{O}_3$ ) (green), normalized by  $\text{CE}_p$ . **(B)** Cumulative probability distributions for single particle counts (solid line) and single-particle mass (dashed) for SOA, normalized by  $\text{CE}_p$ .

prompt particle that vaporizes upon impact, albeit after some time associated with its bouncy journey.

Indeed, when the mass arrival signals for an ensemble of single-particle events are averaged together, we see that prompt and delayed particles have the same peak shape (Figure 5.8). Here, we take the average single-particle mass signal for a given bin of maximum arrival time. We chose two arrival-time bins with times-of-flight equal to 3.21 ms (all prompt particles) and 4.05 (all delayed particles). The similar, sharp peak shape suggests that delayed particles are truly delayed in starting the vaporization process, and not simply slow to evaporate. Thus we conclude that delayed particles must be bouncing around the ionization cage after initially striking the front of the vaporizer before they finally land and vaporize on one of the hot surfaces in the vaporization region (e.g. side of the vaporizer, ionization cage).

The AMS vaporizer is a cylindrical tube furnace ( $R = 3.81$  mm;  $L = 20$  mm) with

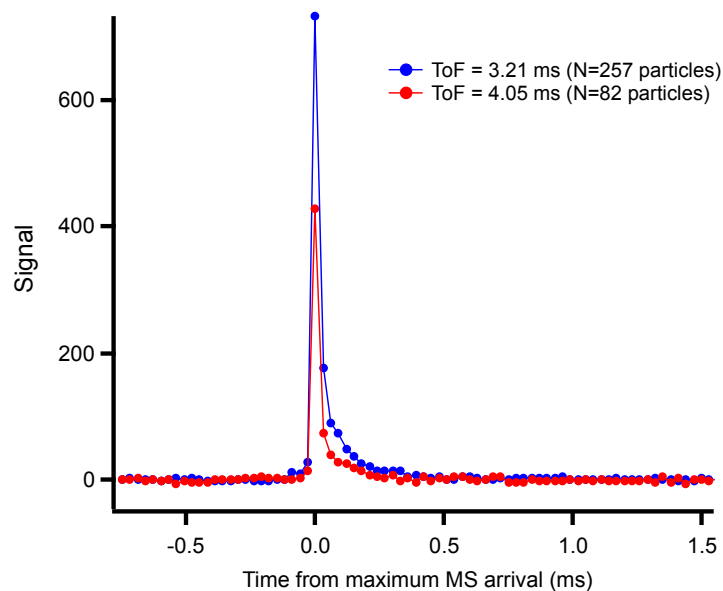


Figure 5.8: Chemical ion signals for two time-of-flight (ToF) bins. The traces represent the average signal for all particles with the same MS arrival time. All particles in each bin were classified as either prompt (ToF = 3.21 ms) or delayed (ToF = 4.05 ms). N is the number of particles used to make the average trace.

a concave beveled cone ( $60^\circ$  included angle) serving as the stop for the particle beam. It is centered within an ionization cage, a rectangular aluminum housing ( $H = 6\text{ mm}$ ;  $W = 8\text{ mm}$ ;  $L = 15\text{ mm}$ ) which is open on each end. The front end of the vaporizer is set back  $\sim 10\text{ mm}$  from the front opening of the ion cage, and  $\sim 2\text{ mm}$  from the ion extraction volume, maximizing the intersection of the vaporized particle plume, the electron beam from the filament, and the axis from ion extraction. Because of the long hot surface of the vaporizer, which is housed inside a sheet-metal cage, our mechanistic picture of particles bouncing around this region before finally landing on a hot surface is plausible. Importantly, for this SOA, the vaporization of the particle still can be thought of as fast—when the particle finally does stick, it is vaporized and ionized on the same timescale as a “prompt” particle. Thus, the “PToF broadening” (shown in Figure 5.2) can be attributed to particles bouncing

around before vaporizing, not slowly boiling off adsorbed material over time, as discussed in Salcedo et al. (2010) for lead salts. Indeed, this explanation is consistent with the decrease in IPP as a function of delay time: when particles vaporize on e.g. the side of the vaporizer, they are in a sub-optimal position for ionization and thus detection of the full single-particle mass Huffman et al., 2009.

As a further check that the SOA particles are rapidly vaporizing—just simply doing so at a time later than would be expected based on their measured size and expected time-of-flight—we increased the temperature of the vaporizer from 600 °C to 800 °C. Were the particles sitting on the vaporizer surface and slowly boiling, we expect this temperature increase to decrease the broadened PToF tail (Figure 5.9a). We do not see this effect (note: the degradation in the organic PToF signal at 800 °C is largely due to low particle numbers at the end of our experiment due to wall loss). However, in an experiment where SOA particles are coated with squalane (liquid at RT,  $CE_p \sim 1$ ), the broadened tail diminishes, further supporting this idea (Figure 5.9b). On the other hand, the PToF distribution for ammonium nitrate can be broadened by decreasing the vaporizer from 600 °C to 200 °C, indicating that these aerosol do stick to the surface, and have a reduced mass flux at lower temperatures, thus spreading the signal arrival out over time-of-flight (Figure 5.9c).

Consistent with this proposed mechanism—that delayed SOA particles are bouncing around and vaporizing on surfaces other than the vaporizer cone—is the difference in mass spectra between prompt and delayed particles. Figure 5.10 shows the difference mass spectrum between prompt and delayed particles for both SOA and ammonium sulfate (which also exhibits a high delayed fraction). Several fragments are biased high in either the prompt or delayed MS (e.g.  $m/z$  43 ( $C_3H_7^+$ ) is higher and  $m/z$  44 ( $CO_2^+$ ) is lower for delayed SOA particles;  $m/z$  81 ( $HSO_3^+$ ) and 98 ( $HSO_4^+$ ) are higher in delayed MS while  $m/z$  48 and 64 are

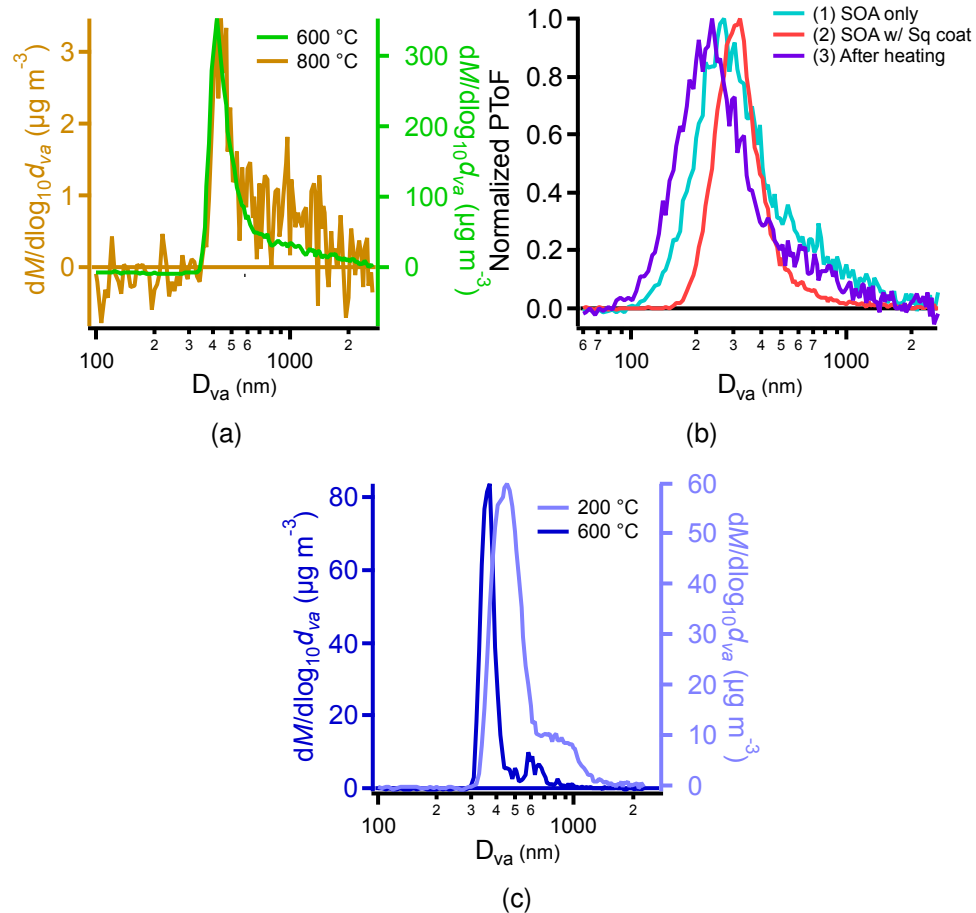


Figure 5.9: Ensemble mass distributions of different particle types under various conditions of the AMS vaporizer. **(A)**  $\alpha$ -pinene derived SOA particles for vaporizer temperatures of the standard 600 °C temperature (green), and 800 °C (brown). Note: the degraded signal at 800 °C is simply a result of wall-loss, as these data were taken at the end of an experiment where particle number was relatively low. **(B)** SOA particles at three stages of a mixed-particle experiment (similar to Chapter 4): homogeneously-nucleated SOA (sky blue), SOA particles coated with squalane (orange), and SOA/squalane particles after an increase in chamber temperature (purple). Note the disappearance of the delayed tail with the condensation of squalane, and the reappearance of the tail with heating despite the decrease in mode diameter. **(C)** Ammonium nitrate at the standard vaporizer temperature (600 °C, dark blue), and low temperature (200 °C, sky blue).

higher in prompt MS for ammonium sulfate particles). On the continuum of loading-dependent  $\alpha$ -pinene SOA composition reported in Shilling et al. (2009), the delayed MS appears less oxidized than the prompt MS. For ammonium sulfate particles, the delayed spectrum appears to be enhanced in acidic fragments. It is possible that

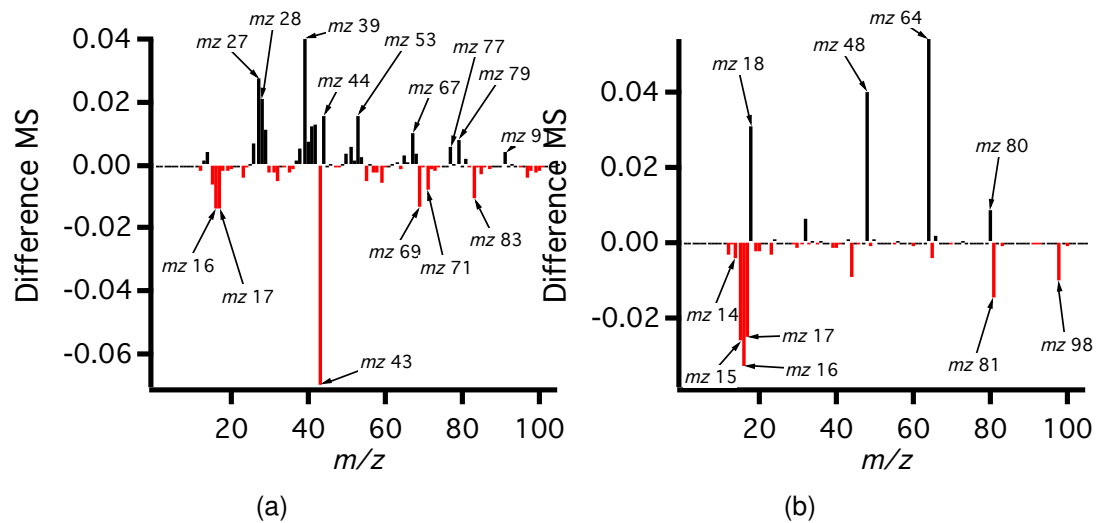


Figure 5.10: Difference plots between prompt and delayed average mass spectra for **(A)** SOA and **(B)** ammonium sulfate. Plot is prepared by first normalizing each spectra by the total signal, and then subtracting the delayed MS from the prompt. Thus, positive fragments are enriched in the prompt MS, while negative are enriched in the delayed MS.

delayed particles are subjected to a wide range of possible temperatures by the surface they eventually land and volatilize on (e.g. ion cage, vaporizer side), and that this can lead to different fragmentation pathways, which could be important for interpreting ambient single-particle spectra.

#### 5.3.4 Collection efficiency as a function of size

As reported previously in the literature, some studies have shown collection efficiency to be size Liu et al., 2013 and composition-dependent Docherty et al., 2013. To investigate any size-dependent collection efficiency that our SOA might have, particles were selected at different mobility diameters by a DMA upstream of the AMS. Figure 5.11a shows  $CE_p$  as a function of selected mobility diameter. LSSP can also provide a size-resolved  $CE_p$  for polydisperse aerosol, as each optically-counted particle has an estimated  $D_{va}$ . Figure 5.11a also shows  $CE_p$  for polydisperse SOA from a smog chamber experiment with good agreement with the

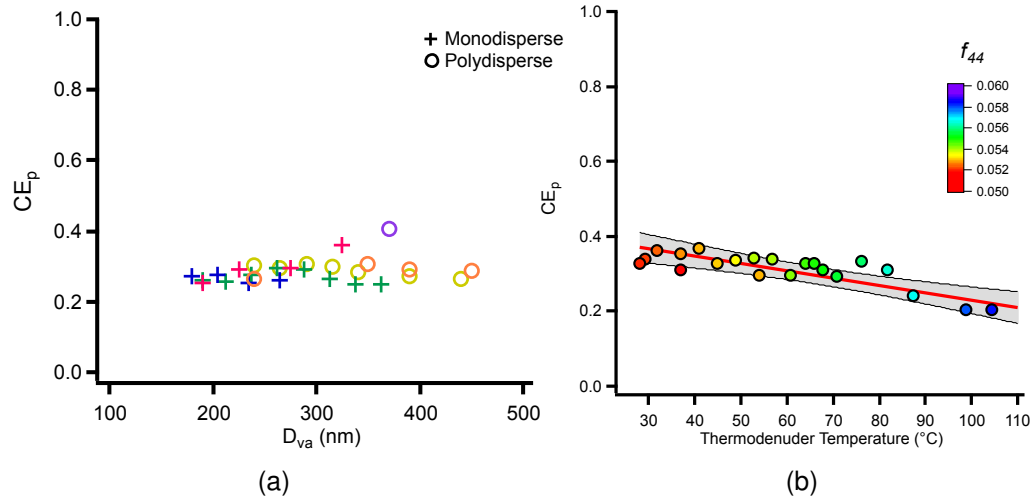


Figure 5.11: **(A)** Particle collection efficiency as a function of  $D_{va}$  for all SOA experiments. Data are from both size-selected experiments (crosses) and polydisperse SOA from a smog chamber (circles), with each color representing a separate experiment. **(B)** Particle collection efficiency (colored markers) as a function of thermodenuder temperature for SOA from  $\alpha$ -pinene, colored by the fraction of m/z 44 ( $f_{44}$ ) to the total organic mass. Confidence intervals (95% CI) for a linear fit are shown (slope:  $-0.0019604 \text{ K}^{-1} \pm 0.000401$ ).

size-selected data.

### 5.3.5 Collection efficiency as a function of volatility

While  $CE_p$  for this SOA is independent of size (for the mobility diameter range 170–460 nm), we do observe a decreasing trend in  $CE_p$  by passing the SOA through a thermodenuder. When we plot  $CE_p$  as a function of thermodenuder temperature (Figure 5.11b), which we use as a proxy variable for the volatility of the aerosol. These results are consistent with the trend shown by Docherty et al. (2013), who saw decreasing  $CE_m$  with increasing oxidation state. It should be noted that this SOA is similarly oxidized ( $f_{44}/f_{57} \approx 6$ ) as the least oxidized SOA from their study with a corresponding  $CE_m$  of  $\sim 0.2$  ( $f_{44}/f_{57} \geq 5$ ). LSSP can be used to verify whether this trend exists for other types of NR-PM<sub>1</sub>.

## 5.4 Conclusions

This study contains four main findings, all aimed at better understanding the nature of collection efficiency for SOA. First, we discuss the nature of the PToF tail artifact for SOA from  $\alpha$ -pinene + O<sub>3</sub>, and show that it arises from delayed particles—those that do not evaporate immediately upon contacting the AMS vaporizer. These data are consistent with previously published findings from Cross et al. (2009) for ambient delayed particles. Secondly, we explore the mechanism of delay for these particles, and, with a novel single-particle data analysis, assert that these are particles bouncing around in the vaporization-ionization region in the AMS. Consistent with this assertion are these other findings for SOA: 1) delayed particles give less signal than prompt particles, 2) vaporizer temperature does not reduce the fraction of delayed particles, but 3) coating the SOA with squalane does decrease the delayed fraction. We also present evidence for a lack of size-dependence for collection efficiency of SOA particles, but a composition-dependence where more heavily oxidized particles have a lower CE than less oxidized particles.

Collection efficiency remains the significant barrier to full quantification in the AMS. However, we show here that single-particle data can help further elucidate the complex interaction between particles and the surface of the AMS vaporizer.

## Bibliography

- [1] M Rami Alfarra. "Chapter Four: Laboratory Characterisation of the Aerodyne Aerosol Mass Spectrometer" (Nov. 2004), pp. 1–20.
- [2] A Asa-Awuku et al. "Mixing and phase partitioning of primary and secondary organic aerosols". *Geophysical Research Letters* 36.15 (Aug. 2009).
- [3] R Bahreini et al. "Measurements of Secondary Organic Aerosol from Oxidation of Cycloalkenes, Terpenes, and m-Xylene Using an Aerodyne Aerosol Mass Spectrometer". *Environmental Science & Technology* 39.15 (Aug. 2005), pp. 5674–5688.
- [4] M R Canagaratna et al. "Chemical and microphysical characterization of ambient aerosols with the aerodyne aerosol mass spectrometer". *Mass Spectrometry Reviews* 26.2 (2007), pp. 185–222.
- [5] J S Craven et al. "Analysis of secondary organic aerosol formation and aging using positive matrix factorization of high-resolution aerosol mass spectra: application to the dodecane low-NO<sub>x</sub> system". *Atmospheric Chemistry and Physics* 12.24 (2012), pp. 11795–11817.
- [6] Eben S Cross et al. "Laboratory and Ambient Particle Density Determinations using Light Scattering in Conjunction with Aerosol Mass Spectrometry". *Aerosol Science and Technology* 41.4 (Mar. 2007), pp. 343–359.
- [7] ES Cross et al. "Single particle characterization using a light scattering module coupled to a time-of-flight aerosol mass spectrometer". *Atmospheric Chemistry and Physics* 9 (2009), pp. 7769–7793.
- [8] Peter F DeCarlo et al. "Field-Deployable, High-Resolution, Time-of-Flight Aerosol Mass Spectrometer". *Analytical Chemistry* 78.24 (Dec. 2006), pp. 8281–8289.
- [9] Peter F DeCarlo et al. "Particle Morphology and Density Characterization by Combined Mobility and Aerodynamic Diameter Measurements. Part 1: Theory". *Aerosol Science and Technology* 38.12 (Jan. 2004), pp. 1185–1205.
- [10] Kenneth S Docherty et al. "Collection Efficiency of the Aerosol Mass Spectrometer for Chamber-Generated Secondary Organic Aerosols". *Aerosol Science and Technology* 47.3 (Mar. 2013), pp. 294–309.
- [11] N M Donahue et al. "Aging of biogenic secondary organic aerosol via gas-phase OH radical reactions". *Proceedings of the National Academy of Sciences* 109.34 (2012), pp. 13503–13508.
- [12] F Drewnick et al. "Intercomparison and evaluation of four semi-continuous PM<sub>2.5</sub> sulfate instruments". *Atmospheric Environment* 37.24 (Aug. 2003), pp. 3335–3350.

- [13] Frank Drewnick et al. "A New Time-of-Flight Aerosol Mass Spectrometer (TOF-AMS)—Instrument Description and First Field Deployment". *Aerosol Science and Technology* 39.7 (July 2005), pp. 637–658.
- [14] J A Huffman et al. "Chemically-resolved aerosol volatility measurements from two megacity field studies". *Atmospheric Chemistry and Physics* 9.18 (2009), pp. 7161–7182.
- [15] J Alex Huffman et al. "Design, Modeling, Optimization, and Experimental Tests of a Particle Beam Width Probe for the Aerodyne Aerosol Mass Spectrometer". *Aerosol Science and Technology* 39.12 (Dec. 2005), pp. 1143–1163.
- [16] J L Jimenez et al. "Evolution of Organic Aerosols in the Atmosphere". *Science* 326.5959 (Dec. 2009), pp. 1525–1529.
- [17] M Kanakidou et al. "Organic aerosol and global climate modelling: a review". *Atmospheric Chemistry and Physics* 5.4 (Mar. 2005), pp. 1053–1123.
- [18] Evangelia Kostenidou, Ravi K Pathak, and Spyros N Pandis. "An Algorithm for the Calculation of Secondary Organic Aerosol Density Combining AMS and SMPS Data". *Aerosol Science and Technology* 41.11 (Oct. 2007), pp. 1002–1010.
- [19] James M Lightstone et al. "Deliquescence, Efflorescence, and Water Activity in Ammonium Nitrate and Mixed Ammonium Nitrate/Succinic Acid Microparticles". *The Journal of Physical Chemistry A* 104.41 (Oct. 2000), pp. 9337–9346.
- [20] S Liu et al. "Organic particle types by single-particle measurements using a time-of-flight aerosol mass spectrometer coupled with a light scattering module". *Atmospheric Measurement Techniques* 6 (2013), pp. 187–197.
- [21] Rafael Lozano et al. "Global and regional mortality from 235 causes of death for 20 age groups in 1990 and 2010: a systematic analysis for the Global Burden of Disease Study 2010". *The Lancet* 380.9859 (2013), pp. 2095–2128.
- [22] Brendan M matthew, Ann M Middlebrook, and Timothy B Onasch. "Collection efficiencies in an Aerodyne Aerosol Mass Spectrometer as a function of particle phase for laboratory generated aerosols". *Aerosol Science and Technology* 42.11 (2008), pp. 884–898.
- [23] Ann M Middlebrook et al. "Evaluation of Composition-Dependent Collection Efficiencies for the Aerodyne Aerosol Mass Spectrometer using Field Data". *Aerosol Science and Technology* 46.3 (Mar. 2012), pp. 258–271.
- [24] Richard L Myers and Wade L Fite. "Electrical detection of airborne particulates using surface ionization techniques". *Environmental Science & Technology* 9.4 (1975), pp. 334–336.

- [25] JF Pankow and WE Asher. "SIMPOL. 1: a simple group contribution method for predicting vapor pressures and enthalpies of vaporization of multifunctional organic compounds". *Atmospheric Chemistry and Physics* 8.10 (2008), pp. 2773–2796.
- [26] P K Quinn et al. "Impacts of sources and aging on submicrometer aerosol properties in the marine boundary layer across the Gulf of Maine". *Journal of Geophysical Research* 111.D23 (Dec. 2006), D23S36.
- [27] C B Richardson and R L Hightower. "Evaporation of ammonium nitrate particles". *Atmospheric Environment (1967)* 21.4 (1987), pp. 971–975.
- [28] Ellis Shipley Robinson, Rawad Saleh, and Neil M Donahue. "Organic Aerosol Mixing Observed by Single-Particle Mass Spectrometry". *The Journal of Physical Chemistry A* 117.51 (Dec. 2013), pp. 13935–13945.
- [29] D Salcedo et al. "Determination of particulate lead using aerosol mass spectrometry: MILAGRO/MCMA-2006 observations". *Atmospheric Chemistry and Physics* 10.12 (2010), pp. 5371–5389.
- [30] D Salcedo et al. "Technical Note: Use of a beam width probe in an Aerosol Mass Spectrometer to monitor particle collection efficiency in the field". *Atmospheric Chemistry and Physics* 7.2 (2007), pp. 549–556.
- [31] John E Shilling et al. "Loading-dependent elemental composition of  $\alpha$ -pinene SOA particles". *Atmospheric Chemistry and Physics* 9.3 (2009), pp. 771–782.
- [32] J G Slowik et al. "Characterization of a large biogenic secondary organic aerosol event from eastern Canadian forests". *Atmospheric Chemistry and Physics Discussions* 9.5 (2009), pp. 18113–18158.
- [33] S Solomon et al. "Climate change 2007: The physical science basis, contribution of working group 1 to the fourth assessment report of the Intergovernmental Panel on Climate Change" (2007).
- [34] Annele Virtanen et al. "An amorphous solid state of biogenic secondary organic aerosol particles". *Nature* 467.7317 (Oct. 2010), pp. 824–827.
- [35] Alla Zelenyuk et al. "A New Real-Time Method for Determining Particles' Sphericity and Density: Application to Secondary Organic Aerosol Formed by Ozonolysis of  $\alpha$ -Pinene". *Environmental Science & Technology* 42.21 (Nov. 2008), pp. 8033–8038.

# Chapter 6

## Conclusions

What unifies this thesis is that each chapter, either directly or indirectly, works towards the goal of better understanding of the phase-state and thermodynamics of aerosols. In Chapter 3, thermodynamic interactions between pure-component and atmospherically-relevant aerosols were directly examined using single-particle mass spectrometry. However, to study thermodynamics of aerosol mixing, one needs to reckon with the kinetics: in chapter 4 we were able to assess the thermodynamics of mixing between SOA and a surrogate for POA, while also uncovering the kinetic constraints to the mixing process, volatility and condensed-phase mass transfer. Finally, in chapter 5, we explored the complex interactions between semi-solid SOA particles and the AMS, a powerful tool for studying aerosol mixing. While disparate when taken separately, taken as a whole these studies further how complex aerosol interactions can be studied in the laboratory.

Since the treatment of phase separation and mixing has a large impact on organic aerosol mass and composition in regional and global models (e.g. Koo, Ansari, and Pandis, 2003), and has only recently been investigated in the lab (albeit indirectly, e.g. Hildebrandt et al., 2011), the first objective of this thesis was to directly test gas-phase mixing between different aerosol populations. Our data showed that mixing through gas-phase exchange can be quantified using single-particle mass spectra, which represents a first step towards assessing activity coefficients between real OA mixtures. Experiments using pure-compound aerosol demonstrated that condensed-phase barriers to mixing (such as low diffusivity), are important to consider alongside the thermodynamics of whether two populations form a single phase at equilibrium. We applied this method towards two atmospherically-relevant systems, and found: 1) aSOA and a hydrophobic surro-

gate for POA did not mix at all, and 2) bSOA absorbed material from aSOA. In both of these “real-world” examples, the result is much more complicated than the assumption used in most regional and global OA models, that organics form a single, well-mixed organic phase (Strader, Lurmann, and Pandis, 1999).

Based on the methods and demonstration of results of Chapter 3, determining the activity coefficients between real OA systems should be the focus of future work. While we explored two interactions (aSOA/hydrophobic POA, and aSOA/bSOA), there are many other important OA types to consider (e.g. how do bSOA and BBOA interact?, etc.). In addition to extending this work to other systems, there are two further avenues of exploration that we recommend be explored. First, how does on-going oxidation chemistry affect mixing? As demonstrated by Dzepina et al. (2009), phase separation between two OA types can drive gas-phase oxidation chemistry that eventually leads to mixing. For example, in the hydrophobic POA/aSOA (of importance in urban outflow), exploring how oxidative processing of the POA drives the two towards miscibility would help better constrain the anthropogenic influence on biogenic aerosol. Secondly, recent works show that both the partitioning (Prisle et al., 2010) and condensed-phase diffusivity (Zhou et al., 2013) of SOA are affected by RH. Thus, a systematic exploration of how RH can both change the thermodynamics and drive the kinetics of mixing in SOA systems should also be an avenue for further mixing work.

While the equilibrium behavior of aerosols is of extreme importance (e.g. for mixing: Robinson, Saleh, and Donahue, 2013), one important question that has emerged in the literature recently is: even if we know the equilibrium state, will OA systems get there fast enough to apply that knowledge to models? The second objective of this thesis was to explore this question for a system containing squalane and SOA. We wanted to investigate the timescale of evaporation of squalane from mixed SOA/squalane particles, as some recent research has concluded that

condensed-phase diffusion is too slow to assume that atmospheric SOA can equilibrate with the gas-phase (Shrivastava et al., 2013). Our results, on the other hand, show that squalane is able to evaporate quite rapidly from these mixed-particles, which we determined to be phase-separated. The implications of this work depend highly on the particle morphology, as the squalane evaporation rate through a thick layer of SOA (core-shell) should likely be quite different than through a squalane-air interface (partially-engulfed). While we were unable to determine the morphology through the particle collection efficiency, we show that CE can be parameterized in this system, and is crucial to do so in performing a comparative volatility analysis between the two materials. We find that, to first order, all of the SOA is less volatile than the squalane, a result that adds to a growing body of knowledge (Ehn et al., 2015) about the extremely-low volatility nature of SOA.

Remaining unfinished in this work, is a quantification of the diffusion coefficient of squalane through SOA. The value of SOA diffusion coefficient has received growing attention recently (e.g. Renbaum-Wolff and Grayson, 2013), as it is a key physical parameter in a handful of processes (e.g. heterogeneous chemistry, mixing, evaporation). We plan to simulate the evaporation of a squalane core from an SOA shell to estimate  $D_{org}$  for this system, and add to the small but growing number of studies that attempt to constrain this important quantity.

Finally, in chapter 5, we explore the nature of collection efficiency in the AMS—the essential tool not only for the work of chapters 3 and 4, but a real-time instrument that has revolutionized the field of organic aerosol in the past ten years (Canagaratna et al., 2007). Despite the power of the AMS, a major limitation to full quantification is collection efficiency; CE is a sensitivity factor that is highly variable between different particle types (literature values range from  $\sim 0.15$  to 1). Previous studies have focused on CE of total OA mass, but in this study we focus on CE on a particle-by-particle basis. In chapter 5, we report CE for SOA derived from

---

$\alpha$ -pinene (which compares well with the previously published work of Docherty et al., 2013), and show that a significant fraction of SOA particles hitting the AMS vaporizer are delayed in reaching the mass spectrometer. We provide compelling evidence that demonstrates that these delayed SOA particles are bouncing around the ionization region of the AMS and landing on surfaces other than the tungsten vaporizer. This leads to lower per-particle signal and affects the mass spectrum (for SOA particles, the MS appears more oxidized for delayed particles, while for ammonium sulfate, the delayed MS appears more acidic). We also find that CE decreases as particles are thermally-denuded, meaning that there is a link between CE and oxidation state and/or volatility. We do not find CE to be a function of size for SOA.

Based on the accumulating number of studies that relate particle bounce to particle phase state (e.g. Virtanen et al., 2010)—indeed, chapter 5 shows that SOA is highly bouncy, and thus possibly a semi-solid—we suggest that future theoretical work be aimed at relating bounce to more fundamental quantities of interest to atmospheric scientists (e.g. viscosity). Additionally, modeling studies of the bounce interaction between particles and the AMS vaporizer have the power to lead to a better designed vaporization region. A new vaporizer design could aim to at either 1) decreasing bounce through modifying the vaporizer itself, or 2) “harness bounce,” by modifying the ionization cage’s temperature and geometry to funnel bouncing particles towards the ion extraction region, and have them vaporize at the standard vaporizer temperature.

## Bibliography

- [1] M R Canagaratna et al. "Chemical and microphysical characterization of ambient aerosols with the aerodyne aerosol mass spectrometer". *Mass Spectrometry Reviews* 26.2 (2007), pp. 185–222.
- [2] Kenneth S Docherty et al. "Collection Efficiency of the Aerosol Mass Spectrometer for Chamber-Generated Secondary Organic Aerosols". *Aerosol Science and Technology* 47.3 (Mar. 2013), pp. 294–309.
- [3] Katja Dzepina et al. "Evaluation of recently-proposed secondary organic aerosol models for a case study in Mexico City". *Atmospheric Chemistry and Physics* 9.15 (2009), pp. 5681–5709.
- [4] Mikael Ehn et al. "A large source of low-volatility secondary organic aerosol". *Nature* 506.7489 (Apr. 2015), pp. 476–479.
- [5] Lea Hildebrandt et al. "Evaluating the Mixing of Organic Aerosol Components Using High-Resolution Aerosol Mass Spectrometry". *Environmental Science & Technology* 45.15 (Aug. 2011), pp. 6329–6335.
- [6] Bonyoung Koo, Asif S Ansari, and Spyros N Pandis. "Integrated approaches to modeling the organic and inorganic atmospheric aerosol components". *Atmospheric Environment* 37.34 (Nov. 2003), pp. 4757–4768.
- [7] Nønne Lyng Prisle et al. "Humidity influence on gas–particle phase partitioning of  $\alpha$ -pinene + O<sub>3</sub> secondary organic aerosol". *Geophysical Research Letters* 37.1 (2010).
- [8] L Renbaum-Wolff and J W Grayson. "Viscosity of alpha-pinene secondary organic material and implications for particle growth and reactivity". *Proceedings of the . . .* 2013.
- [9] Ellis Shipley Robinson, Rawad Saleh, and Neil M Donahue. "Organic Aerosol Mixing Observed by Single-Particle Mass Spectrometry". *The Journal of Physical Chemistry A* 117.51 (Dec. 2013), pp. 13935–13945.
- [10] Manish Shrivastava et al. "Implications of low volatility SOA and gas-phase fragmentation reactions on SOA loadings and their spatial and temporal evolution in the atmosphere". *Journal of Geophysical Research: Atmospheres* 118.8 (Apr. 2013), pp. 3328–3342.
- [11] Ross Strader, Fred Lurmann, and Spyros N Pandis. "Evaluation of secondary organic aerosol formation in winter". *Atmospheric Environment* 33.29 (1999), pp. 4849–4863.
- [12] Annele Virtanen et al. "An amorphous solid state of biogenic secondary organic aerosol particles". *Nature* 467.7317 (Oct. 2010), pp. 824–827.
- [13] Shouming Zhou et al. "Kinetic limitations in gas-particle reactions arising from slow diffusion in secondary organic aerosol". *Faraday Discussions* 165 (2013), p. 391.